YGS Open File 2020–3

Early-stage exploration for geothermal energy resources along the Denali fault near Duke River, Yukon

J.B. Witter Innovate Geothermal Ltd.

Innovate Geothermal

Canadian Northern Economic Development Agency | Agence canadienne de développement économique du Nord

Yukon

Published under the authority of the Department of Energy, Mines and Resources, Government of Yukon https://yukon.ca/en/department-energy-mines-resources.

Printed in Whitehorse, Yukon, 2020.

Publié avec l'autorisation du Ministères de l'Énergie, des Mines et des Ressources du gouvernement du Yukon, https://yukon.ca/en/department-energy-mines-resources.

Imprimé à Whitehorse (Yukon) en 2020.

This, and other Yukon Geological Survey publications, may be obtained from:
Yukon Geological Survey
102-300 Main Street
Box 2703 (K-102)
Whitehorse, Yukon, Canada Y1A 2C6
email geology@gov.yk.ca

Visit the Yukon Geological Survey website at https://yukon.ca/en/science-and-natural-resources/geology.

In referring to this publication, please use the following citation:

Witter, J.B., 2020. Early-stage exploration for geothermal energy resources along the Denali fault near Duke River, Yukon. Yukon Geological Survey, Open File 2020-3, 62 p.

Front cover: Field investigations of the Denali Fault zone in Copper Joe Creek, Kluane Ranges, Yukon.

Preface

This report summarizes the results of a multi-disciplinary study that assesses geothermal potential and identifies targets for several temperature gradient wells along the Denali fault in the Burwash Landing area. Yukon Geological Survey's interest in this region was sparked by the high modeled geothermal gradient indicated by Curie point depth mapping done by Witter and Miller (YGS Open File 2017-3). Curie point depths indicated temperature gradients upwards of 40°C/km in southwestern Yukon in the vicinity of the Denali fault. Within this prospective region the Burwash Landing area was specifically chosen for two reasons: representatives of Kluane First Nation were receptive to the study and keen to engage with Yukon Geological Survey, and Burwash Landing is one of four Yukon communities that relies on diesel for power generation.

Interest in geothermal energy is growing both in Yukon and across Canada; not only for its potential for power generation, but for other applications such as district heating, green houses and aquaculture. While heating homes economically has always been a challenge in Canada's North, food security is an increasingly important issue as governments make efforts to reduce dependence on transported food. In cold climates, geothermal power systems tolerate lower water temperatures, making Yukon an appealing jurisdiction to assess electrical generation opportunities as well.

The study described in this publication is a first in a number of ways. It builds on the approach taken by a similar study along the Tintina fault near Ross River (YGS Miscellaneous Report 18), but more thoroughly integrates geophysical and bedrock geology datasets into a three-dimensional model to identify prospective drill targets. The geological setting examined in this study is a crustal-scale fault system, which makes it unique from other research underway in Canada where the play types of interest are hot sedimentary basins or young volcanic belts. The ultimate goal of this project was to define temperature gradient well targets based on geological criteria and logistical considerations. The seven targets identified in this report lay the ground work for further assessing the geothermal energy potential of this region of Yukon.

The bulk of funding for this project was provided by the Canadian Northern Economic Development Agency through their Strategic Investments in Northern Economic Development program.

Carolyn Relf
Director, Yukon Geological Survey

Table of Contents

Figures

Tables

Abstract

In collaboration with the Yukon Geological Survey, Innovate Geothermal Ltd. performed a multi-component geoscientific investigation in southwestern Yukon to initiate the search for subsurface geothermal energy resources that could be used for direct use applications and, possibly, the generation of electricity. The study area for this project is located near the community of Burwash Landing and straddles the eastern Denali fault zone. The aim of this project is to analyze and interpret a variety of pre-existing and newly-acquired geological and geophysical data sets to identify favourable subsurface targets for a shallow, exploratory geothermal drilling program that could take place in the future. The geoscience work accomplished here includes both 2D map interpretation as well as construction of a 3D geologic model that was tested by geophysical inversion modelling of gravity and magnetic survey data. In addition, a literature review was conducted to identify analogous geothermal structural environments located in similar crustal-scale transform fault zones for comparison with geothermal systems that may be present in the vicinity of the Denali fault. Importantly, geophysical data from this study discovered a right-step in the Denali fault that has the appropriate orientation to form a small pull-apart zone in the Earth's crust within the project area south of Duke River. Such crustal extension may generate fractures and permeability in rocks in the subsurface. Subsurface permeability in geothermal systems provides the pathway for hot geothermal fluids to ascend to drillable depths. This study has identified seven drilling targets, all located in the vicinity of the previously mentioned right-step in the Denali fault. The 3D geologic model generated for this study was utilized to help understand the lithologic domains and structures likely to be encountered by the proposed exploratory boreholes. The distribution of temperature in the subsurface, however, remains a significant unknown. Regional-scale, Curie point depth estimates suggest an average geothermal gradient of ~40°C/km near the eastern Denali fault, but drilling is required to measure actual subsurface temperatures. Based upon the encouraging results of this study, it is recommended that at least two of the seven targets are drilled to depths of 500–1000 m to obtain data on subsurface temperatures, fluids and geology.

Introduction

In early 2019, the Yukon Geological Survey (YGS) engaged Innovate Geothermal Ltd. for assistance with a geothermal exploration program along the Denali fault in southwestern Yukon. YGS has pursued a geothermal energy research program in the territory since 2016, which has included a variety of technical studies as well as community outreach (Fraser *et al.*, 2018). Following consultation with the Kluane First Nation, YGS chose a section along the Denali fault, near the community of Burwash Landing, for a focused geoscientific study to determine if a favourable geological/structural environment might be present that could allow for the ascent of warm geothermal fluids to the near surface, potentially accessible via drilling (Figs. 1 and 2). Burwash Landing depends on diesel generators for electricity and the mean annual temperature in this part of Yukon is -3°C; therefore, a local source of heat and/or power for the community would be of great value.

There are no known hot springs near Burwash Landing; however, there are two primary lines of evidence which suggest that warm geothermal fluids may be present in the subsurface (and are worth looking for) in southwestern Yukon. First, the shallowest depths to the Curie point (580°C) in Yukon are found along the eastern Denali and Duke River fault systems in the southwestern corner of the territory. These data suggest that the average crustal geotherm in this area is elevated and may be on the order of 40°C/km (Witter *et al.*, 2018). Second, the eastern Denali fault is a major, crustal-scale, active dextral fault system that exhibits both strike-slip and reverse motion. This fault trends NW–SE and cuts through the southwestern corner of Yukon. Analogous fault zones, such as the Alpine Fault in New Zealand, have extensive damage zones in the hanging wall which create large-scale rock permeability, which facilitates active circulation of warm geothermal fluids in the subsurface (Townend *et al.*, 2017). Could a similar process be at work along portions of the eastern Denali Fault in which fault-related permeability allows upwelling of warm fluids that have been heated by an elevated crustal geotherm? To test this idea, we specifically selected a project area located in the vicinity of the Duke River valley, ~7 km west of Burwash Landing, for three reasons: 1) recent mapping by Bender and Haeussler (2017) revealed three subparallel strands of the Denali fault which suggests fault complexity, and potentially, a favourable structural environment with permeable subsurface rock formations; 2) the Alaska Highway passes close to the project area to facilitate easy access; and 3) the community of Burwash Landing is located close enough to the project area to benefit in the event that geothermal resources are identified in the subsurface. The project study area itself is 16 km long, it varies from 5–7 km wide, and straddles the northwest-trending Denali fault (Fig. 2).

This report begins with a presentation of the geoscientific background for southwestern Yukon and the project area. Relevant information on volcanism, hot springs, Curie point depth estimates, characteristics of the Denali fault zone, surficial and bedrock geology, as well as a description of structural settings that would be favourable for the formation of geothermal systems are described. Second, to set the stage for the geothermal exploration work undertaken in this study, a summary of the known and unknown facts that are germane to discovery of a geothermal reservoir in the study area is provided. Third, the various geoscience data sets (both existing and newly acquired) that have been analyzed and interpreted for this study are described. Fourth, some comments on the methods used to interpret and model the geoscience data sets are shared. Fifth, the results of both map-based and three-dimensional interpretation of the geoscientific data sets within the project area are presented. And lastly, based upon the aforementioned analysis and interpretation, multiple exploratory geothermal drilling targets are selected. The drill targets are ranked and a rationale for their selection is described.

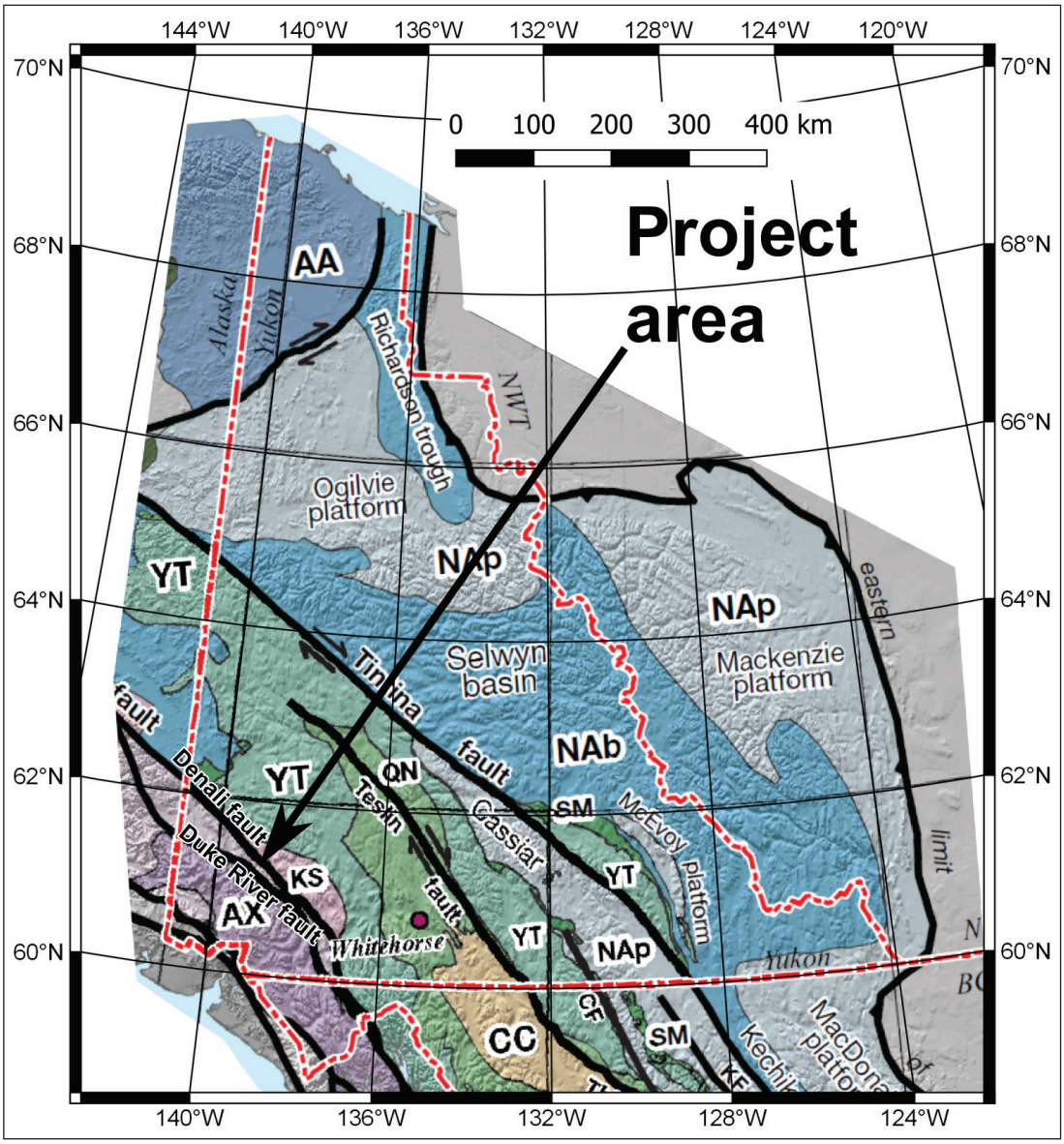

Figure 1. *Map of Yukon illustrating the location of the project area described in this report. Geologic terrane basemap from Nelson et al. (2013). Black lines depict major faults (Colpron and Nelson, 2011). Red dashed lines show provincial/territorial borders.*

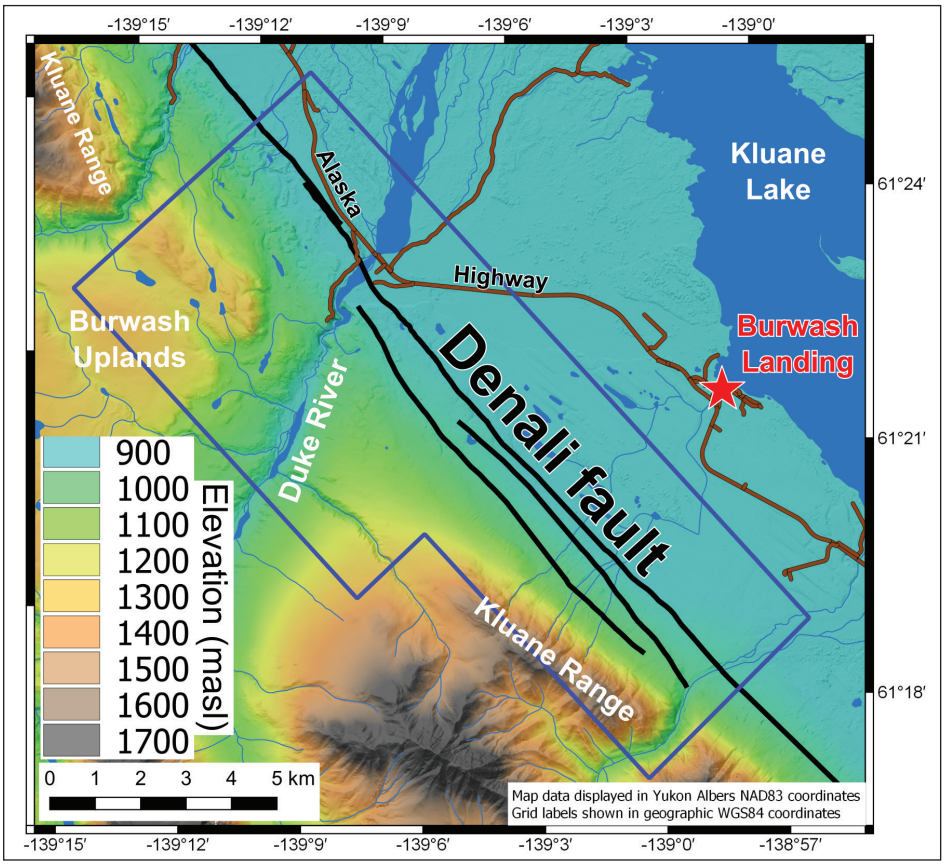

Figure 2. *Map of the Duke River–Burwash Landing area. Project boundary is shown by the blue polygon; roads are in brown. The three strands of the eastern Denali fault mapped by Bender and Haeussler (2017) lie in the central portion of the project area (black lines). Topography with hillshade forms the coloured background.*

Background

Volcanism and Hot Springs

Yukon is not blessed with an abundance of the traditional surface manifestations of geothermal activity: there are few hot springs and even fewer recently active volcanoes in the territory (Global Volcanism Program, 2013; GeoYukon, 2018; Fig. 3).

However, in the Tertiary Period, voluminous active volcanism occurred in southwestern Yukon in the Wrangell volcanic belt, which lies in the vicinity of the Denali and Duke River faults (Skulski, 1988; Skulski *et al.*, 1992). The presence of the Wrangell volcanoes has been explained to be the result of enhanced upwelling of asthenosphere along the edge of the subducted Yakutat slab, coupled with regional transtension associated with major strike-slip faulting (*i.e.*, "leaky" transform faults; Trop *et al.*, 2012; Brueseke *et al.*, 2019). Residual heat from Wrangell volcanic belt magma bodies in Yukon has certainly dissipated in the 10–18 million years since emplacement. However, if localized transtensional motion along the Denali and Duke River fault systems is still occurring today, it could form localized extensional environments that would facilitate the formation of subsurface permeability and provide pathways for the ascent of warm geothermal fluids to shallow reservoirs at drillable depths. Thus, a better understanding of the structural relations and subsurface temperatures in the major, crustal-scale fault systems of southwestern Yukon is key to locating geothermal systems in this area.

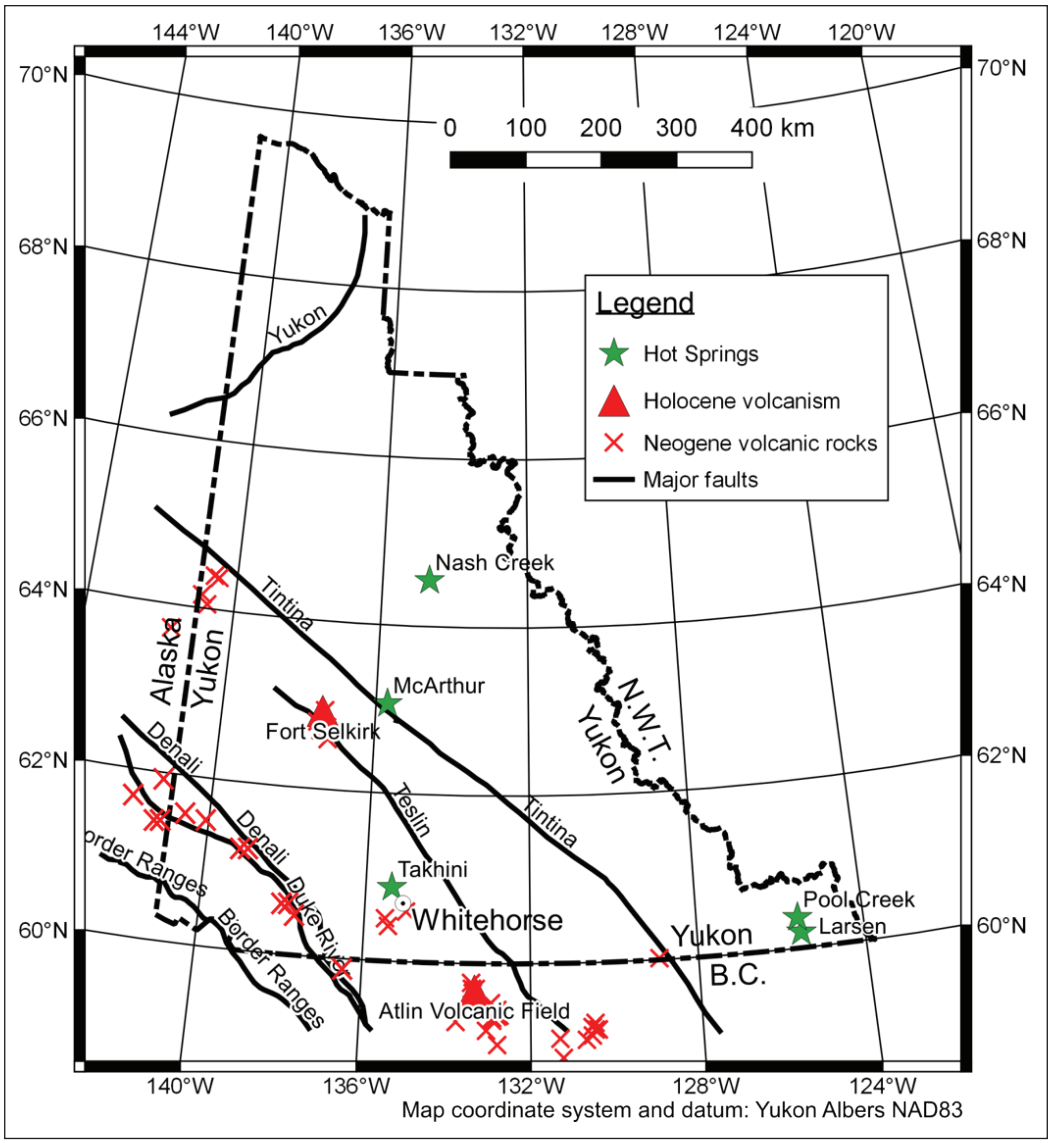

Figure 3. *Map showing Holocene volcanism (red triangles) and hot springs (green stars) in Yukon as well as the locations of Neogene volcanism (red X's). Black lines depict major faults (Colpron and Nelson, 2011).*

Curie Point Depth Map

Curie point depth (CPD) mapping has been used as an initial exploration tool in Yukon to help identify warm *vs.* cool crustal temperatures in the territory (Fig. 4). CPD mapping is a method, originally developed in the 1970s, which uses regional-scale magnetic survey data to map the depth to the Curie point temperature (~580°C) where magnetization in rocks disappears. Regions found to have shallow CPD values are expected to have higher heat flow, higher average thermal gradient, and therefore, a higher likelihood of geothermal energy resources that are accessible via drilling. A study by Li et *al.* (2017) calculated Curie point depths for the entire Earth, with the Yukon data re-plotted by Witter et *al.* (2018). The shallowest CPD values (13–15 km) lie mainly along the Denali and Duke River fault systems in southwestern Yukon. Considering a Curie point temperature of ~580°C, the CPD values of 13–15 km correspond to average crustal temperature gradients of 39–45°C/km. If these estimates are correct, a 2 km borehole along the Denali fault could be expected to reach ~80–90°C. Such a crustal geotherm is elevated compared to the global average of 25–30°C/km.

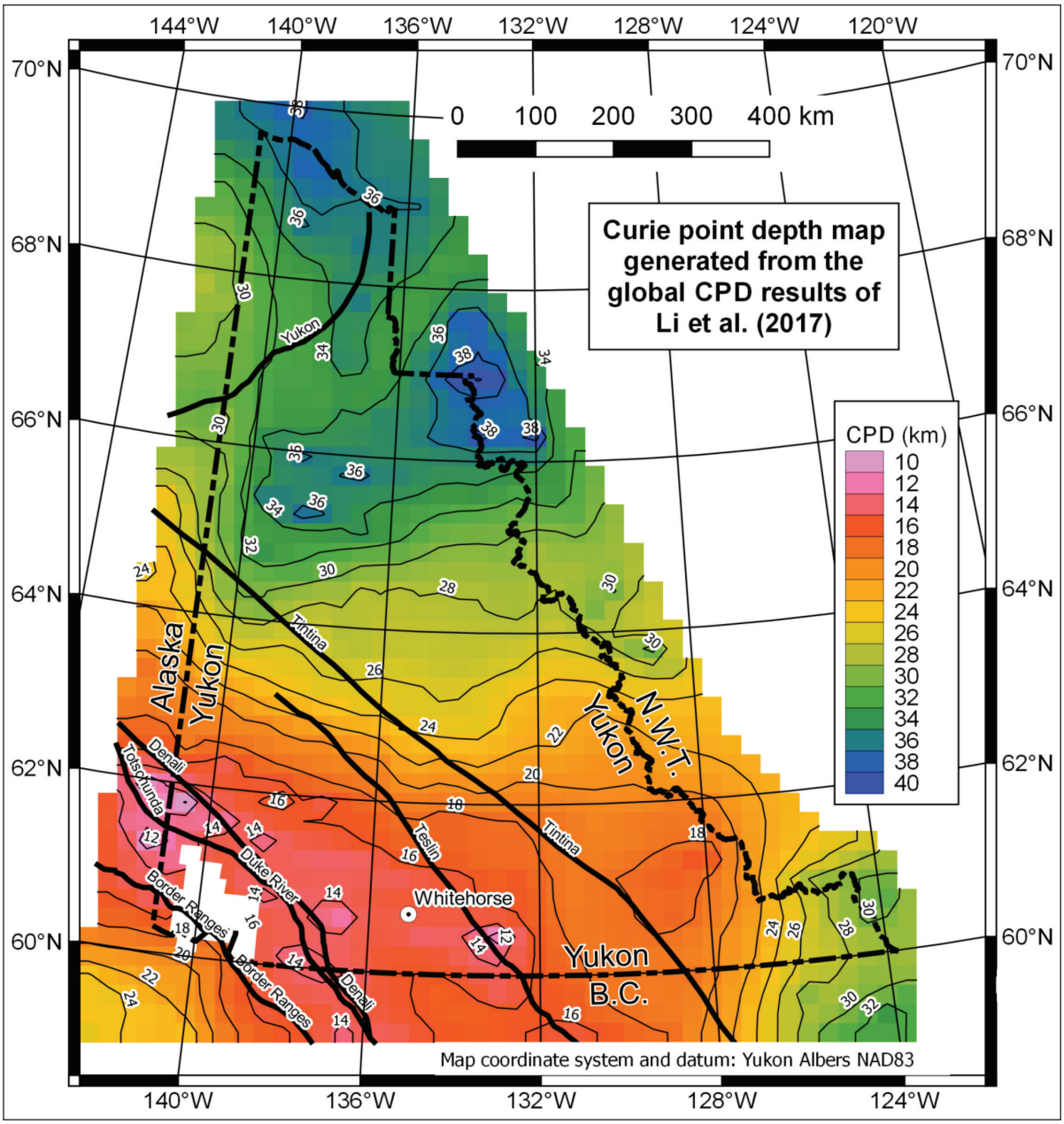

Figure 4. *Curie point depth map for Yukon using data from Li et al. (2017) and re-plotted by Witter et al. (2018). Warm (red) and cool (blue) colours represent shallow and deep CPD estimates, respectively. Contour lines show CPD in units of kilometres below the surface at 2 km depth intervals. Black lines depict major faults (Colpron and Nelson, 2011).*

Denali Fault

The Denali fault is a major intracontinental dextral strike-slip fault, active since the Early Cretaceous, that extends >2000 km from northwestern British Columbia to southwestern Alaska and accommodates ~300–400 km of right-lateral offset (Blais-Stevens et *al.*, 2020; McDermott et *al.*, 2019). The eastern portion of the Denali fault, however, is characterized by both strike-slip and reverse fault motion as evidenced most recently by an earthquake doublet that occurred near the Yukon-BC border in 2017. The earthquake doublet comprised two magnitude 6.2 quakes separated by 2 hours and 1.3 km (Feng et *al.*, 2019). One of the quakes exhibited strike-slip motion while the other showed reverse faulting.

The surface trace of the eastern Denali fault is commonly marked by elongate mounds, tens of metres across and up to 10 m high, separated by depressions. These geomorphic features have been interpreted by Blais-Stevens *et al.* (2020) as sites of local compression and extension, between *en échelon* fault strands, formed during strike-slip movement. Post-glacial offset of these mounds led Blais-Stevens *et al.* (2020) to estimate an average slip rate of ~2 mm/year for the Yukon portion of the Denali fault through the Holocene. Leonard *et al.* (2008) also calculated a deformation rate of 2 mm/year for the eastern Denali fault using earthquake catalog statistics. These two studies estimate *horizontal* deformation on the eastern Denali fault.

A recent study by McDermott *et al.* (2019) used low temperature thermochronometry techniques to investigate *vertical* strain along the eastern Denali fault in the Kluane Ranges, ~40 km SE of the project area in this study. They estimate a total surface uplift rate of 0.2–0.7 mm/year (over the time period 30–10 Ma) for samples collected near the eastern Denali fault. For comparison, Marechal *et al.* (2018) report vertical deformation of 0.9 mm/year for the eastern Denali fault based upon post-glacial geomorphological measurements. Thus, the work of McDermott *et al.* (2019) and Marechal *et al.* (2018) suggest that the vertical motion along the eastern Denali fault may be ~1/10 to ~1/2 the magnitude of the horizontal motion. McDermott *et al.* (2019) point out that vertical strain adjacent to the eastern Denali fault is caused by transpressive deformation which is a far-field response to flat-slab subduction of the Yakutat microplate. A transpressive tectonic regime, however, may not be the full story. Various studies of the Wrangell volcanic belt in Yukon (which lies immediately southwest of the eastern Denali fault) provide strong evidence for zones of transtension associated with the eastern Denali and Duke River faults giving rise to "leaky transform" magmatism (Skulski *et al.*, 1992; Trop *et al.*, 2012; Brueseke *et al.*, 2019). Thus, within the overall transpressive environment, localized transtension may also be present which could give rise to regions of dilatancy within the crust. Such regions should contain subsurface faults, fractures, and permeability which could facilitate geothermal fluid flow.

Favourable structural environments

Favourable structural environments which generate crustal extension, fault dilatancy, and subsurface permeability are essential to the formation of geothermal reservoirs. Faulds and Hinz (2015) analyzed 250 geothermal fields in the Great Basin of the western USA in which they identified 8 characteristic structural settings that are favourable for the formation of geothermal systems. One of these settings is a transtensional pull-apart in a major strike-slip fault zone (Fig. 5). Outside of the Great Basin, the type example of a geothermal system within a transtensional pull-apart is the Salton Sea geothermal field in southeastern California (Younker *et al.*, 1982). In the Salton Sea, right-stepping, right-lateral strike-slip faults of the San Andreas fault zone generate local zones of extension which allow for the ascent of mantle-derived magmas which

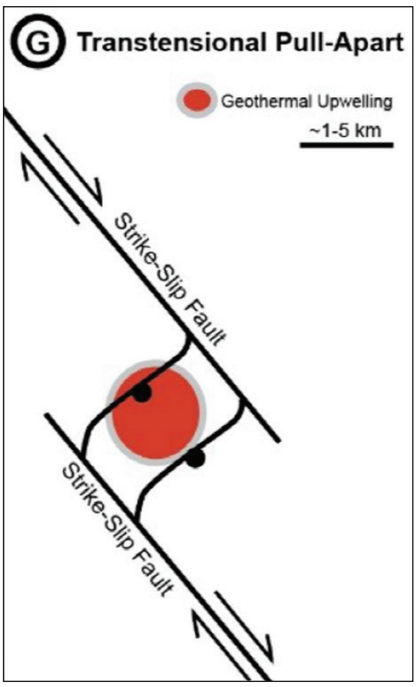

Figure 5. *Schematic diagram of a transtensional pull-apart structural setting which is a favourable geological environment for geothermal fluid upwelling (from Faulds and Hinz, 2015). This schematic represents transtensional pull-aparts that may exist in association with the eastern Denali fault zone. For example, similar to the diagram, the eastern Denali fault zone has a northwest strike, and dextral motion. A right step-over in the fault would create a zone of extension and, possibly, geothermal fluid upwelling.*

drive geothermal systems in the area. Salton Sea geothermal systems are among the largest in the USA. Thus, transtensional pull-aparts are a structural environment that, if found along the eastern Denali fault, would be a favourable environment to find geothermal reservoirs.

An alternate geologic analogue to consider for the eastern Denali fault is the Alpine fault on the South Island of New Zealand which is characterized by oblique transpression (*i.e.*, both strike-slip and thrust motion). In a drilling program on the Alpine fault, Townend *et al.* (2017) found extensive fracturing and forced circulation of meteoric water in the hanging wall, wide fault damage zones (Fig. 6), and measured subsurface temperatures of ~84°C at a depth of only 818 m. The elevated temperature gradient is attributed to rock advection during uplift and exhumation plus fluid advection due to deep groundwater circulation and upwelling (Townend *et al.*, 2017).

A structural environment similar to that described for the Alpine fault may be present in the eastern Denali fault zone. But it would likely be on a smaller scale, because the fracturing, fluid flow, and elevated temperatures observed at the Alpine fault are generated by Quaternary slip rates of 27 mm/year (horizontally) and 6–9 mm/year (vertically), which are ~10 times higher than the slip rates inferred for the eastern Denali fault.

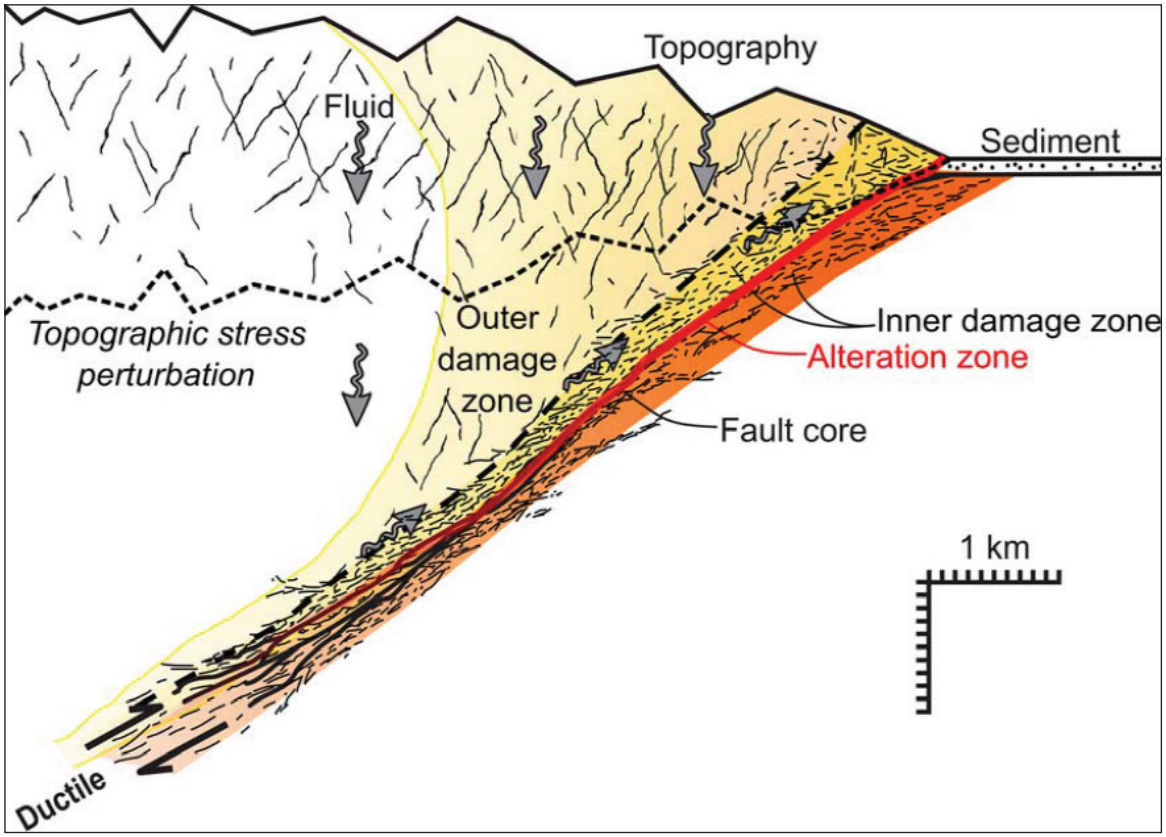

Figure 6. *Schematic cross section of the Alpine fault zone on the South Island of New Zealand (from Townend et al., 2017) which may be structurally analogous to the reverse-faulted portions of the eastern Denali fault zone. The inclined Alpine fault undergoes oblique transpression-type motion and accomplishes two goals germane to the formation of geothermal fluid reservoirs. First, ongoing fault motion brings hot rock material towards the surface (i.e. rock advection) to provide a continually replenishing heat source. Second, extensive fault damage zones, especially in the hanging wall of the fault, create enhanced permeability for deep circulation of meteoric water, heating, and geothermal fluid upwelling.*

Surficial and Bedrock Geology

Surficial geology in the Burwash Landing study area has been mapped by Kennedy (2013). In the lowlands, to the northeast of the Kluane Ranges, bedrock is covered by significant thicknesses of Quaternary-to-recent sedimentary deposits that consist of glacial till and outwash, as well as alluvium and loess. In the town of Burwash Landing, these sediments are at minimum ~390 m thick. Bedrock in the upland portion of the project area has been mapped by Israel *et al.* (2005). Major rock types exposed at the surface within the project area include the following, from youngest to oldest (Fig. 7):

1. Late Triassic to early Cretaceous Tatamagouche Formation which consists of argillite, sandstone, greywacke, conglomerate, and calcareous siltstone;
2. Late Triassic Nikolai Formation which consists dominantly of subaerially erupted basalt lavas;
3. Early Permian Hasen Creek Formation which is composed primarily of marine clastic sedimentary rocks, carbonates, chert, and conglomerates as well as fossiliferous siltstone, turbidites, mudstones, and sandstones (in the Duke River area); and
4. Pennsylvanian to Permian Station Creek Formation which is dominated by volcanic rocks such as breccia, tuff, and epiclastic rocks in addition to basaltic lava.

The Late Cretaceous-aged Kluane schist (Stanley, 2012) is inferred to underlie the surficial sedimentary deposits to the northeast of the Denali fault in the project area. A good summary of the regional geology and tectonic history of the project area can be found in Israel *et al.* (2005).

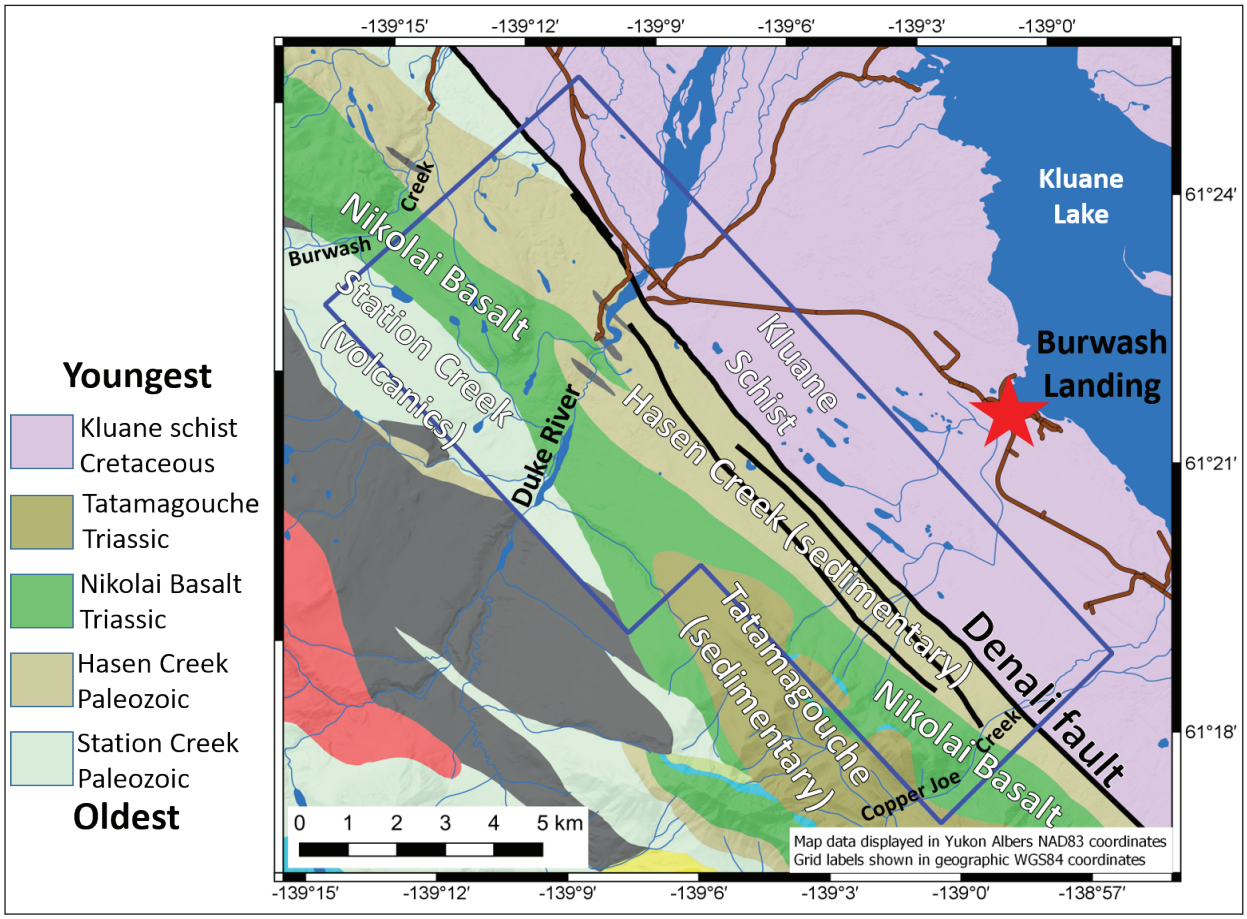

Figure 7. *Geologic map of the project area (blue polygon) and vicinity showing the distribution of bedrock. The surface trace of the Denali fault (black lines) are shown as well as roads (brown lines).*

Geothermal Exploration Summary and Strategy

What do we know?

Existing geoscientific information in the project area, outlined in the previous section, suggests:

a. An elevated average crustal thermal gradient of ~40°C/km is present along the eastern Denali fault zone, based upon Curie point depth mapping.

b. Geological evidence along the eastern Denali fault zone suggests deformation rates of ~2 mm/year (horizontally) and <1 mm/year (vertically) which are relatively modest compared to other crustal scale fault zones.

c. The overall tectonic regime along the eastern Denali fault is a transpressive environment which exhibits both right-lateral strike-slip as well as reverse fault motion.

d. One possible structural environment that would be favourable for geothermal fluid upwelling (if present) along the eastern Denali fault is a transtensional pull-apart within a right-step in the fault zone; indeed Miocene volcanism in the Wrangell volcanic field (immediately to the southwest of the project area) likely occurred due to such a structural environment.

e. Alternatively, the oblique transpressive tectonic environment of the eastern Denali fault may generate hanging wall fracture permeability as well as permeability in an along-fault damage zone which could facilitate deep meteoric fluid circulation, heating, and geothermal upwelling (analogous to the Alpine fault in New Zealand).

f. The multiple mapped (active?) strands of the eastern Denali fault that lie within the project area also suggest a rather wide (minimum 1 km) near-fault damage zone which could potentially create a significant volume of fractured, permeable rock in the subsurface.

g. Favourable rock types, present within the project area, that would tend to maintain open fractures and sustain subsurface permeability include igneous and crystalline metamorphic rocks, specifically, the Kluane schist, Nikolai basalt and the lavas of the Station Creek Formation. Lithological units containing clay-rich rocks (e.g., argillite, mudstone) such as the Hasen Creek and Tatamagouche formations are less likely to have the capacity to maintain open fractures required for permeability.

h. Structurally-controlled, producing geothermal fields are commonly associated with faults that have ruptured in the Quaternary. Thus, structures in the eastern Denali fault zone with Quaternary offset would be more likely to facilitate geothermal fluid flow than older structures.

What do we want to know?

In any geothermal exploration program, the two key requirements for a viable geothermal resource are elevated temperature and adequate rock permeability. Subsurface temperatures in the uppermost few kilometres of the Earth's crust can only be known accurately via downhole measurements in wells. At the present time, the absence of deep wells in the project area prevents us from knowing more about subsurface temperatures than what can be inferred from the Curie point depth map. The task at hand, then, is to attempt to identify where the fractured and permeable rocks exist in the subsurface. By doing so, we will infer where geothermal fluid upwelling might be possible. The exact type of permeability we are in search of is crustal scale fracture permeability that would promote deep (*i.e.*, several kilometres) meteoric water circulation that transports the heat at depth to the surface. The eastern Denali fault zone and/or associated faults may be the crustal scale geologic feature we are looking for that provides a fractured, deep

circulation pathway into the crust. To evaluate, there are a number of important questions to address:

a. For the eastern Denali fault zone, how wide is the system of faults that has ruptured in the Quaternary? In other words, how big is the fault damage zone? How many fault strands are there?
b. Is there a transtensional pull-apart structural environment associated with the eastern Denali fault zone within the project area? If so, where?
c. Is the hanging wall of the eastern Denali fault zone pervasively fractured and if so, does it allow deep infiltration of meteoric water (analogous to what happens at the Alpine fault)?
d. Is there a fault parallel damage zone along the margin of the eastern Denali fault plane (or associated fault planes) that provides a permeable pathway for upwelling geothermal fluids? If so, where exactly are the fault planes in the subsurface?
e. Exactly where in the subsurface are the rock types that are more prone to sustain open fractures, and what is their distribution?

In order to even begin to address such questions, a thorough understanding of the 3D geological and structural framework of the subsurface is required. Thus, a significant amount of the research effort in this study is aimed at building an initial 3D geoscience model of the lithology and faults within the project area. The overall goal is that the 3D geoscience model, generated for this project, serves as a guide for selecting drilling targets that would give direct measurements of subsurface temperature and permeability. The next two sections describe the data and methods used in our attempt to create an initial 3D geoscience model that is consistent with all of the various geoscience data sets available.

Data Used in this Project

A variety of geological and geophysical data sets were collected for this project so that they could be interpreted in conjunction with one another in an attempt to yield an internally consistent 3D geoscience model of the subsurface.

Existing Geoscience Data

Topography

High-resolution, land surface topographic data were used in this study to investigate surface geomorphological features associated with recent faulting and to provide a top surface for the 3D geoscience model. Public domain, 2 m spatial resolution Arctic DEM data (Porter *et al.*, 2018) available through the University of Minnesota were used for this purpose.

Geology

Surficial geology from Kennedy (2013) and bedrock geology from Israel *et al.* (2005) were used to help lay out the initial geologic framework and rock type distribution. Additional bedrock geology data from the Yukon Geological Survey (2018) was used for regions that lie to the northeast of the Israel *et al.* (2005) geologic map. Structural information from Israel *et al.* (2005) provided key information on the strike and dip of rock units to guide the construction of the initial 3D geologic model. The locations of the surface traces of the Bock's Creek fault and the eastern Denali fault were derived from Israel *et al.* (2005) and Bender and Haeussler (2017), respectively.

Airborne Magnetics

Public domain, high-resolution aeromagnetic survey data that covers the southwestern half of the project area were available for this study (Coyle and Oneschuk, 2015). The aeromagnetic survey was conducted by CGG via helicopter, mounted with a rigid stinger, in the spring of 2015. Survey lines oriented NE–SW were spaced 250 m apart with perpendicular tie lines spaced 1000 m apart. The nominal terrain clearance of the survey was 100 m and the magnetic survey data generated were subsequently gridded to a 60 m cell size. Additional, lower resolution aeromagnetic survey data were available that cover the rest of the project area. However, these data were not considered to be of high enough resolution to be beneficial for this study. The high-resolution magnetic survey data were useful for investigating structural relations in the subsurface and were used for 3D magnetic susceptibility inversion modelling to test the initial 3D geological model.

New Geoscience Data Acquired

Gravity

Twelve lines of ground-based gravity data, oriented NE–SW, were collected in the northern 2/3 of the project area in March 2019 by Aurora Geosciences. The gravity survey lines were oriented perpendicular to geologic structure. Line lengths varied from 5–7 km. Each line was spaced 1 km apart and gravity measurements taken along lines spaced 250 m apart. A total of 297 gravity measurements were obtained. Uncertainty in the gravity measurements was estimated at 0.05 mGal. The gravity survey data were useful for investigating structural relations in the subsurface and were also used in 3D density inversion modelling to test the 3D geological model. Details of the gravity data acquisition can be found in Appendix 3.

Extremely Low Frequency–Electromagnetics (ELF-EM)

For this study we used the ground-based ELF-EM method to investigate subsurface variations in electrical resistivity in the project area. Twelve lines of ELF-EM data, oriented NE–SW, were collected by Aurora Geosciences in the northern half of the project area in June 2019. Line lengths varied from 5–7 km. Each line was spaced 1 km apart with ELF-EM measurements spaced 250 m apart along the lines. A total of 329 ELF-EM measurements were obtained. Frequencies measured included: 11, 22, 45, 90, 180, 360, 720, and 1440 Hz. Average reading time at each station was 3 minutes. The Aurora Geosciences field personnel made every effort to co-locate the ELF-EM stations with the gravity stations collected earlier in the year. A greater number of ELF-EM stations were collected, compared to gravity stations, due to improved field conditions in June when the ELF-EM survey was undertaken; however, the footprint of the ELF-EM survey is the same as the gravity survey. Details of the ELF-EM data acquisition can be found in Appendix 4.

Geological Field Work and Rock Property Measurements

From July 23–27, 2019, new geological fieldwork was conducted in the project area. Participants in the fieldwork included: Jeff Witter (project lead; consultant), Tiffani Fraser (Yukon Geological Survey), and Liam Maw (student intern). Goals of the geological fieldwork were to:

a. compare actual rock types found in the field with rock units on the geologic map of Israel *et al.* (2005);
b. collect hand samples of the major rock units for rock property measurements (*e.g.*, density and magnetic susceptibility); and
c. observe major fault structures exposed in river valley walls.

In order to achieve these goals, foot traverses were conducted up three river valleys that lie within, or immediately adjacent to, the project area. The three river valleys are: Burwash Creek, Duke River, and Copper Joe Creek. Fifty-one rock samples were collected from all five of the major rock units shown in Figure 7. Magnetic susceptibility was measured on outcrop and hand samples in the field while density was measured on hand samples in the Yukon Geological Survey laboratory in Whitehorse.

InSAR Deformation Analysis

Interferometric Synthetic Aperture Radar (InSAR) is a satellite-based method which measures fine-scale ground deformation over large areas. As part of this project, the Yukon Geological Survey engaged TRE-Altamira to perform an analysis of InSAR data collected over the project area in an attempt to measure recent ground deformation associated with movement on either side of the Denali fault. InSAR data used in the analysis included 108 ascending and 116 descending images, collected by the Sentinel-1 satellite, covering the time period 2014–2019. Estimated deformation measurement precision is <1 mm/year. A description of the method can be found in Appendix 5.

Methodology

Map-based Interpretation

In an effort to better characterize the structural and geological framework within the project area, the following data sets were interpreted using a map-based approach: topography, gravity, magnetics, ELF-EM, geology, rock properties, and InSAR. All map-based interpretation was performed with the software QGIS (qgis.org).

A map-based interpretation of the high-resolution Arctic DEM data was key to help confirm the surface traces of known faults and to discern possible new fault traces. Both hillshade and slope visualization of the Arctic DEM 2 m resolution data were employed to interpret surface fault traces.

Various filters were applied to the gravity and magnetic survey data to aid map-based interpretation of the spatial extent of dense and magnetic rock units as well as the orientation of fault structures that lie under cover. These filters include: first vertical derivative, total horizontal gradient, tilt derivative, and analytic signal (magnetics only).

Map-based interpretation of ELF-EM data was performed on in-phase divergence plots that covered the frequency range 22–720 Hz. These plots were used as part of the structural interpretation.

The gravity, magnetic, and ELF-EM geophysical data were interpreted in map view in conjunction with the mapped geology (e.g., Israel *et al.*, 2005) and rock properties to better understand structures and lithologic contacts in the project area.

2D Geophysical Inversion Modelling

2D geophysical inversion modelling was performed by Aurora Geosciences on the ELF-EM data to generate 12 electrical resistivity profiles along the ELF-EM survey lines. The REBOCC inversion code (Siripunvaraporn and Egbert, 2000) was used to perform the 2D inversions. Two channels of data (11 Hz and 1440 Hz) were too noisy and not included in the inversion modelling. Near the surface, 2D inversion model cells were 125 m horizontally and 20 m vertically. Cell thickness increased to 50 m at 600 m depth and then 100 m at 1 km depth. The topography was assumed to be flat for the purposes of the 2D inversion modelling; resistivity model results were adjusted after-the-fact to conform to topography. Reference model resistivity values of 10, 100, and 1000 ohm-m were tried at the outset of the 2D inversion modelling effort with a 10 ohm-m half space returning reliable 2D inversion results for most of the lines. However, for 5 out of 12 of the lines, the 10 ohm-m reference model gave unsatisfactory results. For these lines, the inversion model result from an adjacent line was used as a reference model to achieve satisfactory results. Additional details of the 2D inversion of the ELF-EM data can be found in Appendix 4.

3D Geological and Geophysical Modelling

3D Geologic Modelling

An initial 3D geologic model was constructed for the project area to aid in interpretation and to serve as a constraint for 3D gravity and magnetic inversion modelling. Rhinoceros software (www.rhino3d.com) was used to build the 3D geologic model as surfaces that represent geologic horizons and faults. The 3D geologic model was built to honour the bedrock geology map of Israel *et al.* (2005), Denali fault traces of Bender and Haeussler (2017), and surficial geology map of Kennedy (2013). The 3D geologic model was extended to depth by using geologic cross section C-D from Israel *et al.* (2005) as a guide. This cross section lies near the southern end of the project area. The rock unit thicknesses and geologic structures (*i.e.*, folds/faults) from this cross section were projected towards the northwest (along strike) through the project area, while at the same time honouring the surface geology. The thickness variations of the Quaternary sediment cover in the project area were inferred from the 2D ELF-EM inversion profiles.

3D Inversion Modelling of Gravity Data

3D geophysical inversion modelling of gravity data was performed as part of the effort to better understand the 3D geologic framework of the project area. Gravity data are sensitive to changes in subsurface rock density and rock density can be used as a proxy for rock type, provided sufficient density contrasts between rock units are present. The 3D inversion modelling of gravity data pursued here was guided by both the 3D geological model described above as well as representative rock density measurements to yield a geologically reasonable result. The inversion algorithm employed for the modelling is the open source SimPEG code (Cockett *et al.*, 2015). We used both rock property and geologically-constrained inversion strategies as described by Fullagar and Pears (2007) and Fullagar *et al.* (2008). In addition, we use spatially variable mixed Lp norms for the model regularization as described in Fournier and Oldenburg (2019). The 3D gravity model volume was 3 km thick and we assumed a background density value of 2.75 g/cm^3. The 3D model mesh consists of 100 m cells in the X and Y directions with model cell thicknesses of 25 m (from 0–1500 m depth), 50 m (from 1500–2500 m depth), and 100 m (from 2500–3000 m depth). Two kilometres of padding cells were added to the model volume on the sides and bottom to minimize edge effects. The topographic surface of the 3D geophysical model volume was created from a 10 m resolution DEM derived from the Arctic DEM data set. A total of 297 gravity data points, with an average measurement error of 0.05 mGal, were used in the inversion modelling. The gravity data consisted of Complete Bouguer Anomaly gravity values with a terrain correction density of 2.75 g/cm^3. The gravity data were upward continued by 50 m prior to inversion modelling to minimize near surface effects and model artifacts.

3D Inversion Modelling of Magnetic Data

Magnetic data are sensitive to variations in the magnetic susceptibility of rocks in the subsurface, such as mafic and ultramafic rocks, both of which have been mapped in the project area. Due to the presence of the strongly magnetic Nikolai basalt rock unit in the project area, 3D geophysical inversion modelling of magnetic data was also performed to help better define the 3D distribution of the Nikolai basalt and other magnetic rock units. Similar to the gravity modelling, described above, the 3D inversion modelling of magnetic data was guided by both the 3D geological model described above as well as representative rock sample measurements of magnetic susceptibility to help ensure that the inversion model result is geologically reasonable. The magnetic inversion modelling also used the open source SimPEG code (Cockett *et al.*, 2015) and spatially variable mixed Lp norms for the regularization (Fournier and Oldenburg, 2019). The 3D model mesh and padding are the same for the magnetic modelling as for the gravity modelling. Similarly, the thickness of the 3D magnetic model is 3 km. A total of 12,831 magnetic survey data points were used in the inversion modelling. Magnetic field parameters used for the inversion modelling include declination (20.2°), inclination (76.05°), and total field strength (56,694 nT). Lastly, for simplicity, we assume that remanent magnetization of rocks is not present in the project area.

Results

Map-based Interpretation

Topographic data

The aim of the interpretation of the high resolution Arctic DEM topography data was two-fold: a) to confirm the surface features that demarcate the three surface traces of the eastern Denali fault as mapped by Bender and Haeussler (2017) and b) to look in detail at other parts of the project area in an attempt to identify other surface features which may indicate fault structures. Following the example of others (e.g., Bender and Haeussler, 2017; Blais-Stevens *et al.*, 2020) we re-mapped linear sediment mounds and other surface features that mark the previously recognized surface trace of the eastern Denali fault. Re-interpretation of the eastern Denali fault using Arctic DEM data largely confirmed the three strands identified in previous studies (Fig. 8). Crosscutting relationships of surficial glacial features observed in the Arctic DEM data suggest that two of the strands of the eastern Denali fault may merge rather than remain parallel (point M in Fig. 8).

In other parts of the project area, we used the Arctic DEM to map subtle linear surface features, such as sudden changes in slope, that may mark additional fault structures. A series of NW-trending structures were identified that lie to the SW of the eastern Denali fault strands. These inferred structures were connected with fault zones that were observed in Burwash Creek, Duke River, and Copper Joe Creek during geological fieldwork in summer 2019 (Fig. 8). In addition, on the flanks of the Duke River valley, slope changes have been inferred to represent NE-trending normal faults. Lastly, linear strings of mounds or other metre-scale surface features were not observed in the Arctic DEM data along the Bock's Creek fault or other faults mapped by Israel *et al.* (2005) within the project area which may suggest little to no Quaternary offset on these structures.

Magnetic survey data

The aeromagnetic survey data from 2015 covers only the southwestern half of the project area (Figs. 9 and 10). Within the project area, the Total Magnetic Intensity (TMI) data with an IGRF-correction and Reduction to Pole (RTP) applied have an overall range from -1300 nT to +1800 nT; but, the majority of the data lie in the range -900 to +100 nT.

Magnetic anomalies are generally elongate in a NW–SE direction, parallel to geologic strike. Compared to bedrock geologic mapping (Fig. 7), magnetic highs generally correspond to areas mapped as Nikolai basalt and the lowest magnetic anomalies correspond to areas mapped as Tatamagouche Formation (*i.e.*, sedimentary rocks). An exception to this association is a strongly magnetic, lozenge-shaped anomaly which lies in the centre of the project area on the margin of the high-resolution magnetic survey data (Fig. 9). The size, shape, and rock type of the body causing this magnetic anomaly is not known.

The available high-resolution magnetic survey data lie largely to the SW of the main strands of the eastern Denali fault mapped by Bender and Haeussler (2017) which precludes a detailed analysis of magnetic anomalies on both sides of these active fault structures. However, regional magnetic data show that anomalies on the NE side of the Denali fault are broad, featureless, and weak. The Bock's Creek fault appears to separate strongly magnetic rocks to the NE (Nikolai basalt) from moderately magnetic rocks to the SW (Station Creek Formation) consistent with the mapping of Israel *et al.* (2005). The large body of very strongly magnetic rocks that lies

outside and to the SW of the project area consists of peridotite, dunite, and gabbro of the Kluane ultramafic suite.

A more detailed look at the magnetic survey data using the tilt derivative (Fig. 10) accentuates the NW-SE trending magnetic features. The tilt derivative map also reveals a N–S trending right-step in the otherwise NW-oriented magnetic trends. The right-step is located on the eastern shore of the Duke River, in an area mapped as Nikolai basalt and it is bounded by one of the NE-trending normal faults inferred from the Arctic DEM data. Apart from this single example, there appears to be only weak correlation between the specific faults inferred in this study and the boundaries of the observed magnetic anomalies.

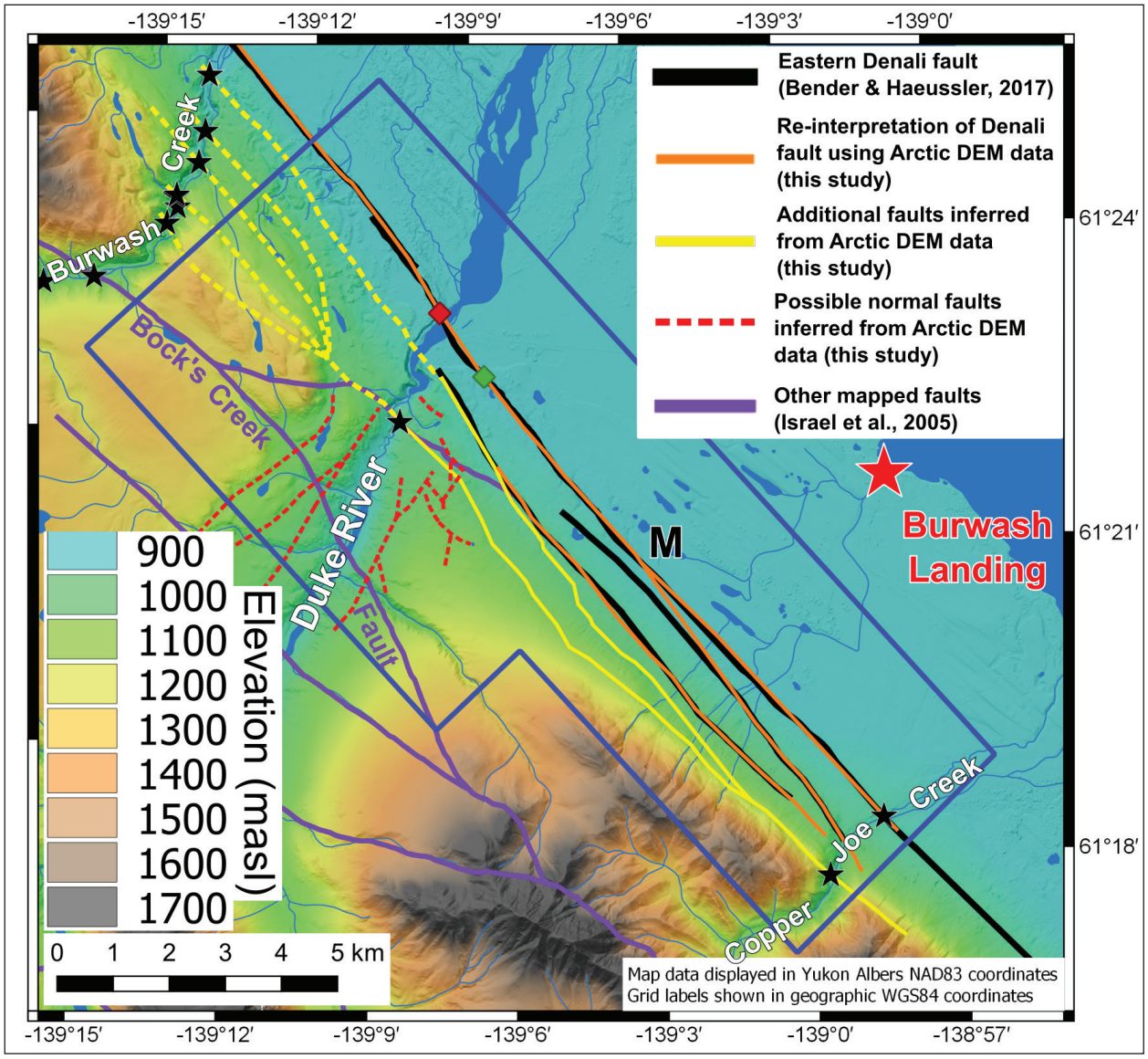

Figure 8. *Map showing fault structures interpreted from Arctic DEM topographic data. The three strands of the eastern Denali fault mapped by Bender and Haeussler (2017), shown as black lines, match well with those interpreted from Arctic DEM data for this study (orange lines). Red and green diamonds represent a river bluff exposure of the eastern Denali fault and a trench dug across the eastern Denali fault, respectively (Blais-Stevens et al., 2020). Black stars represent major fault structures observed in the field in river valley walls. Additional, NW-trending fault structures were also interpreted (yellow lines; dashed where less certain) from Arctic DEM data. NE-trending features are also interpreted on the flanks of the Duke River valley (red dashed lines) which may represent normal faults. Topography with hillshade forms the coloured background. Project area boundary is the blue polygon. See text for further explanation.*

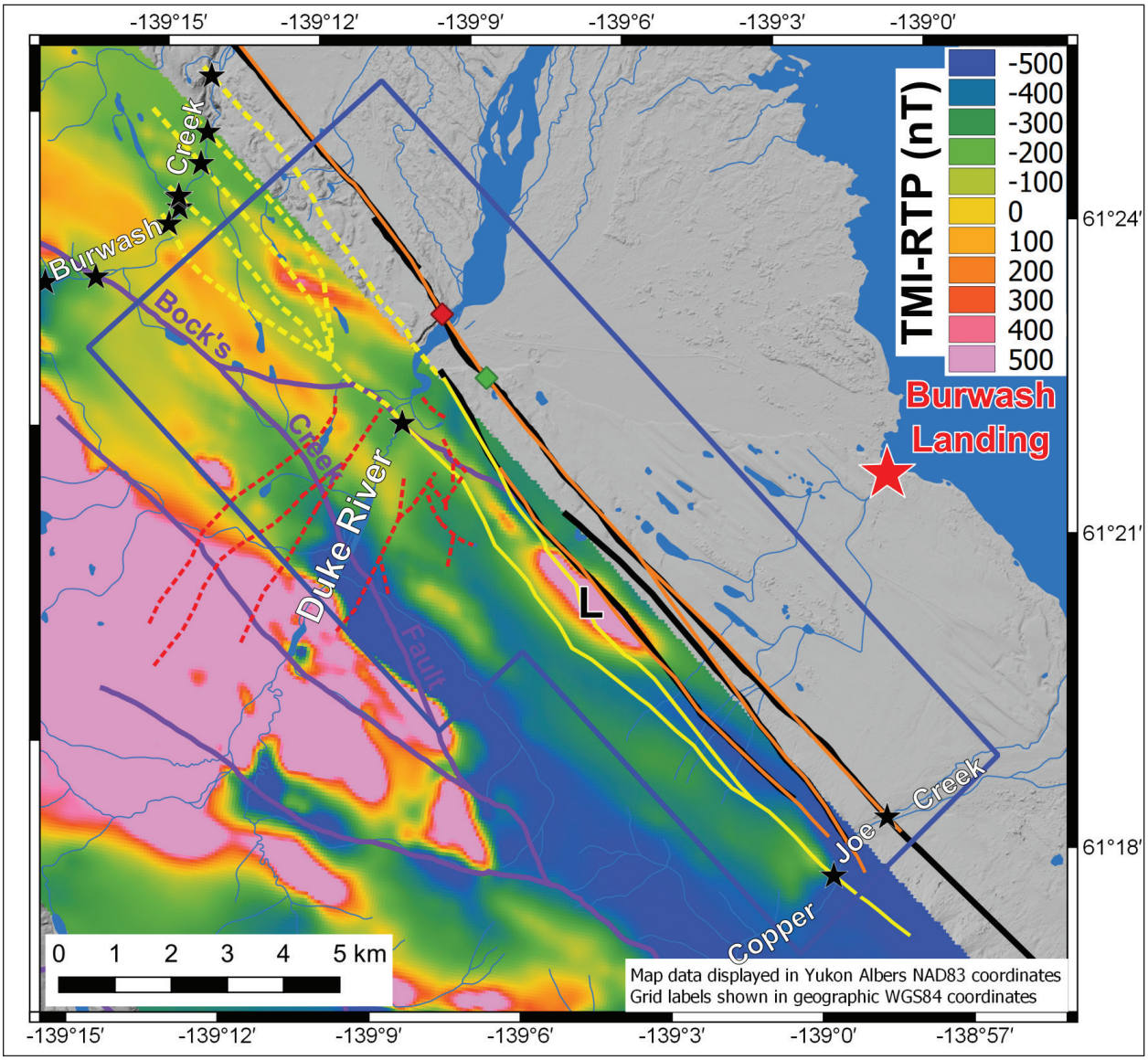

Figure 9. *High resolution aeromagnetic survey data from 2015 covers the SW half of the project area gridded with a 60 m cell size. Total Magnetic Intensity with Reduction to Pole applied (TMI-RTP) is shown here. Fault annotation and other symbols are the same as in Figure 8. Grey background is hillshade topography in the area with no high-resolution magnetic data. Project area boundary is the blue polygon. The "L" marks the location of the lozenge-shaped magnetic high anomaly referred to in the text.*

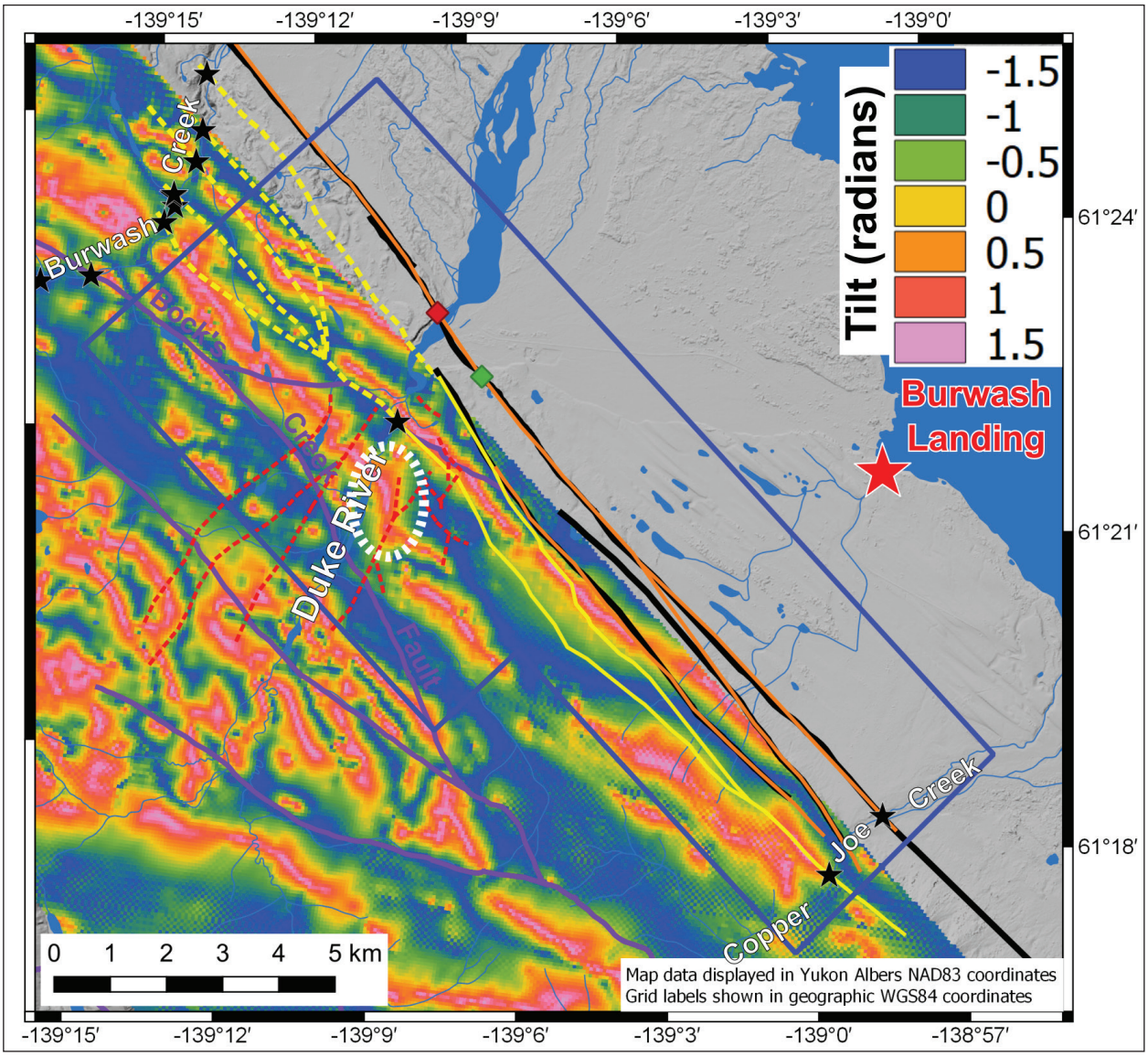

Figure 10. *High resolution aeromagnetic survey data from 2015 with the tilt derivative applied to enhance the magnetic features. Fault annotation and other symbols are the same as in Figure 8. Grey background is hillshade topography in the area with no high-resolution magnetic data. Project area boundary is the blue polygon. White stippled oval marks a right-step in the NW-trending magnetic high anomalies.*

Gravity data

Residual Complete Bouguer Anomaly (CBA) gravity data collected for this study, with a terrain correction density of 2.75 g/cm^3, has a range from -17 to +15 mGal (Fig. 11). The residual values were calculated by subtracting the average CBA value from all gravity data points (*i.e.*, the regional gravity signal is assumed to be flat). The gravity response within the project area consists of gravity lows in the lowlands to the NE progressing to gravity highs in the uplands to the SW. The NW strike of the gravity signal parallels the surface trace of the eastern Denali fault and the Kluane mountain range. On the central-SW side of the project area, a weak relative gravity low lies in the Duke River valley and follows a portion of the Bock's Creek fault. This gravity low observed in the Duke River valley corresponds to the zone of normal faulting inferred from

the Arctic DEM data. A total horizontal gradient (THG) filter was applied to the gravity data to highlight the zone of greatest horizontal change in the gravity (Fig. 12). THG maps are commonly used in gravity interpretation to infer fault contacts since THG high anomalies represent zones of strong density contrast. The THG map generated for the project area reveals a sub-linear high in the horizontal gradient that parallels the surface trace of the eastern Denali fault. Furthermore, in the central part of the project area, just east of the Duke River, a small-scale, right-step is observed in the horizontal gradient of the gravity. This right-step is located ~1.5 km NE of a similar right-step observed in the magnetic data.

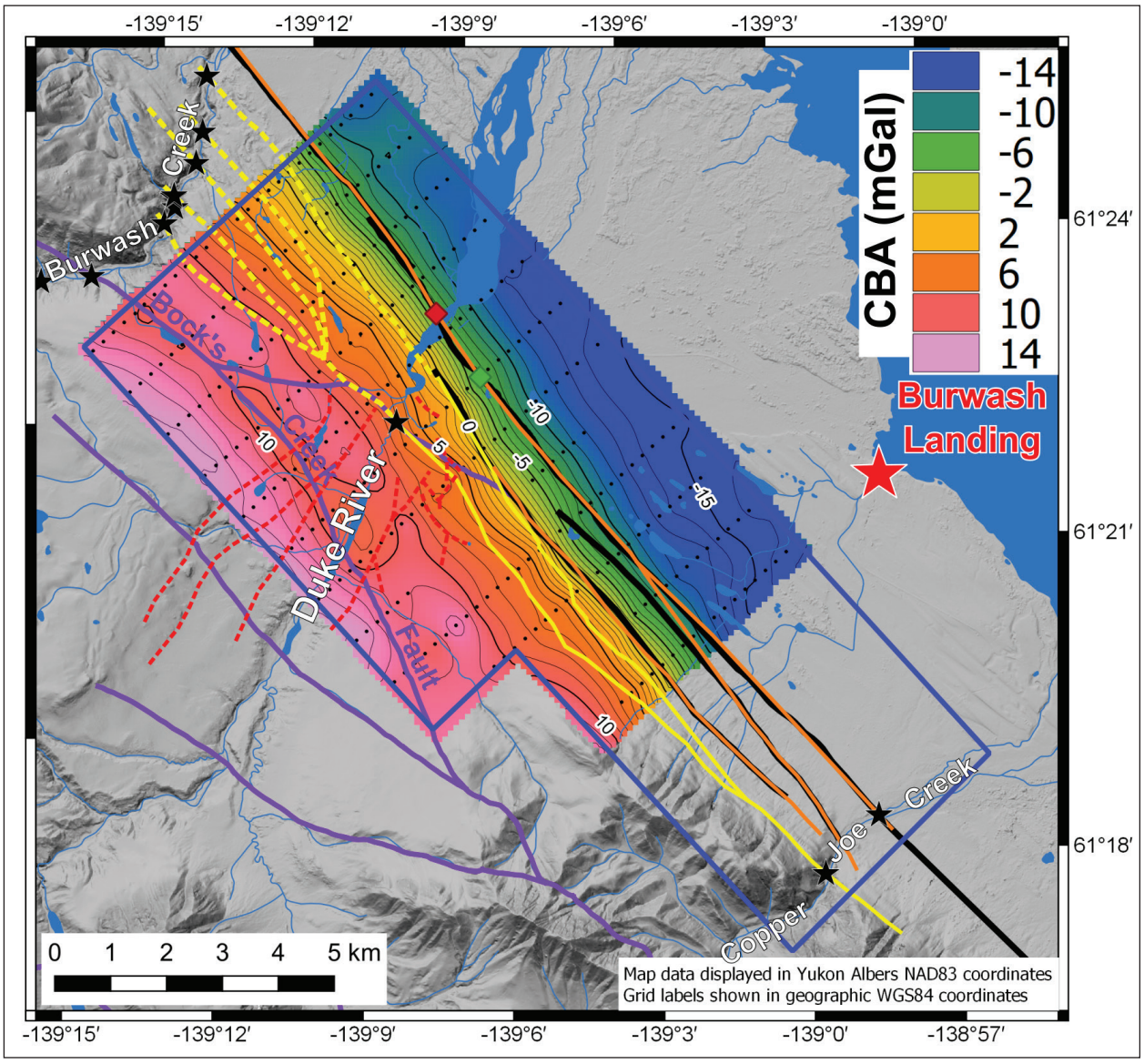

Figure 11. *Complete Bouguer Anomaly (CBA) gravity data gridded with a 100 m cell size. Black dots represent gravity survey stations. Gravity contour lines are shown at 5 mGal (black lines) and 1 mGal (thin gray lines) intervals. Fault annotation and other symbols are the same as in Figure 8. Grey background is hillshade topography in the area with no gravity data. Project area boundary is the blue polygon. See text for further explanation.*

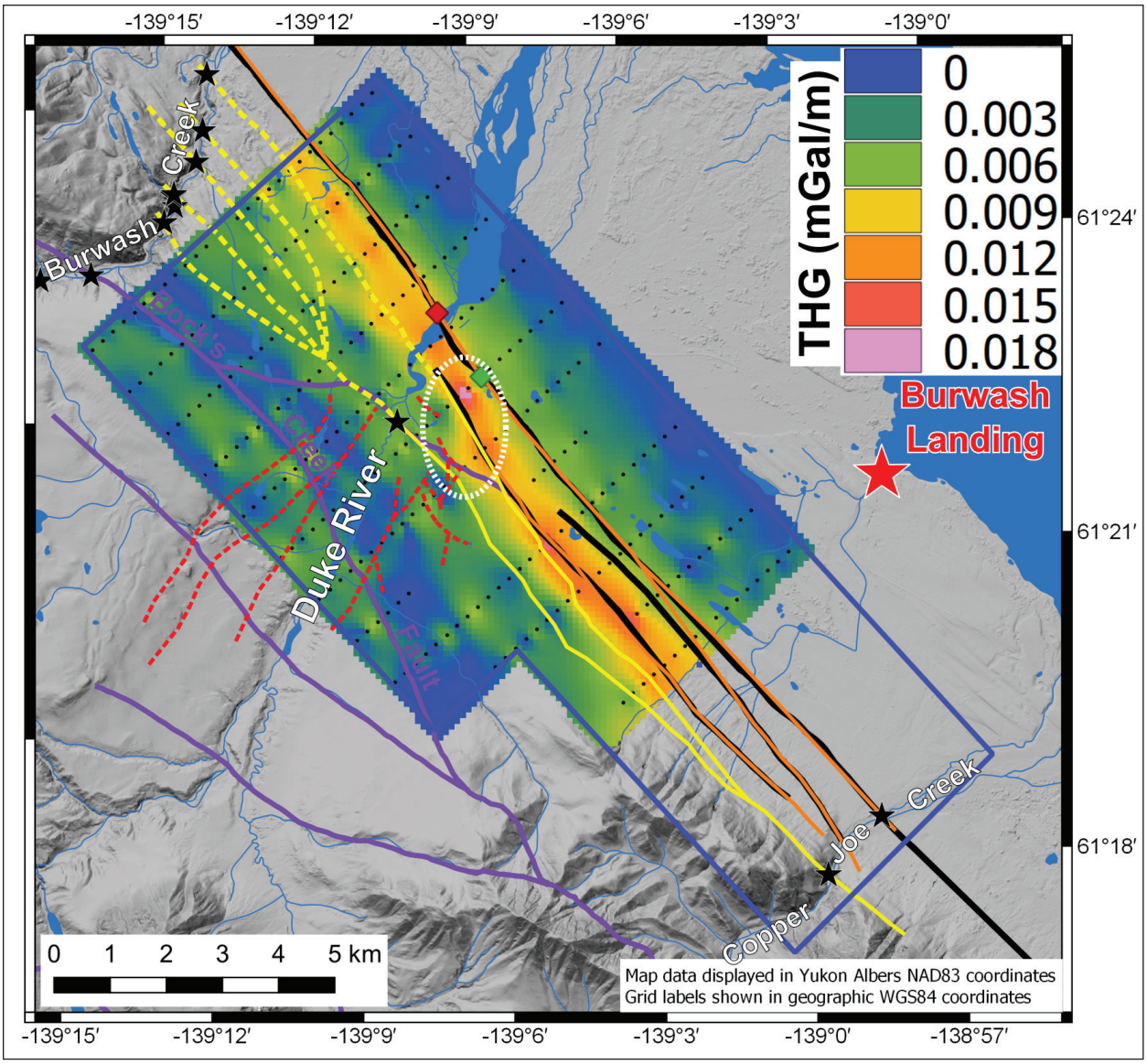

Figure 12. *Gravity survey data with the total horizontal gradient (THG) filter applied. Black dots represent gravity survey stations. Fault annotation and other symbols are the same as in Figure 8. Grey background is hillshade topography in the area with no gravity data. Project area boundary is the blue polygon. White stippled oval marks a right-step in the NW-trending THG high anomaly.*

ELF-EM data

Part of the ELF-EM deliverables provided by Aurora Geosciences included in-phase divergence maps calculated at different ELF-EM survey measurement frequencies. In-phase divergence maps reflect subsurface resistivity variations at different depths with higher/lower frequencies related to shallower/deeper depths, respectively. Figure 13 shows an in-phase divergence map at 360 Hz (relatively shallow depth). Zones of high in-phase divergence correlate well with both the surface trace of the eastern Denali fault as well as the mapped Bock's Creek fault. From this spatial association, we infer that high in-phase divergence represents zones of subsurface faulting. A third zone of high in-phase divergence is observed to lie between the Bock's Creek and eastern Denali faults (Fig. 13). This third, central zone also exhibits a N-S trending right-step on the east side of the Duke River, in the same general area as the right-steps observed in the gravity and magnetic interpretations.

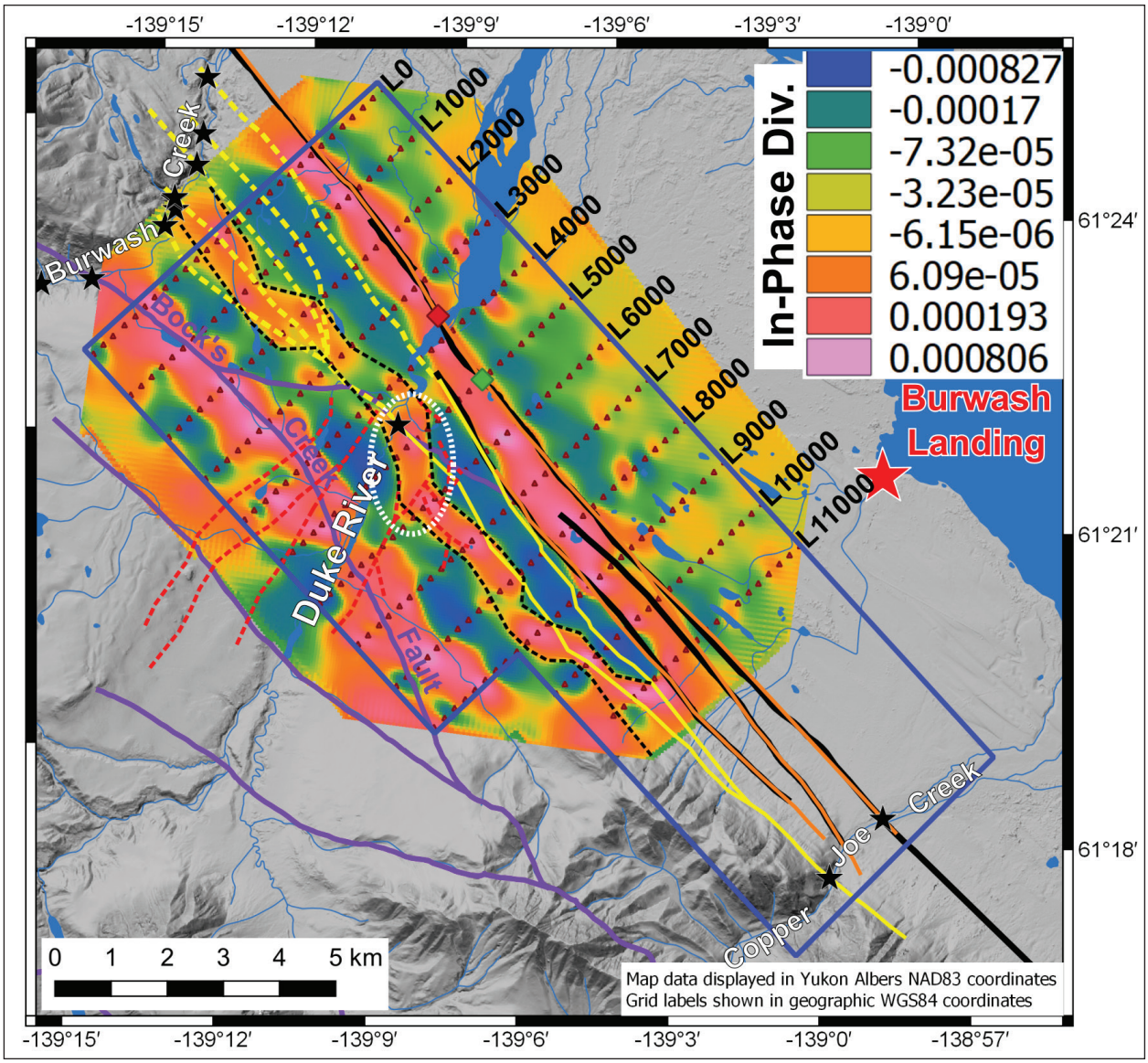

***Figure 13**. In-phase divergence plot at 360 Hz generated from the ELF-EM survey data. Red triangles represent ELF-EM survey stations. Black labels are ELF-EM survey line numbers. Black dotted lines mark the central zone of high in-phase divergence. White stippled oval marks a right-step in this central high anomaly. Fault annotation and other symbols are the same as in Figure 8. Grey background is hillshade topography in the area with no ELF-EM survey data. Project area boundary is the blue polygon.*

Rock property data

As part of this project, 51 rock samples were collected for rock property measurements including density and magnetic susceptibility (Appendix 2). These samples were collected from outcrops in the Burwash Creek, Duke River, and Copper Joe Creek valleys (Fig. 14) and represent the five major rock types present within the project area (see Fig. 7). These new data were merged with an additional 53 sets of rock property measurements available from the YGS archive. The YGS archival samples were previously collected in southwestern Yukon and also represent the five major rock units present in the project area.

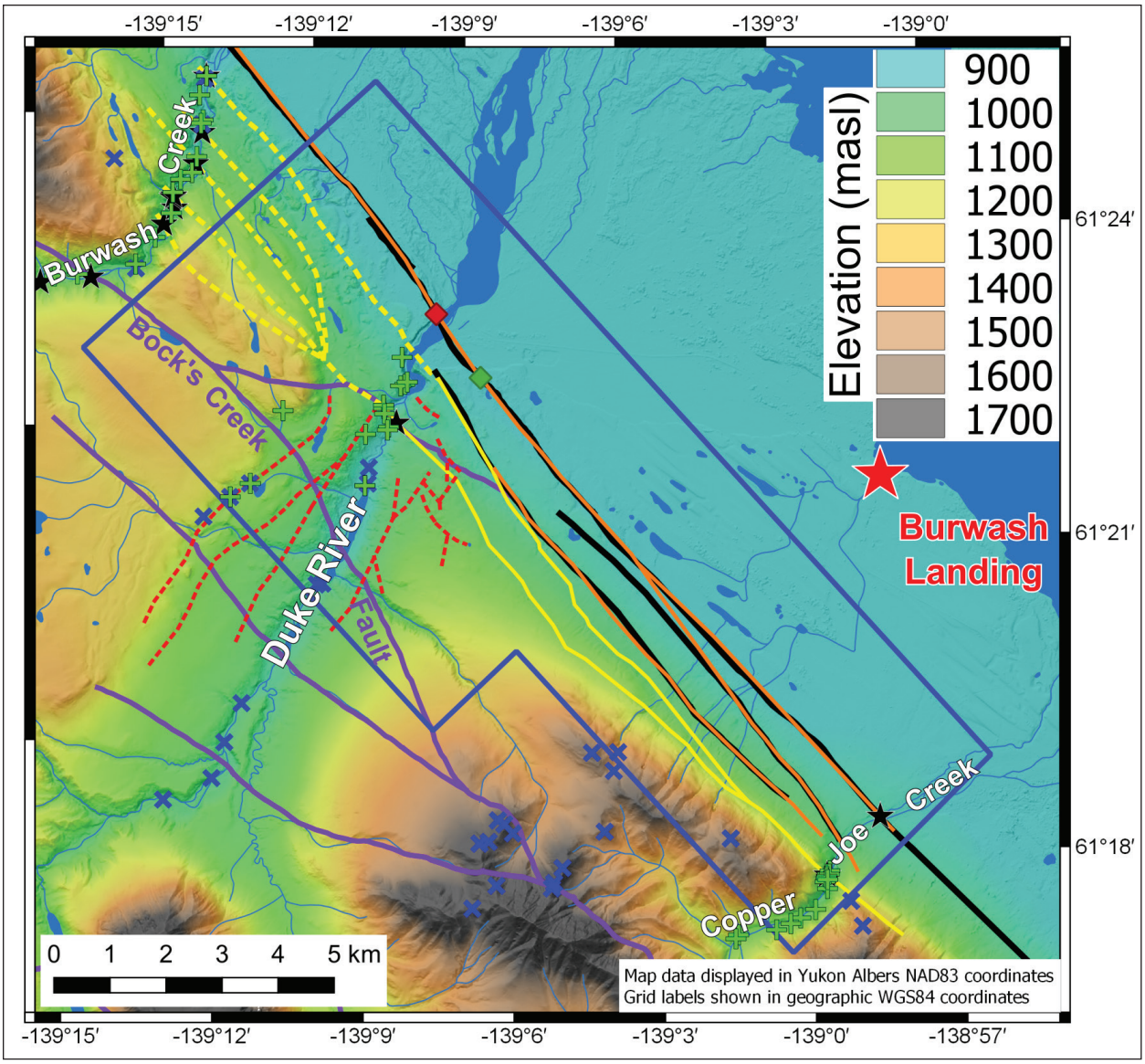

Figure 14. *Map of the project area showing locations of rock samples collected for rock property measurements (i.e., density and magnetic susceptibility). Green crosses represent rock samples collected in this study; blue X's represent rock samples from the YGS archive for which rock property measurements were already available. Topography with hillshade forms the coloured background. Fault annotation and other symbols are the same as in Figure 8.*

The rock property data were categorized according to the major rock unit to which they belong and were graphed as box and whisker plots for better visualization of their distribution (Fig. 15). Simple statistics (*i.e.*, maximum, minimum, mean and 1σ standard deviation) were calculated to assess the variation in the results (Table 1). The average rock property values shown in Table 1 are assumed to be representative of each rock unit and, therefore, were used as starting and reference values in the 3D geophysical inversion modelling.

Overall, the magnetic susceptibility values of all but one of the major rock units have a similar, low value (~0.3×10^{-3} SI). In essence, the Kluane schist, Station Creek, Hasen Creek and Tatamagouche formations are magnetically indistinguishable from one another. The exception is the Nikolai basalt unit which has a highly variable, but much higher average magnetic susceptibility (~10×10^{-3} SI).

The rock density data reveals that the Kluane schist, Hasen Creek and Tatamagouche formations have the lowest average density (2.70–2.73 g/cm^3) and are essentially indistinguishable from one another with respect to density. The Station Creek Formation has a higher average density (2.83 g/cm^3) yet this unit has enough density variability that it overlaps substantially with other rock units. The Nikolai basalt has the highest average density (2.92 g/cm^3) of all the rock units in the project area.

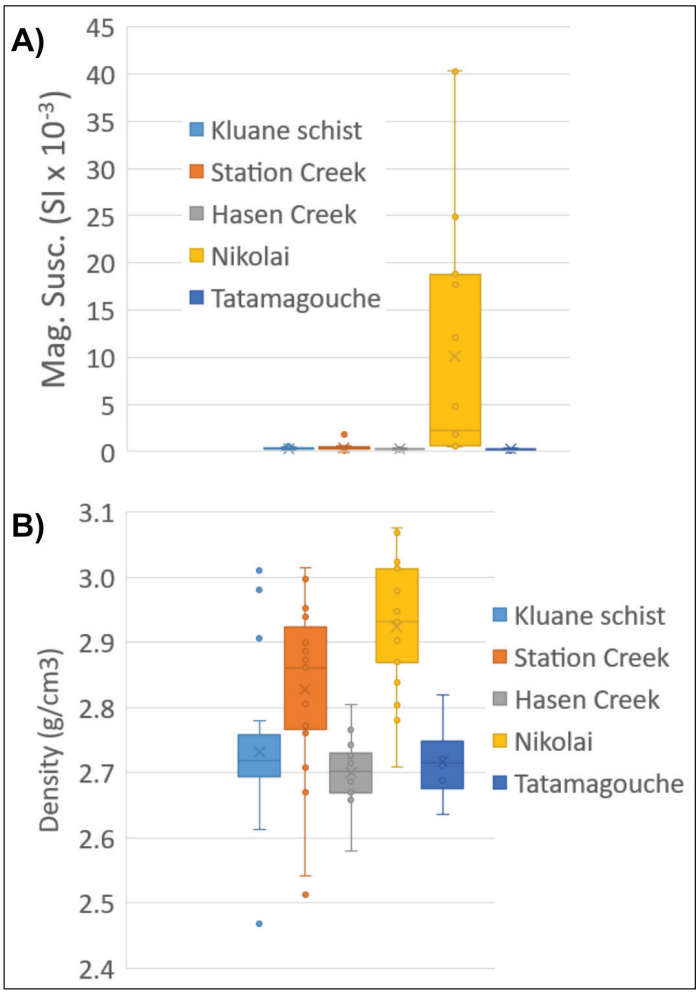

Figure 15. *Box and whisker plots of* ***A)*** *magnetic susceptibility and* ***B)*** *density, categorized according to the five major rock types found in the project area. Mag. Susc. = magnetic susceptibility.*

Table 1. *Simple statistics of data categorized according to rock type. n = number of measurements.*

A) Magnetic susceptibilty

Rock unit	Minimum (SI x 10^{-3})	Maximum (SI x 10^{-3})	Average (SI x 10^{-3})	1σ Std. Dev. (SI x 10^{-3})	n
Kluane schist	0.20	0.52	0.31	0.08	33
Station Creek	0.07	1.86	0.45	0.39	18
Hasen Creek	0.19	0.34	0.28	0.05	14
Nikolai	0.55	40.30	10.10	13.24	19
Tatamagouche	0.16	0.35	0.24	0.08	6

B) Density data

Rock unit	Minimum g/cm^3	Maximum g/cm^3	Average g/cm^3	1σ Std. Dev. g/cm^3	n
Kluane schist	2..47	3.01	2.73	0.10	33
Station Creek	2.51	3.02	2.83	0.13	21
Hasen Creek	2.58	2.80	2.70	0.05	14
Nikolai	2.71	3.07	2.92	0.10	19
Tatamagouche	2.64	2.82	2.72	0.06	6

InSAR analysis

The goal of the InSAR analysis in this study was to measure tectonic movements associated with the eastern Denali fault (or other faults) within the project area. If tectonic movement could be detected, this would help identify areas more likely to have undergone fracturing that might suggest subsurface permeability. At the project area, InSAR data were analysed over a 5-year period (2014–2019) and significant ground deformation was detected. However, strong evidence for tectonic motion is not apparent in the InSAR data. Instead, the ground deformation measured by InSAR appears to be more near-surface in origin and associated with freeze/thaw processes acting on permafrost.

The InSAR data available for this study included images collected by both ascending and descending Sentinal-1 satellites. This method of data collection enabled the InSAR ground deformation measurements to be decomposed into east-west and vertical components. The eastern Denali fault is a NW-trending, right-lateral, strike-slip fault and so, considering the east-west component of movement, we would expect the rocks on the east side of the fault to move east and the rocks on the west side of the fault to move west. Such deformation patterns, however, are not observed in the InSAR data (Fig. 16). Instead, east-directed deformation appears to coincide with slopes that have an east-facing component to them and, similarly, west-directed deformation is associated with west-facing slopes.

The vertical deformation measurements made by InSAR show subsidence occurring over most of the project area (Fig. 17). Areas of uplift observed in the InSAR data coincide mostly with the stream beds of Burwash Creek and Duke River. Work by other researchers show evidence for uplift of the Kluane range (e.g., McDermott *et al.*, 2019) which is not apparent in the InSAR data.

A plausible explanation for the InSAR measurements is that near-surface deformation is caused by long-term melting of permafrost as the Arctic landscape warms. For example, widespread subsidence of the land surface is consistent with year-on-year melting of permafrost. The observed “uplift” in the river valleys may simply be a reflection of sediment accumulation in the stream bed over time. Similarly, a plausible explanation for the observed east–west deformation patterns recorded by InSAR is downslope creep processes associated with long-term warming and melting of permafrost. This would explain the observed correlation between east-west deformation direction and slope aspect.

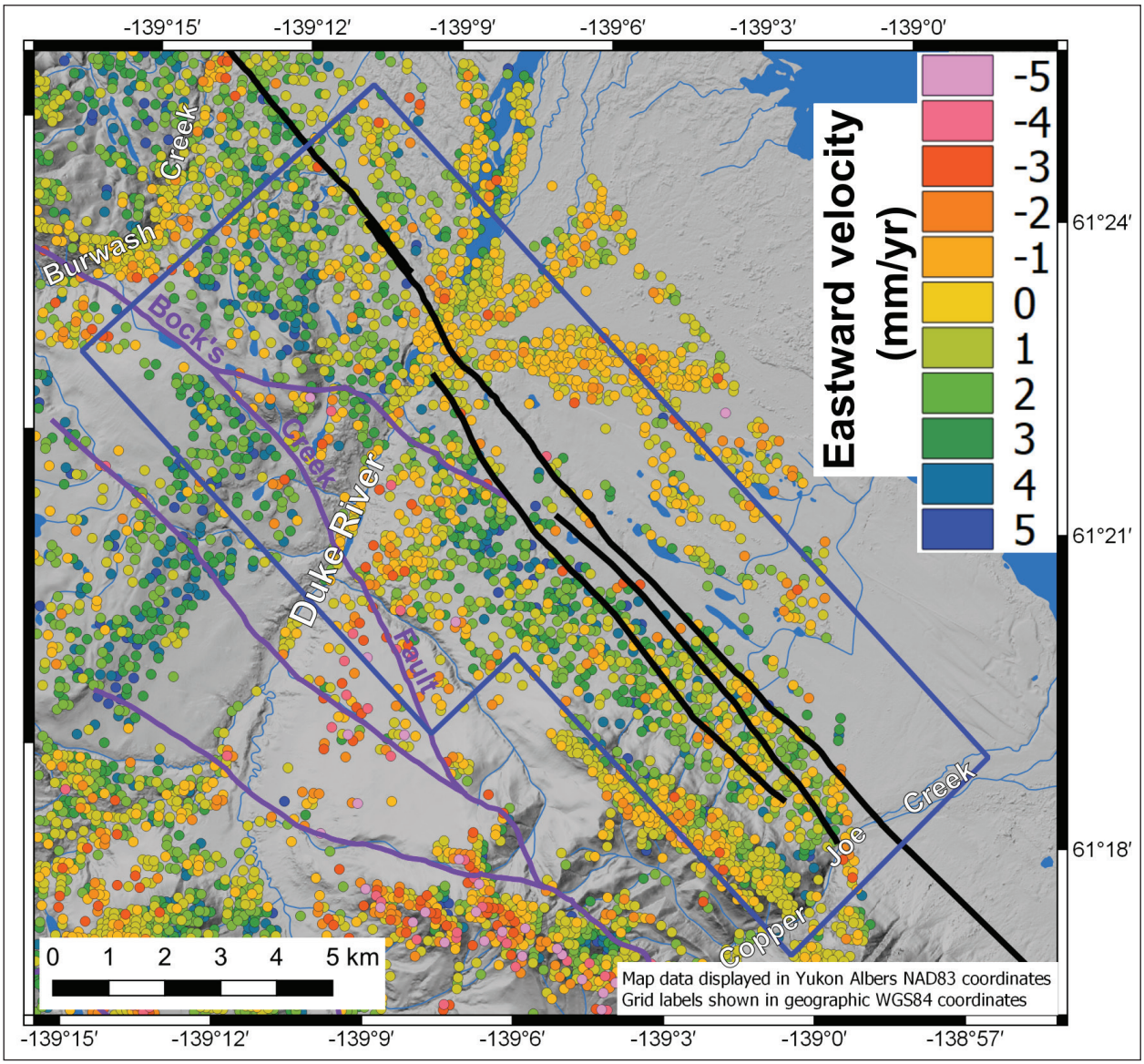

Figure 16. *Map view of InSAR deformation results showing east–west velocity in mm/year. InSAR data points (dots) show eastward movement (positive values; blue-green) mainly on east-facing slopes. In some areas, westward movement (negative values; orange-red-pink) are found on west-facing slopes. Flat areas show no east-west movement (yellow). Grey background is land surface topography with hillshade.*

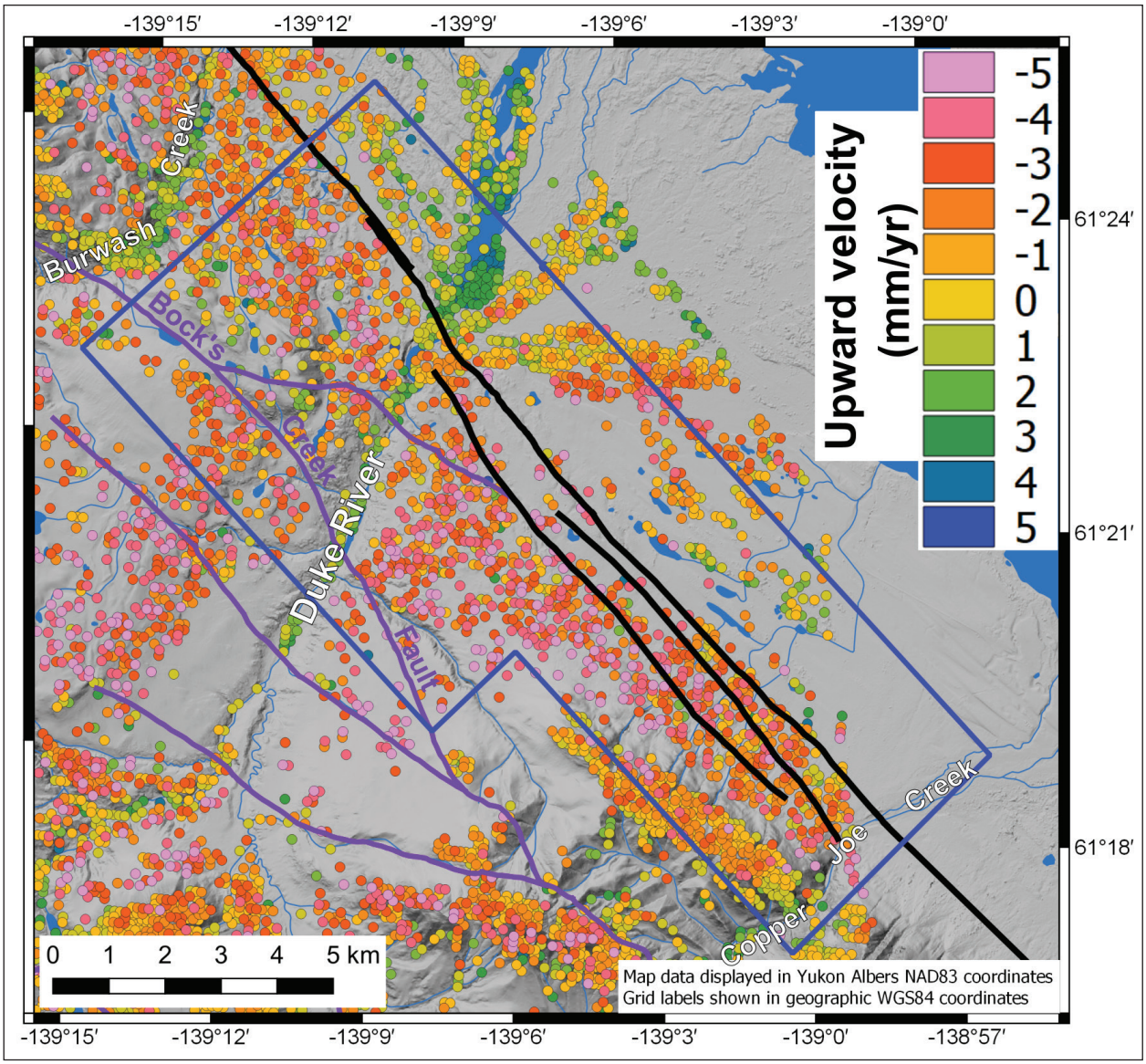

Figure 17. *Map view of InSAR deformation results showing vertical velocity in mm/year. InSAR data points (dots) show upward movement (positive values; green) mainly in Burwash Creek and the Duke River valley. Downward movement, or subsidence (negative values; orange-red-pink) are found across most of the study area. Grey background is land surface topography with hillshade.*

2D Resistivity Model Interpretation

Twelve 2D resistivity profiles, oriented NE-SW and spaced 1 km apart were generated by Aurora Geosciences through inversion modelling of the ELF-EM data that were collected for this study. The electrical resistivity values returned in the 2D resistivity models span the range 5–3000 ohm-m and reach depths up to ~1.5 km below ground surface. Two example resistivity profiles are shown in Figures 18 and 19.

The ELF-EM profiles clearly demarcate one stratigraphic layer in the project area: Quaternary sediments. In each profile, we observe an electrically resistive surface layer (500–3000 ohm-m and <500 m thick) present in the northeastern portion of the project area, in the lowlands east of the Kluane range front. This resistive layer is interpreted, geologically, as freshwater-bearing glacial and alluvial sediments sitting on top of more conductive bedrock. The layer is laterally continuous from profile-to-profile and has been stitched together in three dimensions in order

to help construct the distribution of Quaternary sediments in the 3D geologic model. The spatial distribution of resistive Quaternary sediments inferred from the 2D ELF-EM profiles is also consistent with surficial geology mapping by Kennedy (2013). Apart from Quaternary sediments, no other stratigraphic layers have been inferred from the ELF-EM profiles.

Electrical resistivity values in the bedrock are variable across the project area (Figs. 18 and 19). In a 2–3 km wide zone that straddles the surface traces of the eastern Denali fault, bedrock resistivity values are low (5–60 ohm-m). We infer that these low bedrock resistivity values in the vicinity of the fault zone may represent either: a) zones of fractured rock infiltrated by electrically conductive fluids; b) fractured and altered bedrock which contains conductive minerals such as clays; or c) graphite-bearing bedrock. The bedrock geology in this area has been inferred to be Kluane schist to the east and Hasen Creek Formation to the west of the Denali fault (Yukon Geological Survey (2018); however, the bedrock in this area is hidden by the overlying sediments. Stanley (2012) reports that both subtypes of Kluane schist (muscovite-rich and biotite-rich) contain abundant fine-grained graphite, which is an electrically-conductive (*i.e.*, low resistivity) mineral. Thus, the low resistivity bedrock revealed in the ELF-EM profiles in the vicinity of the eastern Denali fault would be consistent with graphite-bearing Kluane schist. However, the bedrock resistivity variations revealed by the ELF-EM profiles suggest a more complicated story.

There is no evidence in the ELF-EM resistivity profiles to suggest a simple and sharp resistivity boundary at the eastern Denali fault separating Kluane schist (on the NE) from Hasen Creek Formation (on the SW). Instead, in the vicinity of the Denali fault strands, the zones of low resistivity observed in the ELF-EM profiles are discontinuous and some anomalies form narrow, vertical features (Figs. 18 and 19). The discontinuous distribution of resistivity in the subsurface may suggest dismemberment of the crust into blocks by faulting. Similarly, the vertically-oriented resistivity anomalies may represent vertically-oriented geologic structures (*i.e.*, faults) that are associated with alteration. Unfortunately, the actual subsurface dip angles of the three strands of the eastern Denali fault within the project area are not known, and therefore a direct comparison of dip angles with the resistivity profiles is not possible. It is important to point out that the width spanned by the three, subparallel, mapped strands of the eastern Denali fault is no more than ~1 km. This contrasts markedly with the much wider zone (2–3 km) of discontinuous, low resistivity bedrock which lies on either side of the eastern Denali fault zone. This observation suggests that, over geologic time, faulting along the eastern Denali fault zone may have affected a much wider zone and/or low resistivity Kluane schist may be present as fault slivers on both the east and west sides of the currently active trace of the eastern Denali fault.

The region to the SW of Bock's Creek fault is characterized by low-to-moderate resistivity values (50–200 ohm-m). The Station Creek Formation is present to the southwest of this fault (Israel *et al.*, 2005), thus, low-moderate resistivity values may be representative of the Station Creek Formation. The dip angle of the Bock's Creek fault is not known and the resistivity patterns in the ELF-EM profiles suggest a variety of dip angles for the fault (Figs. 18 and 19).

The central portion of the project area that lies between the eastern Denali Fault and Bock's Creek fault, is dominated by moderate-to-high resistivity values (100–3000 ohm-m). Nikolai basalt and Hasen Creek Formation have been mapped in this area (Israel *et al.*, 2005); however, the mapped distribution of these rock units does not correlate consistently with high or low subsurface resistivity values. This suggests that the subsurface geology is likely more complex than surface mapping indicates. For example, zones of high resistivity in areas mapped as Nikolai basalt (Fig. 18) may indicate massive unfractured basalt lavas. On the other hand, moderate resistivity values in areas mapped as Nikolai basalt (Fig. 19) may indicate: a) fractured and clay-altered basalt, b) fractured basalt hosting conductive fluids, or c) a rock type other than Nikolai basalt.

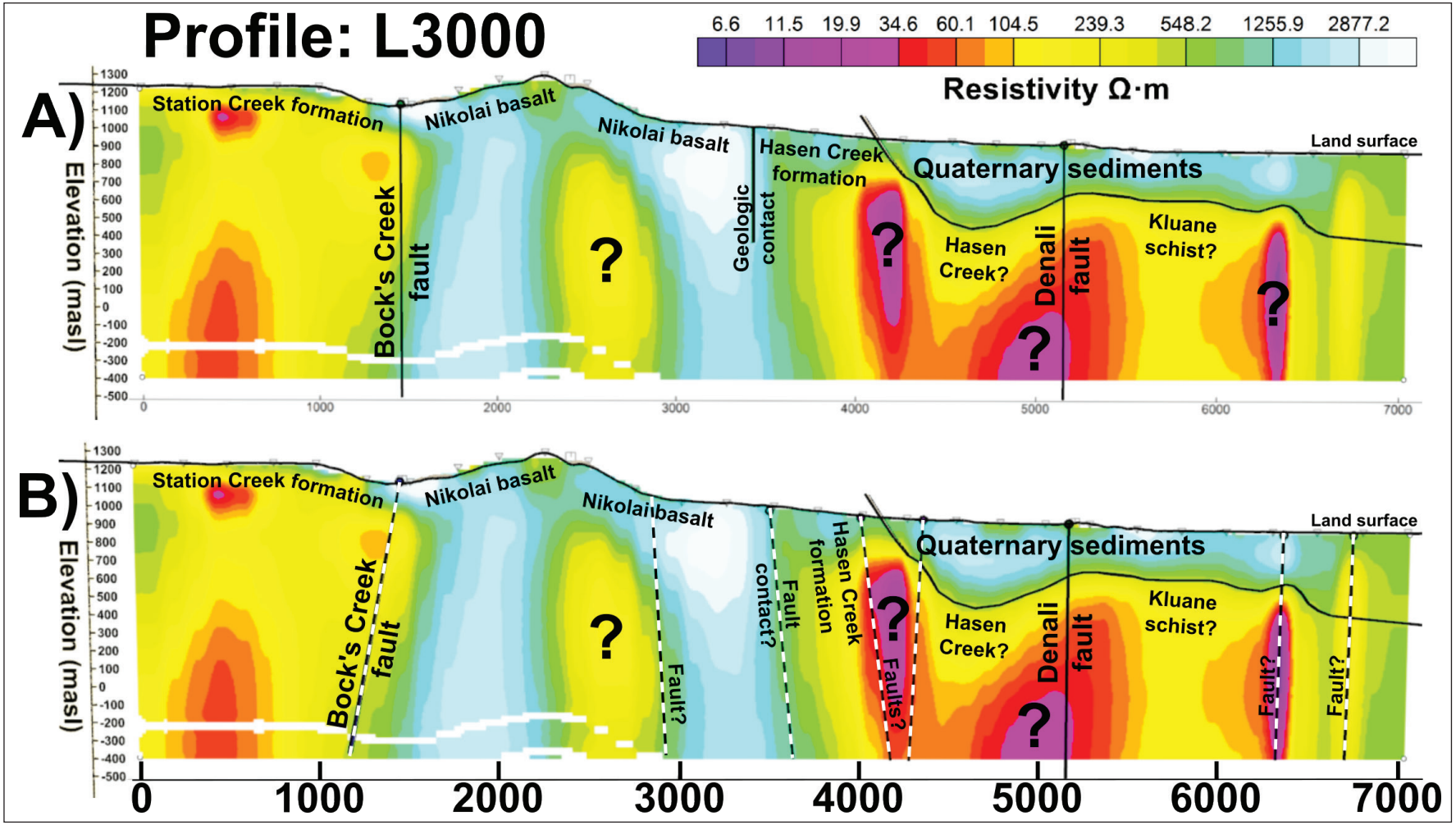

Figure 18. *Two interpretations (A and B) of ELF-EM resistivity profile L3000 in the northern part of the project area where there is only one mapped strand of the eastern Denali fault. Purple-pink-red colours represent low electrical resistivity (e.g., high conductivity) and green-blue-white colours represent high electrical resistivity (i.e., low conductivity). Interpretation* **A** *includes the major fault structures and bedrock geology mapped at the surface (Israel et al., 2005; Bender and Haeussler, 2017). Interpretation* **B** *includes additional fault structures (white dashed lines) inferred from the ELF-EM profile. The base of the Quaternary sediments is assumed to lie at ~250 ohm-m (i.e., between yellow and green). Question marks denote subsurface resistivity anomalies that remain unexplained. See Figure 13 for the location of the profile within the project area. Horizontal scale is in metres. See text for discussion.*

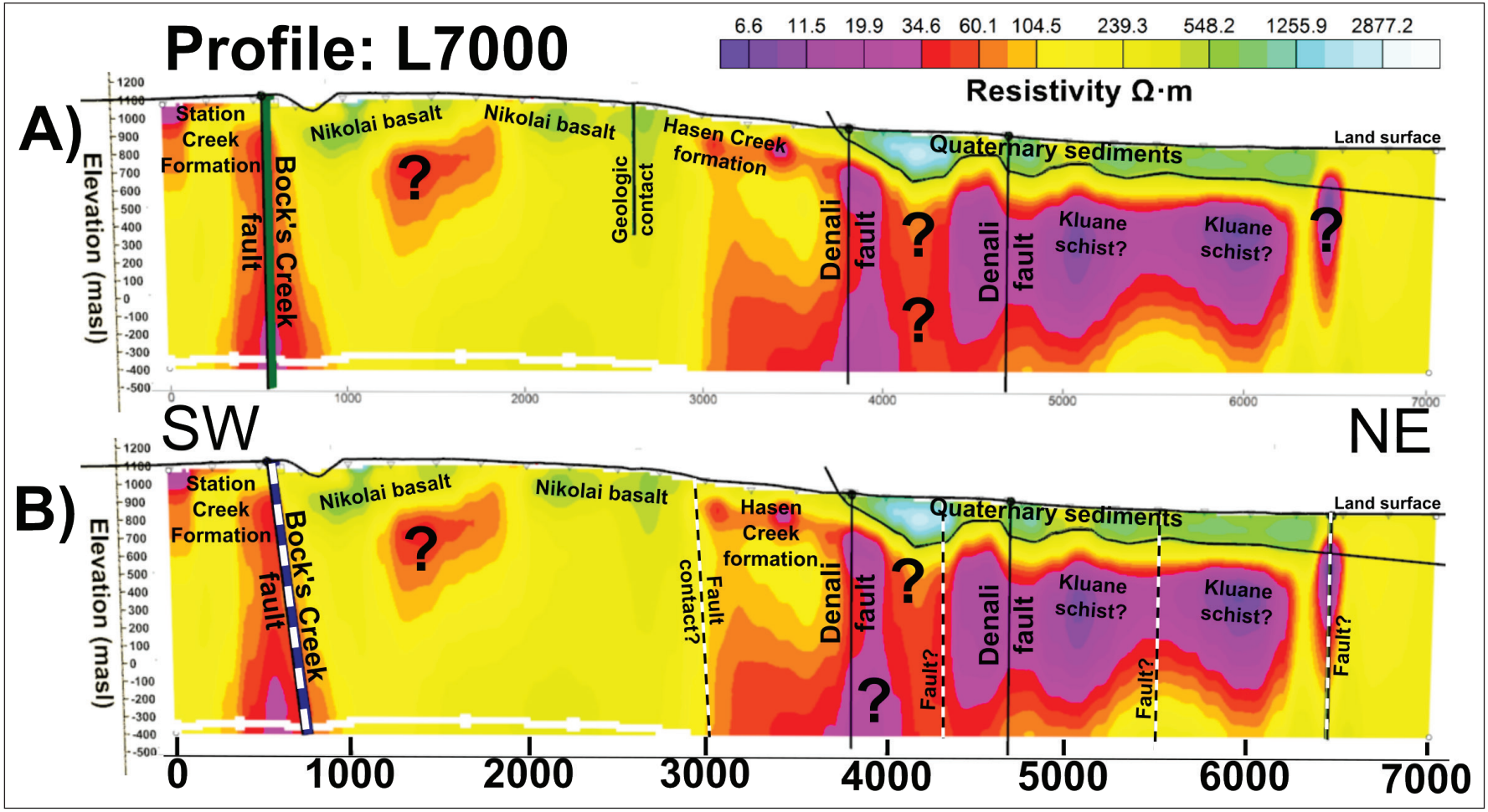

Figure 19. *Two interpretations (A and B) of ELF-EM resistivity profile L7000 in the central part of the project area where there are two mapped strands of the eastern Denali fault. Purple-pink-red colours represent low electrical resistivity (e.g., high conductivity) and green-blue-white colours represent high electrical resistivity (i.e., low conductivity). Interpretation* **A** *includes the major fault structures and bedrock geology mapped at the surface (Israel et al., 2005; Bender and Haeussler, 2017). Interpretation* **B** *includes additional fault structures (white dashed lines) inferred from the ELF-EM profile. The base of the Quaternary sediments is assumed to lie at ~250 ohm-m (i.e., between yellow and green). Question marks denote subsurface resistivity anomalies that remain unexplained. See Figure 13 for the location of the profile within the project area. Horizontal scale is in metres. See text for discussion.*

Structural interpretation of the ELF-EM resistivity profiles is challenging because of uncertainty surrounding the spatial relationship between resistivity and an inferred fault structure. For example, in some cases fault boundaries can separate two different rock units that have contrasting resistivity. However, in other cases, a fault zone itself can form the resistivity anomaly due to hydrothermal alteration in the fault plane and adjacent fault damage zones (*i.e.*, a fault zone conductor; Hoffmann-Rothe *et al.*, 2004; Ingham and Brown, 1998; Unsworth and Bedrosian, 2004a,b). In other words, in some cases, it is unclear whether to infer a fault structure through the centre of a resistivity anomaly or along the margin of one.

3D Geological and Geophysical Model Interpretation

An initial 3D geologic model was built to provide a 3D lithologic framework within which to interpret the gravity and magnetic data (Fig. 20). The 3D geologic model contains six major rock units, honours the surface geologic mapping of Israel *et al.* (2005) and incorporates the Denali fault surface traces of Bender and Haeussler (2017). However, many assumptions went into the creation of this initial 3D geologic model. For example, all major faults and the contact between the Hasen Creek Formation and the Nikolai basalt are assumed to be vertical. The bottom contact of the Quaternary sediment layer was assumed to lie at ~250 ohm-m in the ELF-EM resistivity profiles. Lastly, the thickness and folding in each of the bedrock units were assumed to be similar to those shown in cross section C-D of Israel *et al.* (2005). Due to these many assumptions, the initial 3D geologic model is certainly not intended to be a 100% accurate depiction of the subsurface. Rather, the initial 3D geologic model is meant to be as realistic as possible; a starting 3D geologic framework which can be subsequently tested and improved with geophysical data and/or drilling.

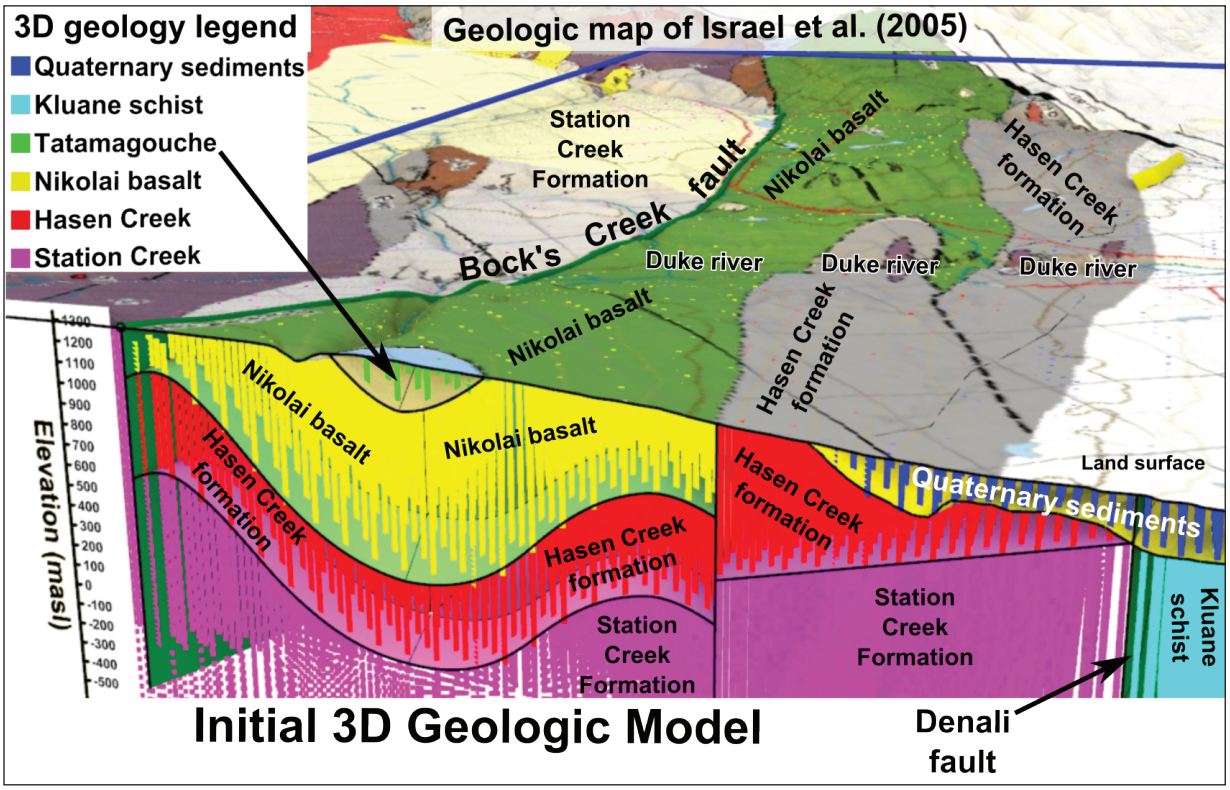

Figure 20. *3D perspective view (looking to the NNW) of a portion of the initial 3D geologic model used for the 3D geophysical inversion modelling. The upper boundary of the 3D geologic model is surface topography draped with the geologic map of Israel et al. (2005). The distribution of rock units in the subsurface is depicted with various colours defined by the 3D geology legend (upper left). The horizontal and vertical scales are equal.*

For this project, both gravity and magnetic survey data are available for 3D geophysical inversion modelling to test the initial 3D geologic model. For the 3D inversion modelling of the gravity data, each of the six rock units in the initial 3D geologic model were assigned starting density values based upon rock property measurements (Table 1). Similarly, for the 3D inversion modelling of the magnetic data, the six rock units were given starting magnetic susceptibility values also based on rock property measurements (Table 1). Quaternary sediments were assigned an assumed density value of 2.0 g/cm^3 and a magnetic susceptibility value of 0.3×10^{-3} SI. The gravity and magnetic inversion modelling were performed separately (*i.e.*, not a joint inversion), but in each case the inversion algorithm adjusted the rock property values in the model cells until a match was achieved with the measured gravity/magnetic survey data. For the case of the gravity inversion modelling, a match was achieved when the root-mean-squared (RMS) misfit, calculated for the 3D density model, equaled the average measurement error of the gravity survey data (*i.e.*, 0.05 mGal). The actual calculated RMS misfit obtained for the 3D density model is 0.047 mGal. A similar, but slightly more relaxed metric was used for the magnetic inversion modelling. The estimated error on the magnetic survey measurements was not reported, but we assume that it does not exceed 10 nT. We used this value as a target during the magnetic inversion modelling and the output 3D magnetic susceptibility model achieved an RMS misfit of 8.2 nT. A more stringent target misfit value would have required longer computing times and generated a magnetic model that is visually indistinguishable from the one presented here.

In summary, the outcome of the gravity inversion modelling is a new 3D rock density model and the result of the magnetic inversion modelling is a new 3D magnetic susceptibility model (Fig. 21). These two rock property models are used to highlight areas where the initial 3D geology is incompletely understood and needs to be updated. Example cross sections through the rock property models are shown in Figures 22 to 25.

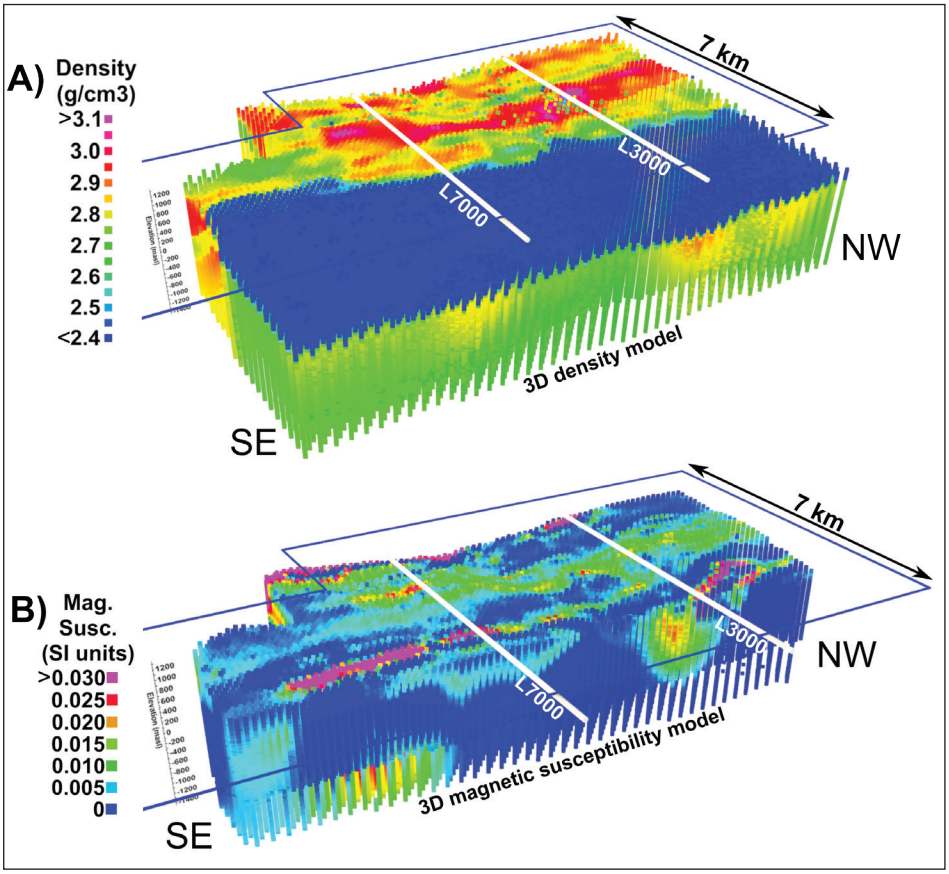

Figure 21. *3D perspective view looking towards the west of:* ***(A)*** *3D density model generated from geophysical inversion modelling of gravity data (coloured blocks represent the rock density values for each model cell according to the density legend); and* ***(B)*** *3D magnetic susceptibility model generated from geophysical inversion modelling of magnetic data (coloured blocks represent the rock magnetic susceptibility values for each model cell according to the magnetic susceptibility legend). Blue polygon shows the project boundary. The locations of 2D profile lines L3000 and L7000 are shown.*

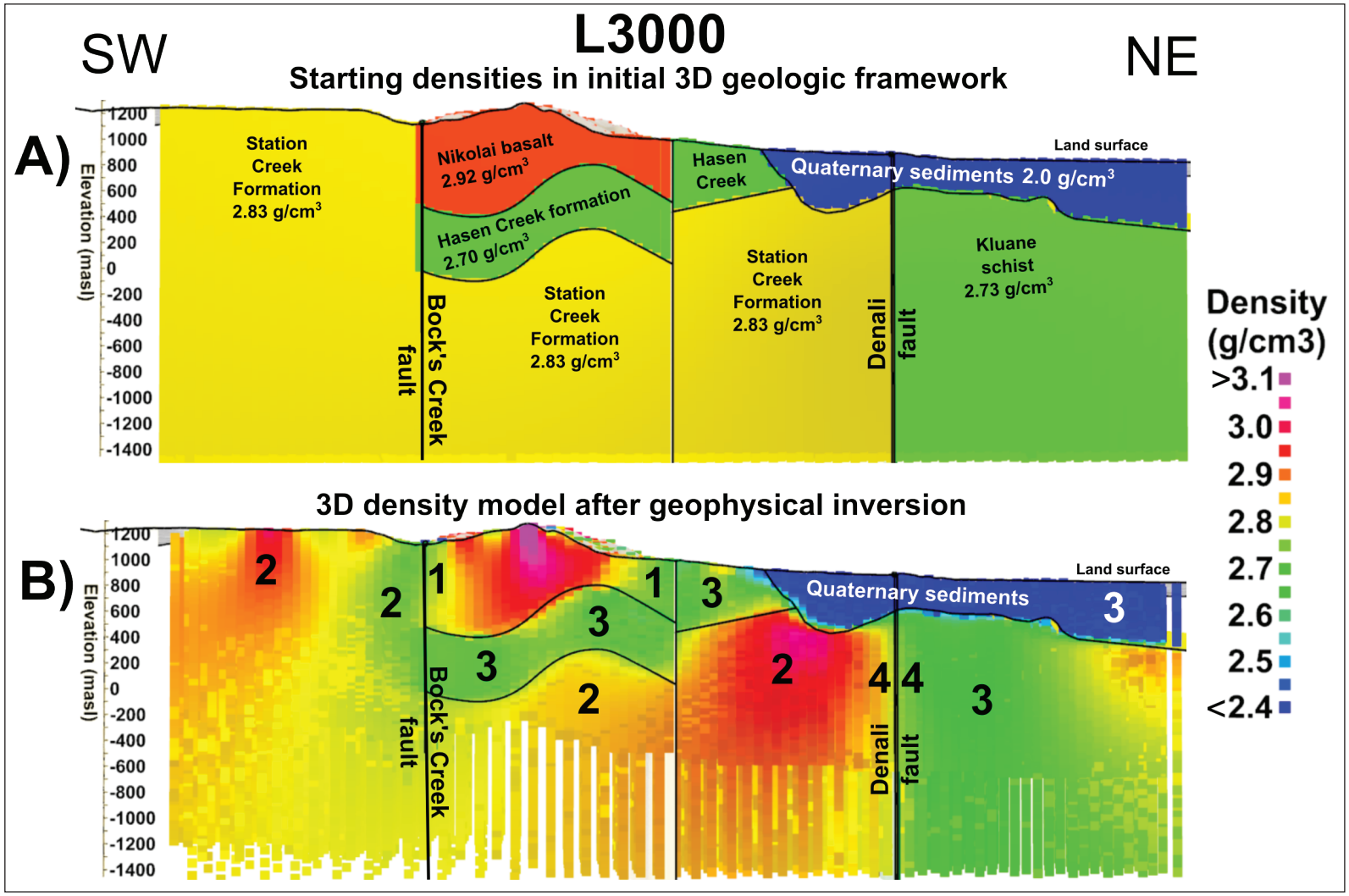

Figure 22. *Density models along profile L3000 showing:* **(A)** *starting density values in the initial 3D geologic model and* **(B)** *model densities generated by the geophysical inversion that are in agreement with the measured gravity survey data. The results show that the spatial extent of high-density Nikolai basalt may be less than originally assumed (the 1s in B above), Station Creek Formation has variable densities and may actually be different rock types (2s), three of the rock units (Hasen Creek, Kluane schist, and Quaternary sediments) match the starting density and 3D geology fairly well (3s), the Denali fault defines a boundary between rocks with markedly different densities (4s). The horizontal and vertical scales are equal.*

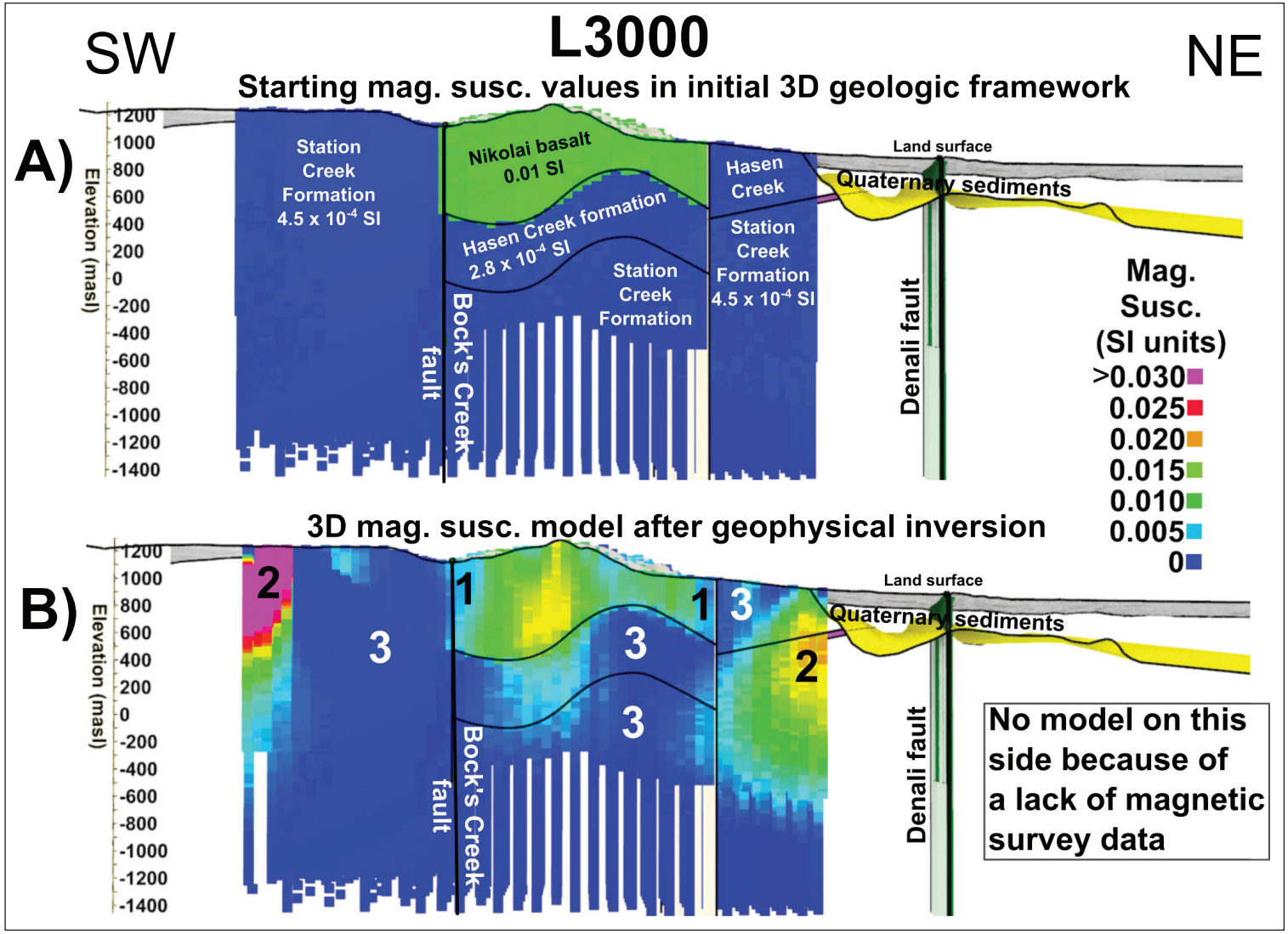

Figure 23. *Magnetic susceptibility models along profile L3000 showing:* ***(A)*** *starting magnetic susceptibility values in the initial 3D geologic model and* ***(B)*** *model magnetic susceptibility values generated by the geophysical inversion that are in agreement with the measured magnetic survey data. The results show that the strongly magnetic Nikolai basalt almost fills the region originally assumed (the 1s in B above), Station Creek Formation contains strongly magnetic rocks in two areas (that correspond to zones of elevated density) and are likely different rock types (2s), large portions of the Hasen Creek and Station Creek formations have low magnetic susceptibility as predicted (3s). Horizontal and vertical scales are equal.*

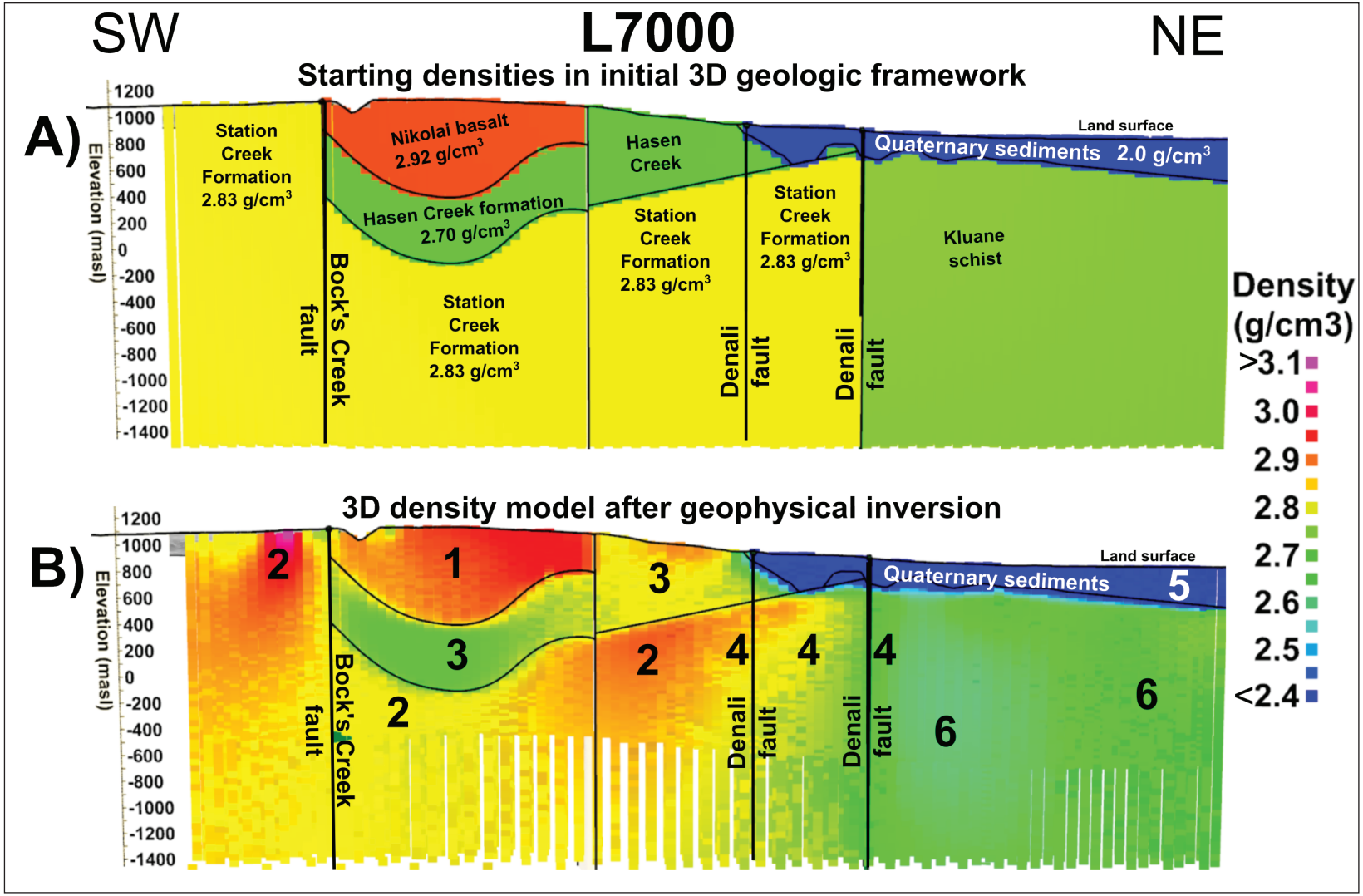

Figure 24. *Density models along profile L7000 showing:* **(A)** *starting density values in the initial 3D geologic model and* **(B)** *model densities generated by the geophysical inversion that are in agreement with the measured gravity survey data. The results show that high-density Nikolai basalt fills the region originally assumed (the 1s in B above), Station Creek Formation has variable densities and may consist of different rock types (2s), Hasen Creek Formation matches the starting density and 3D geology in some areas, but not others (3s), a gradational change in rock density spans the two strands of the Denali fault which may suggest varying rock types across the fault zone (4s), the Quaternary sediment unit matches the starting density and 3D geology well (5s), and subtle density variations exist within the Kluane schist unit (6s). Horizontal and vertical scales are equal.*

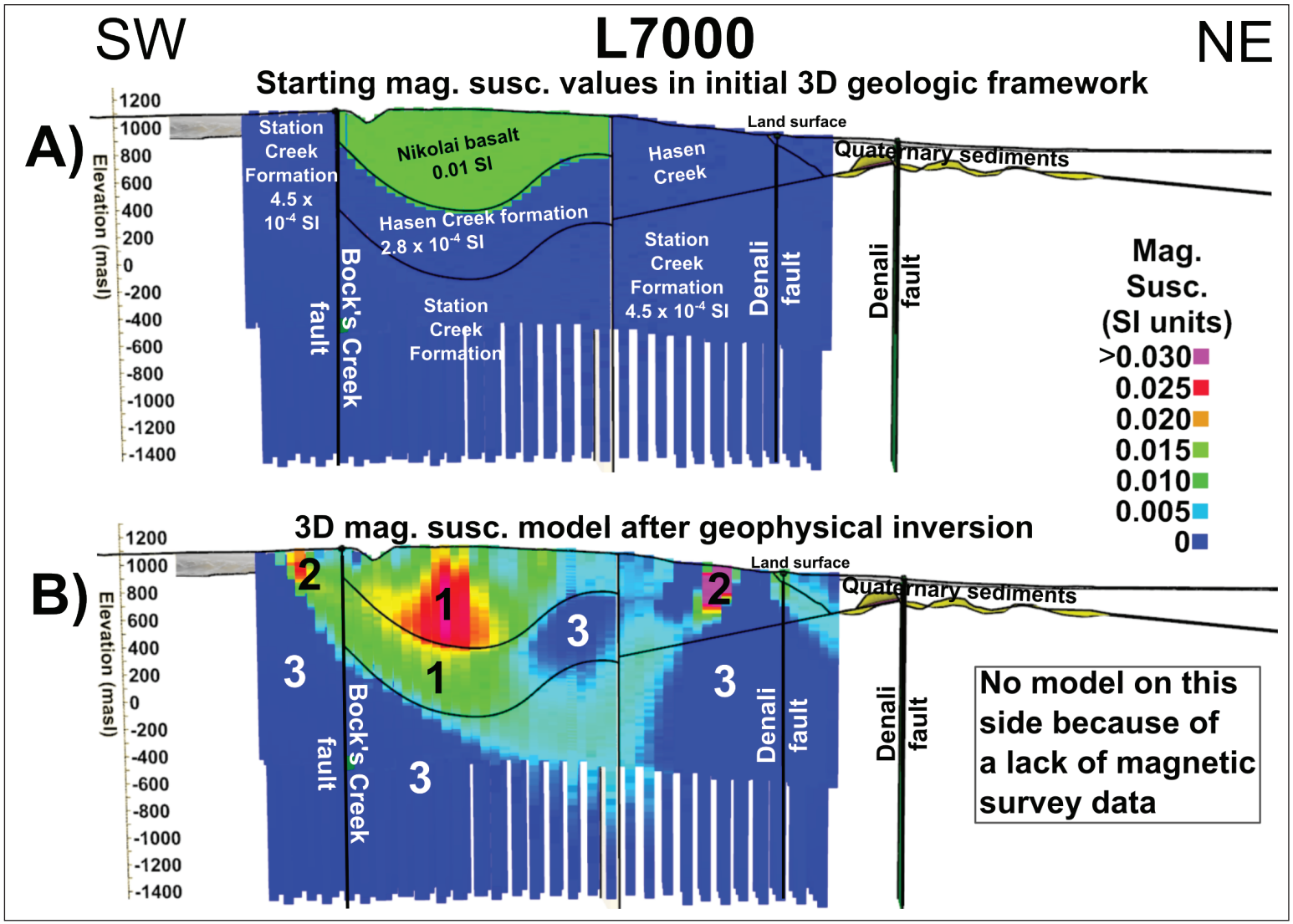

Figure 25. *Magnetic susceptibility models along profile L7000 showing:* ***(A)*** *starting magnetic susceptibility values in the initial 3D geologic model and* ***(B)*** *model magnetic susceptibility values generated by the geophysical inversion that are in agreement with the measured magnetic survey data. The results suggest that the strongly magnetic Nikolai basalt may fill a larger volume than originally assumed (the 1s in B above), the Hasen Creek and Station Creek formations contain small bodies of strongly magnetic rocks in two areas (that correspond to zones of elevated density) and are likely different rock types (2s), portions of the Hasen Creek and Station Creek formations have low magnetic susceptibility (3s). Horizontal and vertical scales are equal.*

Discussion

In Section 3.2, a number of questions were posed regarding what we would want to know in order to better understand the subsurface and target exploratory geothermal wells. In this section, I attempt to provide answers to these questions, to outline what we have learned and what remains to be investigated in the effort to find geothermal resources within the project area.

The first question has to do with the width of the eastern Denali fault zone and, by extension, the width of the potentially permeable fault damage zone associated with Quaternary movement on these fault planes. Based upon linear strings of mounds on the land surface, the width of Quaternary deformation along the eastern Denali fault is as much as ~1 km. However, geophysical data, such as the ELF-EM resistivity profiles and subtle features in the 3D density model suggest that the fault damage zone may be significantly wider, up to 2–3 km wide. If true, such a wide fault damage zone could potentially create large volumes of fractured, permeable rock to enable deep circulation and ascent of geothermal fluids.

The second question asks if a transtensional pull-apart structural environment is present in the project area. The gravity, magnetic and ELF-EM geophysical data sets all suggest that a right-step in the right lateral Denali fault system is present and that the geometry is consistent with a localized pull-apart zone. This right-step is located on the south side of Duke River, approximately 0.5–3 km southwest of the Alaska Highway.

The third question asks whether the pervasively fractured hanging wall on the Alpine fault in New Zealand (Fig. 6) is an accurate analogue to the eastern Denali fault. The extensive fracturing associated with the Alpine fault facilitates deep infiltration of meteoric water that allows for geothermal heating. The geophysical data in this study are not capable of providing direct evidence for subsurface permeability. In addition, interpretation of the geophysical data has not revealed new evidence to estimate the actual dip angles of the different strands of the eastern Denali fault that are located in the project area. The eastern Denali fault strands are likely oriented vertically based upon the strike-slip motion recorded for this fault. However, a borehole that intersects the Denali fault would help answer this question more conclusively. A drilling program would also be the best way to address the question of the extent of fracturing in the subsurface rocks near the fault zone.

The presence or absence of fault-parallel damage zones (*i.e.*, potential permeability) and the exact locations of fault planes that have these damage zones is the topic of the fourth question. For any geothermal exploration program, finding subsurface permeability is key. The highest potential for permeability likely lies in fault damage zones near the active segments of the eastern Denali fault or other faults. We did not find strong, incontrovertible evidence for subsurface permeability in this study for areas away from the eastern Denali fault. For example, NE–SW trending normal faults have been inferred in the Duke River valley based upon subtle changes in slope in the Arctic DEM data. However, an alternate explanation could be that these slope features are glacial in origin. If these normal faults are real, the amount of Quaternary offset is likely small (*i.e.*, metres to tens of metres) which would suggest that the amount of subsurface fracturing is not large. To more adequately address this question, more detailed geologic mapping coupled with exploratory drilling is required.

The last question has to do with the location of the different rock types in the subsurface that would be more prone to sustain open fractures. The 3D geophysical modelling in this study helped to address this question. The Nikolai basalt rock unit is more likely to sustain open fractures and permeability than a clay-rich rock unit such as the Hasen Creek Formation. Mafic volcanic rocks, like basalt, are usually dense and magnetic. Therefore, in the 3D density

and magnetic susceptibility models generated for this study, it is possible to identify which areas in the subsurface are more likely to be both dense and magnetic and which areas are not. The portions of the geophysical models that are dense and magnetic are more likely to be basalt and thus would make better drilling targets at this exploratory stage of the project.

There is still considerable uncertainty in our understanding of the 3D geologic framework in the project area. Additional geologic mapping and drilling are required to develop a clearer understanding of the subsurface. An initial 3D geologic model was built as part of this study; some portions of the geologic model are in agreement with the 3D geophysical models but other parts are not. It must be mentioned here that, as with all geophysical models, non-uniqueness is a problem such that even if a geophysical model is mathematically correct, it is not necessarily geologically correct. With these limitations in mind, a number of subsurface targets have been selected as initial exploratory boreholes.

Proposed Drilling Targets

A key goal of this project is to identify favourable locations for the drilling of exploration boreholes. The purpose of such boreholes is to measure subsurface temperatures, assess subsurface fracturing and permeability, and increase understanding of subsurface geology. Presented here are seven proposed drill sites, all of which lie in the vicinity of Duke River. This portion of the project area was chosen due to proximity to the observed right-step in the eastern Denali fault and the NE-trending normal faults inferred in the Duke River valley. The available evidence suggests that, within the project area, the Duke River valley exhibits the highest level of subsurface structural complexity. A structurally complex environment has the highest likelihood of containing fractured, permeable rock units in the subsurface, which could potentially facilitate the ascent of hot geothermal fluids. Other parts of the project area either: 1) do not have strong evidence for subsurface structural complexity; 2) do not have evidence for normal faulting; or 3) do not show evidence for bending or step-overs in the eastern Denali fault zone.

The drill sites proposed here have been ranked from most to least-favourable. The highest ranked location is Site #1 and the lowest is Site #5. Three sites, #4a, #4b and #4c all have an equivalent favourability. Accessibility varies from site-to-site and has been included, along with geoscientific information, as an important factor in the ranking. Maps of the geoscientific data, focused on the Duke River area, are presented in Figures 26 through 31. In addition, Figures 32 through 37 show interpretations of the subsurface along two separate profiles (L4000 and L5000) that run nearly through the proposed drill sites. Table 2 and Table 3 are compilations of the geoscientific and access information for each of the proposed drill locations. Table 4 provides the locations of the drill sites. The recommended depth of exploratory boreholes in the Duke River area is 500 m to 1 km. In order to test the thermal and geologic variability amongst the proposed boreholes, I recommend that at least two out of the seven proposed holes are drilled. What follows here is a discussion of each of the proposed drill sites from the most to least-favoured. Note the author has not visited all of these proposed sites: the landscape and access limitations have only been assessed through inspection of satellite images on the GeoYukon website (https://mapservices.gov.yk.ca/GeoYukon).

Site #1: This location has been selected as most favourable as it strikes a balance between notable geoscientific indicators and relatively easy access. This site is located ~250 m SE of Duke River in a flat area that lies ~350 m SW of the end of a gravel spur road that connects to the Alaska Highway (Fig. 26). Satellite images do not show an existing road to this site (Fig. 27). However, the flat terrain and proximity to an existing gravel road should make access to this site relatively uncomplicated. Geologically, the bedrock at this location has been mapped as the Hasen Creek Formation (Israel *et al.*, 2005; Fig. 28). However, ELF-EM data suggest a relatively thick cover of Quaternary sediments here (described below). This site is also located between two strands of the eastern Denali fault as mapped in this study and by Bender and Haeussler (2017). The presence of a significant fault contact in this area is corroborated by both the ELF-EM anomaly (Fig. 29) and horizontal gravity gradient high (Fig. 30) at this same location. Furthermore, Site #1 is located on the edge of the right-step in the Denali fault zone as shown in the horizontal gravity gradient map (Fig. 30). In the subsurface beneath Site #1, the geophysical models suggest a few hundred metres of electrically resistive, low density Quaternary sediments underlain by several hundred metres of rocks with moderate-to-high conductivity and anomalously high-density (Figs. 32 and 34). The high-density rocks are likely crystalline igneous or metamorphic rocks which would be more likely to sustain fractures, compared to sedimentary rocks. The moderate-to-high conductivity signature could indicate the presence of geothermal brines or clay alteration. Alternatively, the higher conductivity values near 1000 m depth at Site #1 may arise from the presence of graphite-bearing Kluane schist, which cannot be ruled out in this location.

Site #2: This location is considered the second most-favourable due to some positive geoscientific indicators, but largely because of the ease of access. This site is in a flat area located at the end of a gravel spur road that connects to the Alaska Highway (Figs. 26 and 27). Site #2 is located immediately adjacent to the active strand of the eastern Denali fault. The exact location of the Denali fault plane is slightly different in this study and in the study by Bender and Haeussler (2017) and Site #2 is positioned between the two interpretations. The subsurface geology is expected to be a few hundred metres of Quaternary sediments underlain by faulted bedrock. This site lies on the margin of the ELF-EM anomaly (Fig. 29) and horizontal gravity gradient high (Fig. 30) that mark the eastern Denali fault zone. Similar to Site #1, Site #2 is located on the edge of the right-step in the Denali fault zone as shown in the horizontal gravity gradient map (Fig. 30). The 3D density model suggests that the bedrock beneath Site #2 lies at the contact between lower density rocks to the NE and higher density rocks to the SW (Fig. 32). Interestingly, the resistivity profile derived from ELF-EM data shows an unusual, highly conductive anomaly ~100 m below the surface at Site #2. This is unexpected since the near surface geology in the vicinity of Site #2 is dominated by resistive Quaternary sediments. This zone of elevated conductivity in the shallow subsurface could represent: a) electrically conductive minerals (e.g., clay) associated with large-scale transform faulting; b) electrically conductive minerals associated with hydrothermal alteration precipitated out of circulating geothermal fluids; c) electrically conductive geothermal brines circulating in the near surface; or d) a large boulder of graphite-bearing Kluane schist. Below this conductivity anomaly, the ELF-EM profile shows moderate conductivity (~200 ohm-m) over several hundred metres, reaching even more conductive values (~40 ohm-m) at a depth of ~1 km. The regions in the subsurface with moderate conductivity are unlikely to be Kluane schist due to the high graphite content reported in these rocks.

Site #3: This location is difficult to access but has a uniquely favourable geoscientific characteristic which places it as the 3rd most-favourable site. Site #3 is located ~1.5 km from the end of the gravel spur road (mentioned above; Fig. 26) and at the end of an off-road vehicle trail that is visible in satellite images on the GeoYukon website (Fig. 27). It is also located ~400 m SW of the southern strand of the eastern Denali fault. The geology of the area is expected to be a thin cover of Quaternary sedimentary material underlain by Hasen Creek Formation bedrock (Figure 28). Site #3 is located immediately SW of the right-step in the Denali fault zone as shown in the horizontal gravity gradient map (Fig. 30). However, it is positioned relatively far (1–1.5 km) NE of the right-step anomalies observed in the ELF-EM and magnetic survey maps (Figs. 29 and 31). In the subsurface, the 3D density model suggests a stratigraphy of a few hundred metres of Hasen Creek Formation underlain by several hundred metres of Station Creek Formation (Fig. 35). Meanwhile, the 3D magnetic model suggests weakly magnetic rocks in the subsurface which is consistent with our current understanding of the geology (Fig. 36). The two key geological indicators which make Site #3 attractive are a) a NE-dipping contact in the ELF-EM resistivity profile (Fig. 37) and b) a NE-dipping fault, located nearby, that was observed in the field as part of this study. Figure 37 suggests that rocks under Site #3 are separated by a contact (fault?) with strongly conductive rocks on the NE side and moderately conductive rocks on the SW side. The down-to-the-NE dip orientation observed in the ELF-EM profile is remarkably similar to the dip of a fault zone observed in the field on the south wall of the Duke River valley (~650 m along strike from Site #3; black star in Fig. 26). Most large-scale faults observed in river valley walls in this study dip down-to-the-SW. The large fault observed in the Duke River valley wall is the only one dipping in the opposite direction, which suggests it may be an antithetic fault occupying a zone of complex geological structures. Site #3 has been positioned so that a 1 km borehole would pass through the presumed subsurface extension of the large fault observed in the Duke River valley wall. Lastly, Site #3 is also located on the margin of a zone of minor, inferred normal faults mapped from high-resolution Arctic DEM data (Fig. 26).

Site #4a: This site is easily accessible along a gravel road, ~2.5 km from the Alaska Highway, on a flat bluff on the north side of the Duke River (Fig. 26). This location is in a dense thicket of trees so some clearing of vegetation would be required to make space for drilling. Geology at the site is expected to be a thin covering (*i.e.*, <10 m) of surficial sediments underlain by Nikolai basalt (Fig. 28). Indeed, Nikolai basalt crops out in the river bluff only 100 m from the site. This site is located well away from both the right-step seen in the gravity map (Fig. 30) and the right-step in the magnetic map (Fig. 31). However, this site is positioned on the north edge of the right-step recognized in the ELF-EM map (Fig. 29). Site #4a is inferred to be located in the hanging wall of the NE-dipping fault zone observed in the Duke River valley wall (the same as that described for Site #3). Site #4a is located ~500 m along strike from this antithetic, NE-dipping fault. However, geophysical models do not provide corroborating evidence for this interpretation. For example, the 3D density and 3D magnetic models show varying rock property values with depth that only partially agree with the expected subsurface geology (Figs. 32 and 33). And the resistivity profile shows strongly resistive rocks (~1000 ohm-m) under Site #4a to depths >1 km (Fig. 34). Thus, despite easy access to this site, there is still substantial uncertainty in the geologic interpretation of the subsurface at this location.

Site #4b: This location has some intriguing geoscience characteristics; however, it appears to be rather inaccessible. Site #4b is positioned on the south side of the Duke River, ~2.5 km from the Alaska Highway, on a gently sloping bluff above the river bottom (Fig. 26). There are no known roads or trails that extend into this area (Fig. 27). Geologically, Site #4b is expected to be underlain by Hasen Creek Formation rocks (Fig. 28). Although, this site is >1 km away from the right-step in the gravity map, it is located within the right-step ELF-EM anomaly (Fig. 29) and at the north end of the right-step magnetic anomaly (Fig. 31). In addition, Site #4b is positioned near to normal faults inferred from Arctic DEM data. The subsurface geophysical models (Figs. 35 and 36) suggest that the low density and weakly magnetic Hasen Creek Formation is underlain by a much denser and strongly magnetic rock unit (Nikolai basalt?). This zone of dense and magnetic rock under Site #4b is characterized by a broad zone of moderately resistive (~200 ohm-m) rock as seen in the ELF-EM profile (Fig. 37). If these dense and magnetic rocks are Nikolai basalt, then the moderate resistivity values may suggest that these rock units are more fractured, permeable, and/or altered compared to massive, unaltered, impermeable lava (which generally has high resistivity values). Overall, the upsides of this location include proximity to the right-step and suggestions of subsurface permeability. But the obvious downside for this site is lack of access.

Site #4c: Similar to Site #1, Site #4c is located between two strands of the eastern Denali fault and is meant to take advantage of presumably fractured rocks within the fault zone. Site #4c is located ~700 m SE of Site #1 and ~1 km from the gravel spur road mentioned above (Fig. 26). It has some favourable geoscientific characteristics; however, access to this site is not ideal. Satellite images on the GeoYukon website suggest that Site #4c has no road access but, instead may be located on an off-road vehicle trail (Fig. 27). The geology at this site includes Quaternary sediments underlain by either the Hasen Creek Formation or possibly the Station Creek Formation (Fig. 28). What is intriguing about this site is that it is located in the centre of the right-step in the in the Denali fault zone as shown in the horizontal gravity gradient map (Fig. 30). Furthermore, the 3D density model suggests that the zone between the two strands of the Denali fault is gradational and not characterized by a single sharp density contrast (Fig. 35). This is significant because a gradual change in density across the Denali fault zone would be more consistent with a wide, highly fractured fault zone than would a sharp lateral change in density. The resistivity signature in the ELF-EM profile under Site #4c is similar to that seen at Site #1, specifically, electrically resistive, low-density Quaternary sediments underlain by several hundred metres of rocks with moderate-to-high conductivity (Fig. 37).

Site #5: This location is considered the least-favourable of those presented here because of a lack of strong geoscientific indicators, however it is included here as it is a site with relatively easy access that would test the subsurface in the upper reaches of the Duke River valley. Site #5 is located ~4 km from the Alaska Highway, along a gravel road in a flat area near some cabins on the north side of the Duke River (Figs. 26 and 27). It is located ~600 m NE of the Bock's Creek fault and within the area of inferred normal faults in the Duke River valley. The subsurface geology is expected to be a thin cover of fluvial sediments underlain by Nikolai basalt (Fig. 28). The geophysical data do not paint a favourable picture for Site #5 since it lies outside of both the right-step observed in the magnetic and ELF-EM data and the right-step seen in the gravity data (Figs. 29 and 31). In the subsurface, geophysical modelling results lack consistency. The 3D density model suggests ~500 m of dense Nikolai basalt underlain by ~500 m of lower density Hasen Creek rocks (Fig. 35). The 3D magnetic model, however, suggests strongly magnetic rocks from the surface to deeper than ~1 km (Fig. 36). Lastly, the resistivity profile from the ELF-EM data shows elevated resistivity values in a relatively narrow zone beneath Site #5 (Fig. 37). These geophysical results conflict with the current understanding of the subsurface stratigraphy at this location and reveal substantial uncertainty at this location. Overall, the value of Site #5 is that it is an easily accessible spot to test subsurface temperatures in an area situated to the SW of the structurally complex right-step feature. Drilling at Site #5 would answer the question: are subsurface temperatures different inside *vs.* outside the right-step in the Denali fault zone? One of the downsides of Site #5 is that it is not proximal to any faults (certain or inferred), thus subsurface permeability may be low.

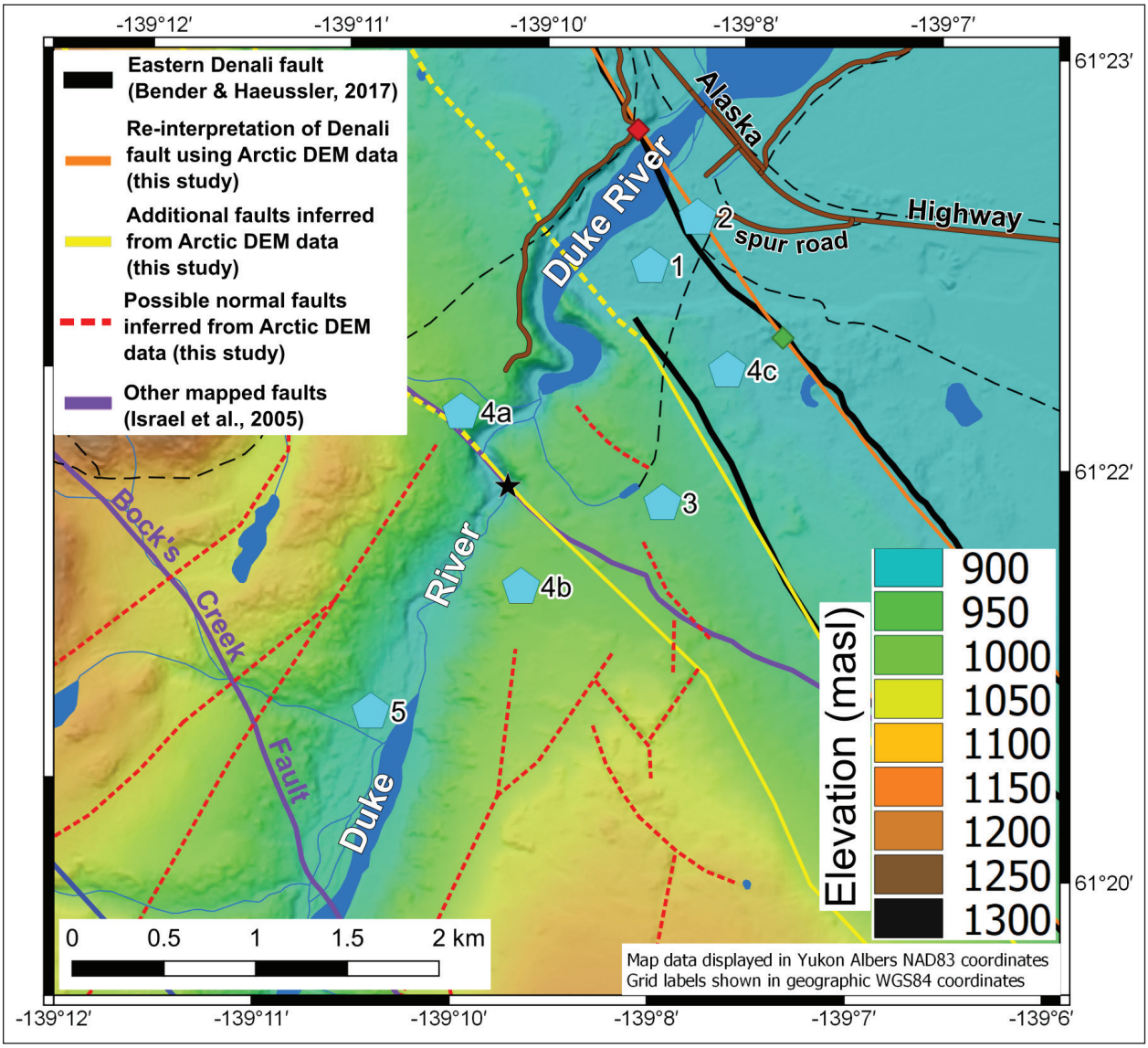

Figure 26. *Map showing the seven proposed drilling locations (blue pentagons), topography, and fault structures from this study and other studies (defined in legend). Red and green diamonds represent a river bluff exposure of the eastern Denali fault and a trench dug across the eastern Denali fault, respectively (Blais-Stevens et al., 2020). The black star shows the location of a major fault structure observed in the field in the Duke River valley wall. Roads are in brown. Dashed black lines mark trails.*

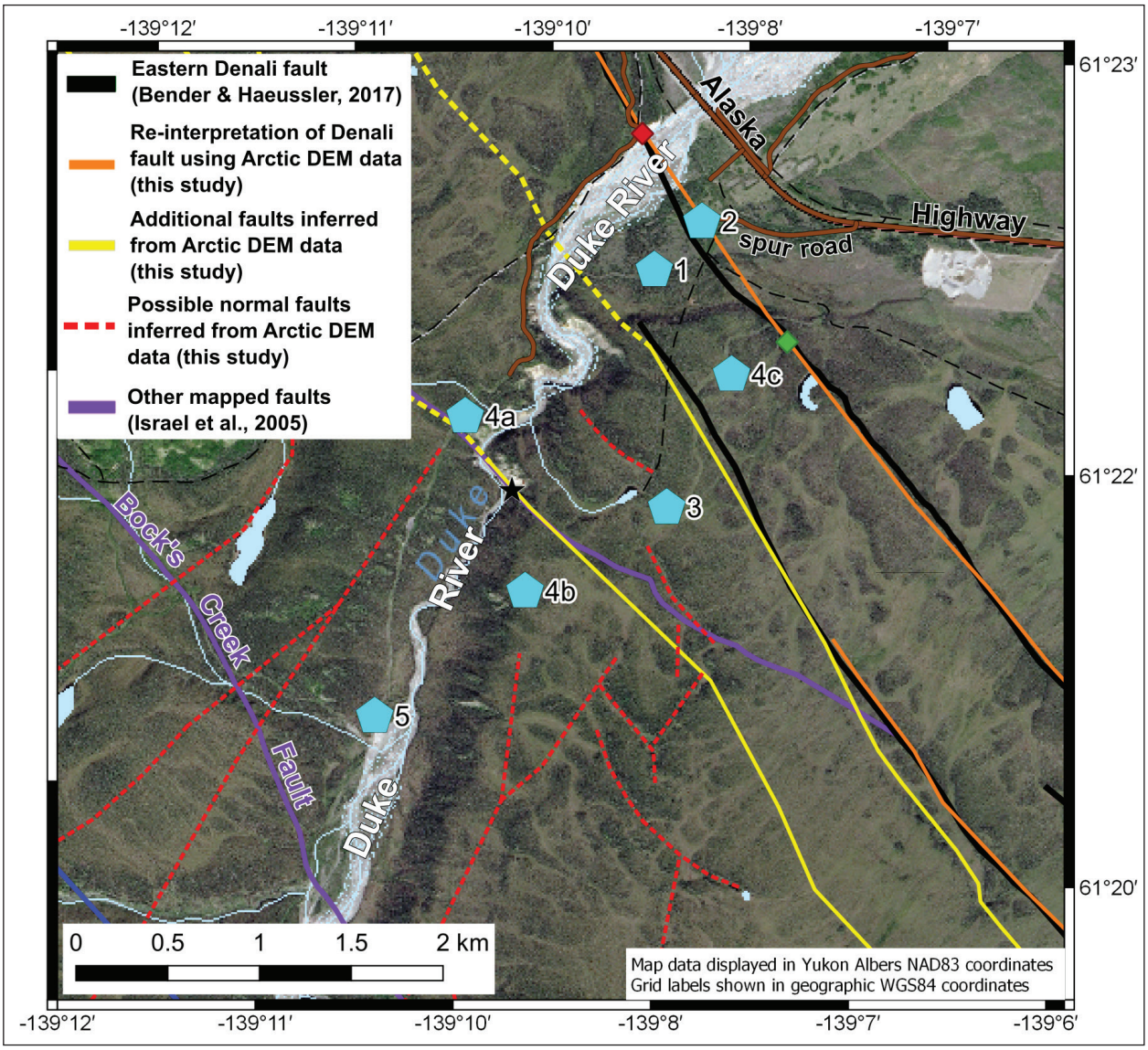

Figure 27. *Map showing the seven proposed drilling locations (blue pentagons) and a medium resolution satellite image of the area from the GeoYukon website (https://mapservices.gov.yk.ca/GeoYukon). Fault annotation and other features are the same as in Figure 26.*

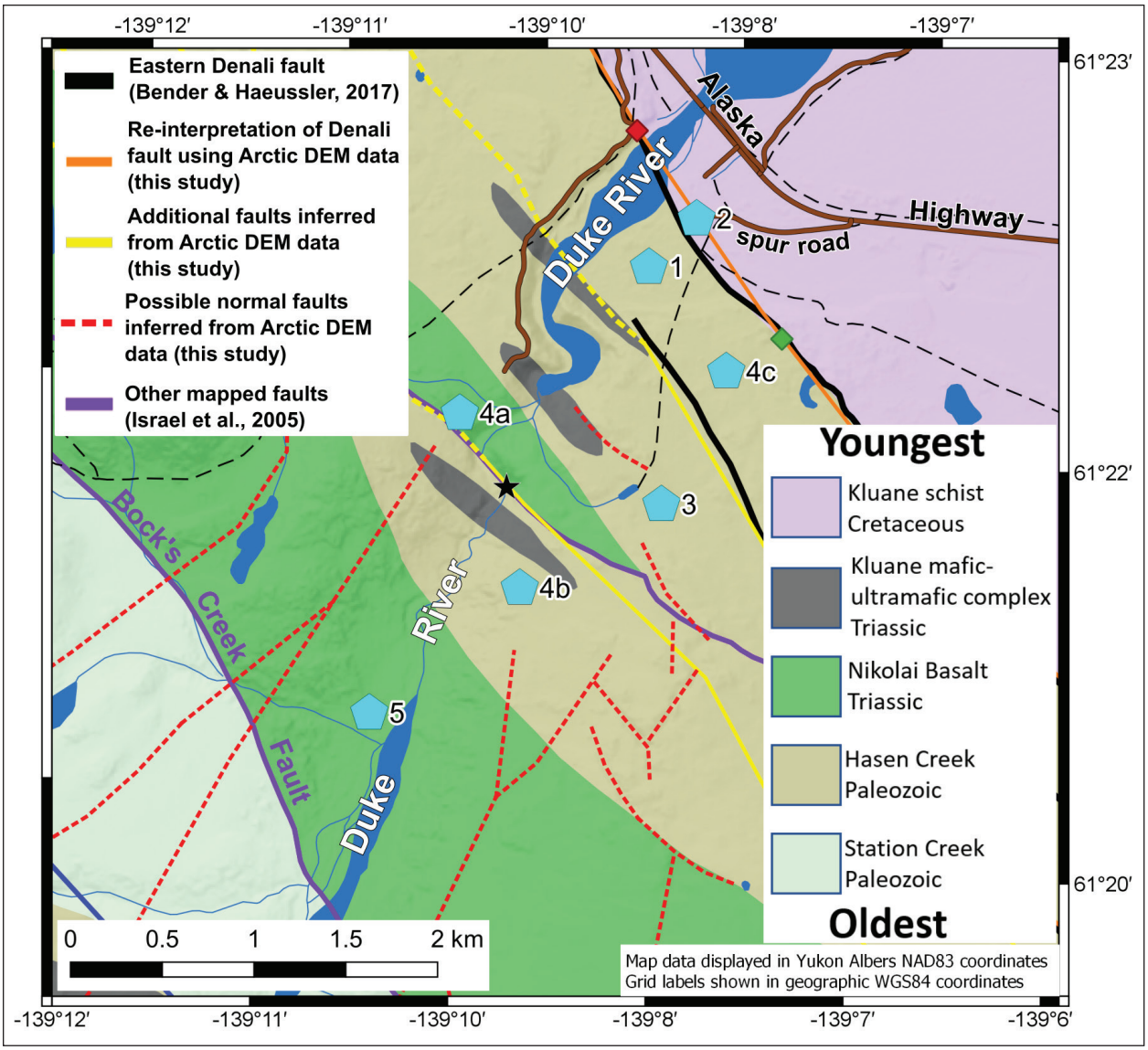

Figure 28. *Map showing the seven proposed drilling locations (blue pentagons) and bedrock geology from the GeoYukon website. Fault annotation and other features are the same as in Figure 26.*

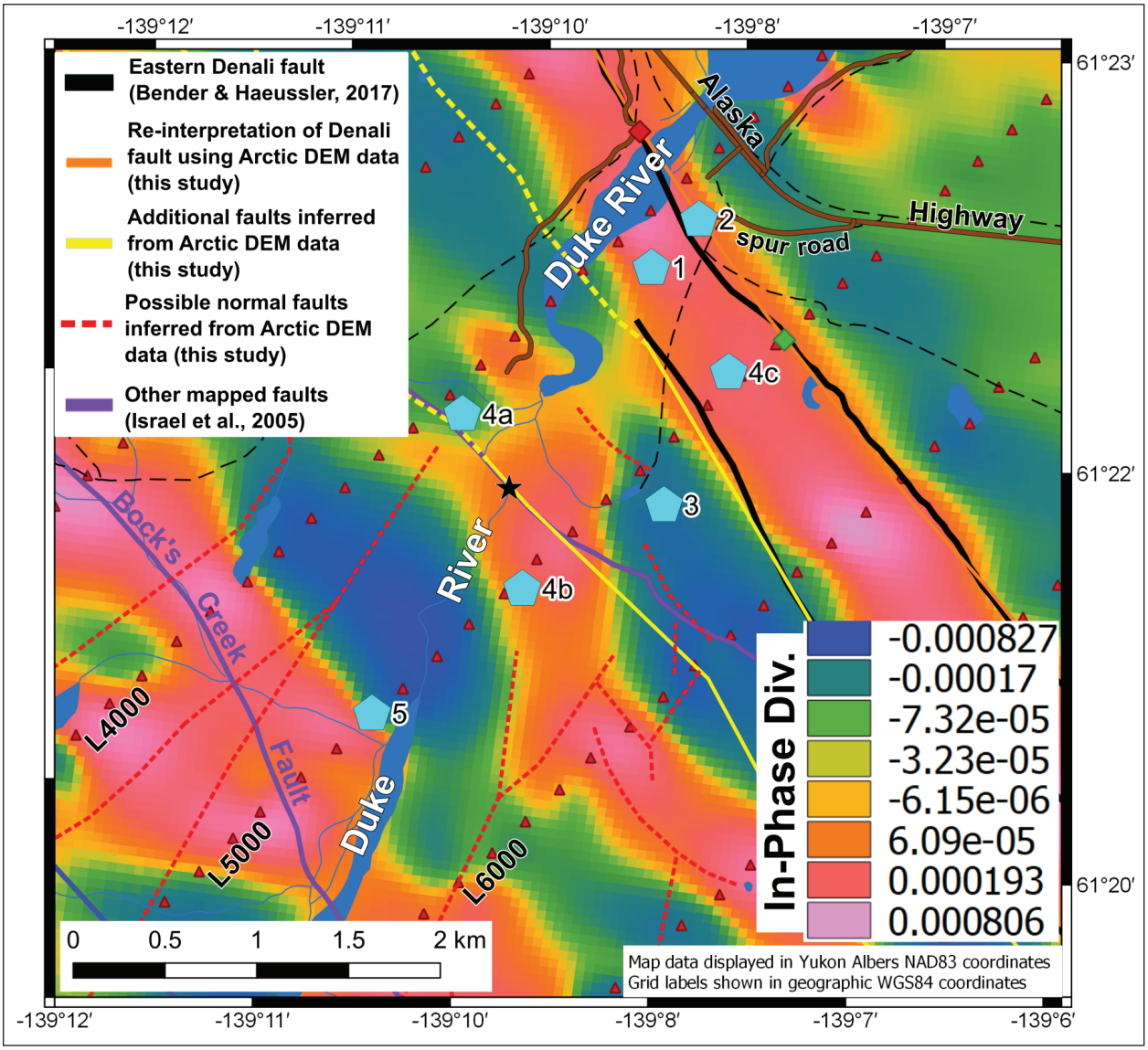

Figure 29. *Map showing the seven proposed drilling locations (blue pentagons) and the in-phase divergence map at 360 Hz derived from the ELF-EM geophysical survey. Fault annotation and other features are the same as in Figure 26. The lines of red triangles mark the locations of NE–SW profiles (e.g., L4000, L5000, etc.) along which geological and geophysical cross sections have been generated in Figure 32 through Figure 37.*

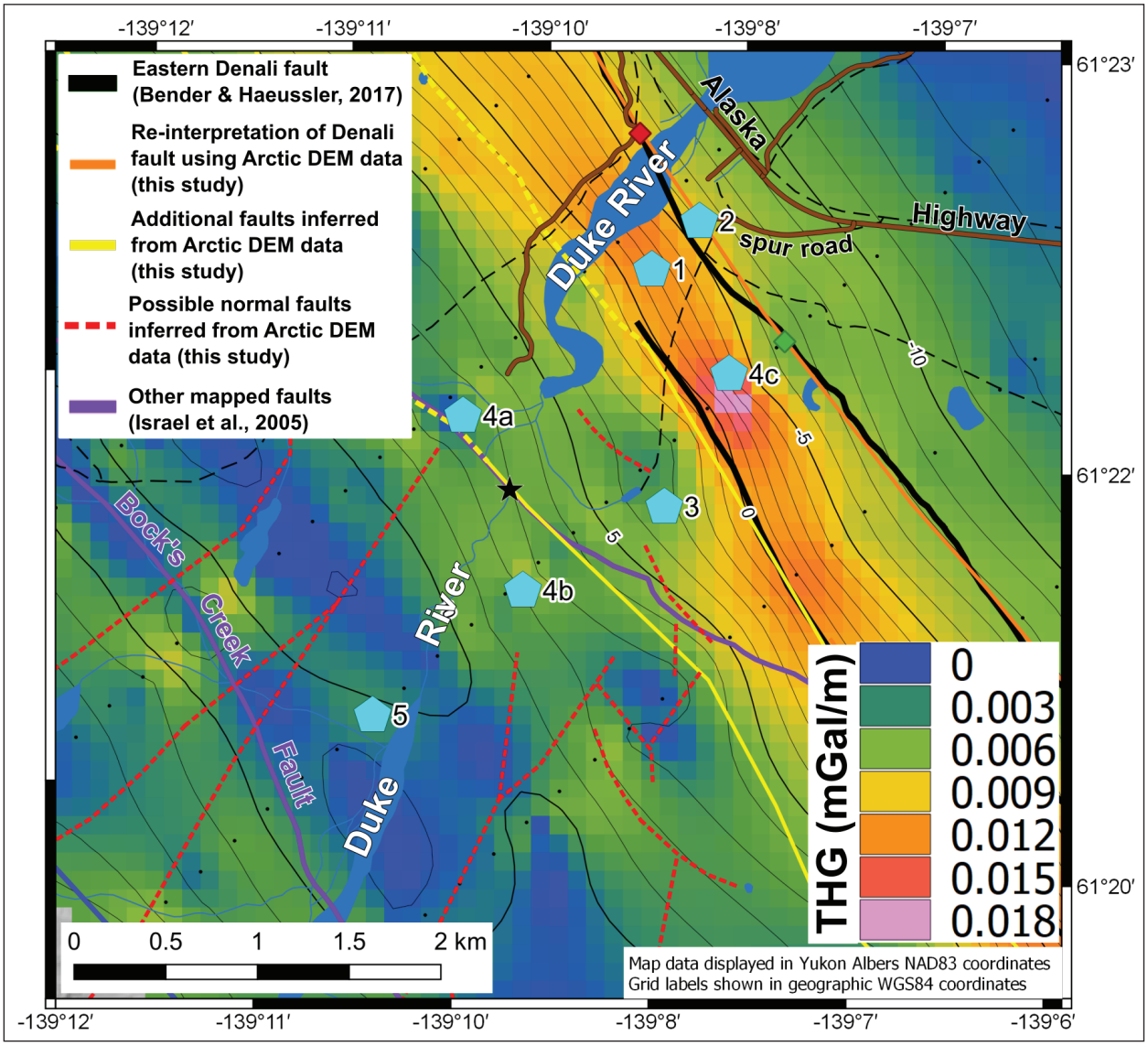

Figure 30. *Map showing the seven proposed drilling locations (blue pentagons) and the total horizontal gradient gravity map (colors defined in the legend) with contour lines from the Complete Bouguer Anomaly map (thick black lines = 5 mGal contours and thin black lines = 1 mGal contours). Fault annotation and other features are the same as in Figure 26.*

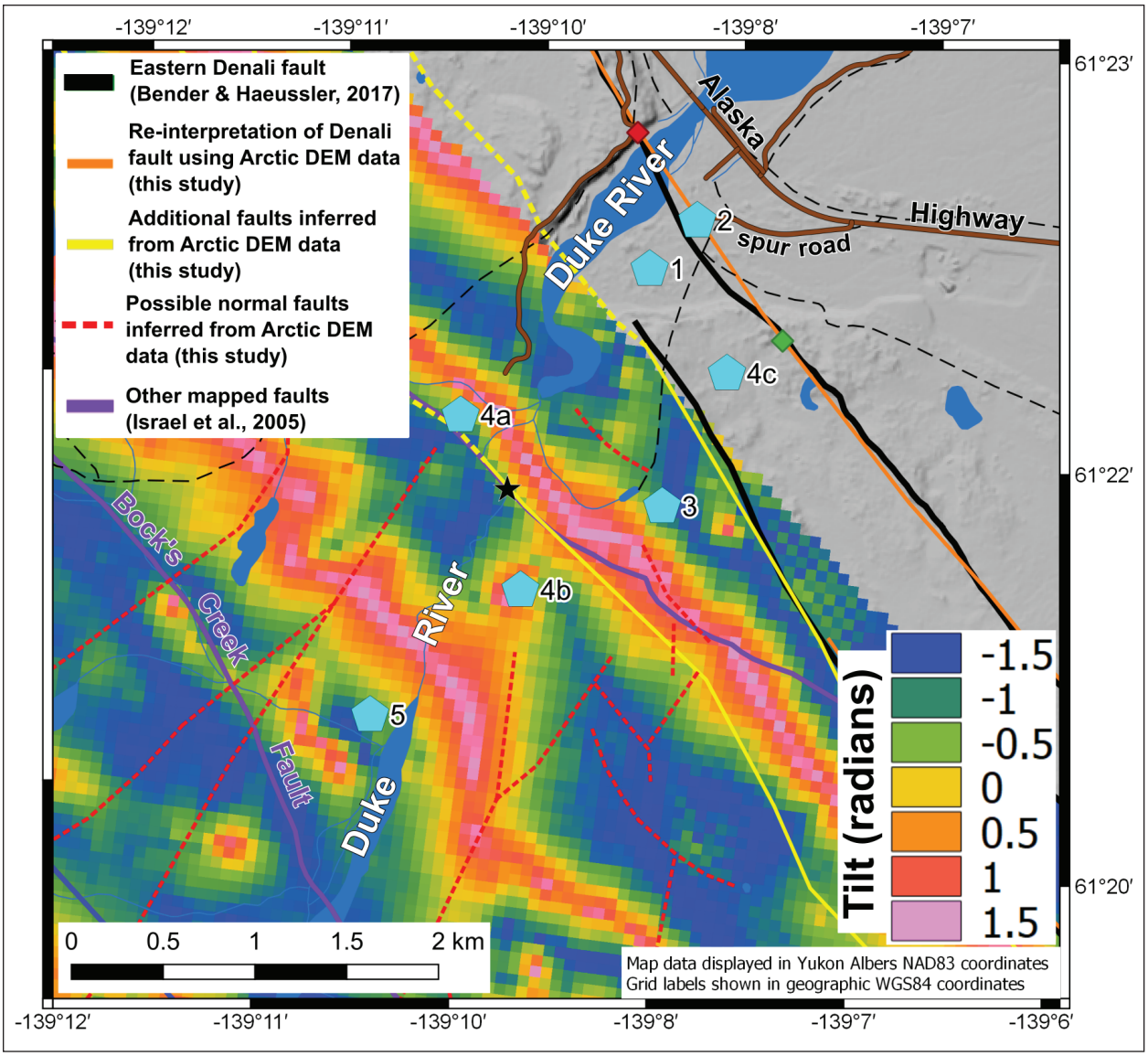

Figure 31. *Map showing the seven proposed drilling locations (blue pentagons) and the aeromagnetic survey data from 2015 with the tilt derivative applied. Fault annotation and other features are the same as in Figure 26.*

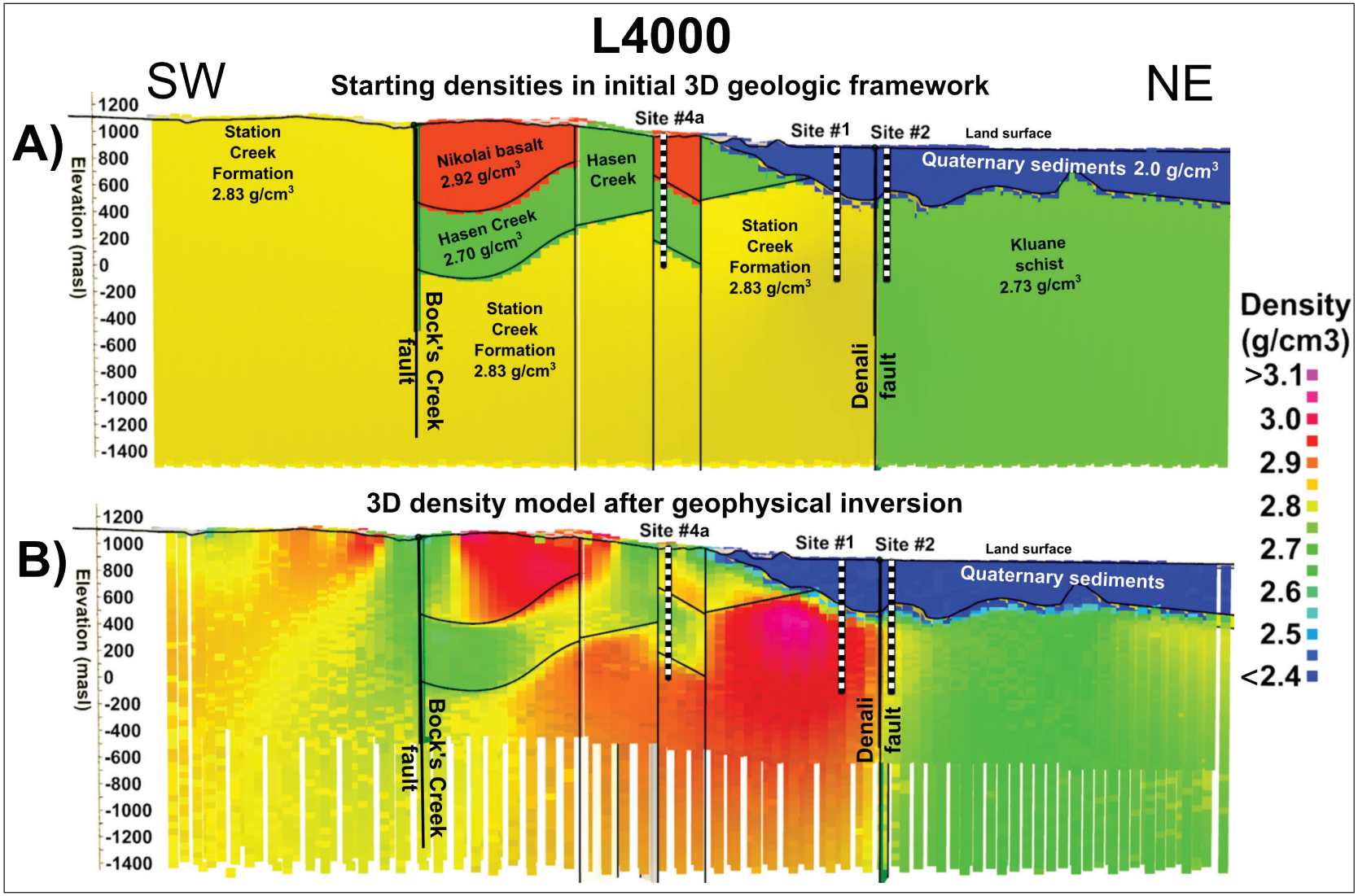

Figure 32. *Density models along profile L4000 showing:* **(A)** *starting density values in the initial 3D geologic model and* **(B)** *model densities generated by the geophysical inversion that are in agreement with the measured gravity survey data. One kilometre deep proposed boreholes are shown as black/white dashed lines and are labeled. The boreholes have been projected onto the cross-section from their original locations by < 200 m. Horizontal and vertical scales are equal. Location of profile is shown in Figure 29.*

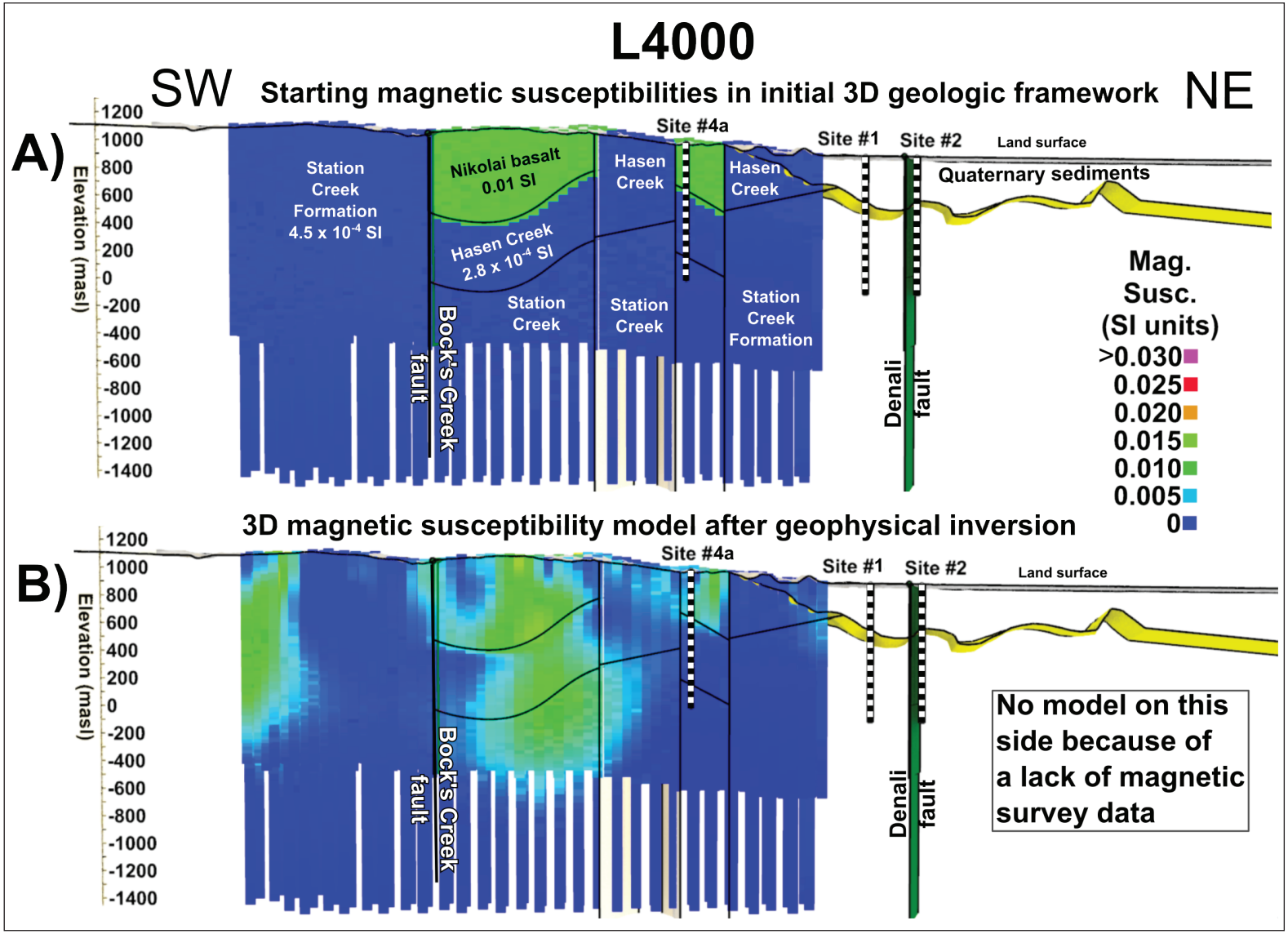

Figure 33. *Magnetic susceptibility models along profile L4000 showing:* ***(A)*** *starting magnetic susceptibility values in the initial 3D geologic model and* ***(B)*** *model magnetic susceptibility values generated by the geophysical inversion that are in agreement with the measured magnetic survey data. One kilometre deep proposed boreholes are shown as black/white dashed lines and are labeled. Horizontal and vertical scales are equal.*

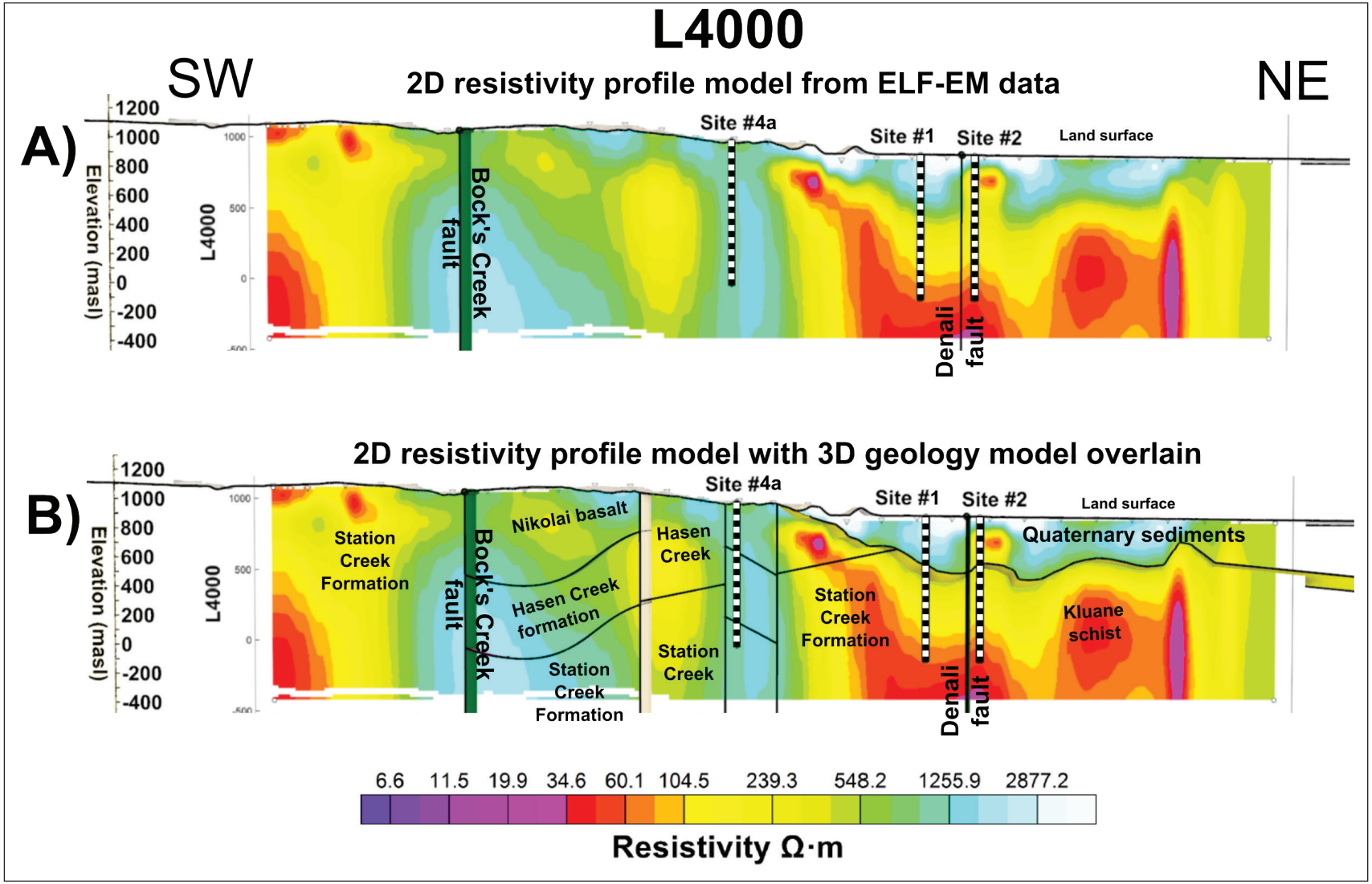

Figure 34. *ELF-EM resistivity model along profile L4000 showing:* ***(A)*** *the original model and* ***(B)*** *the resistivity profile with the 3D geologic model overlain. One kilometre deep proposed boreholes are shown as black/white dashed lines and are labeled. Horizontal and vertical scales are equal.*

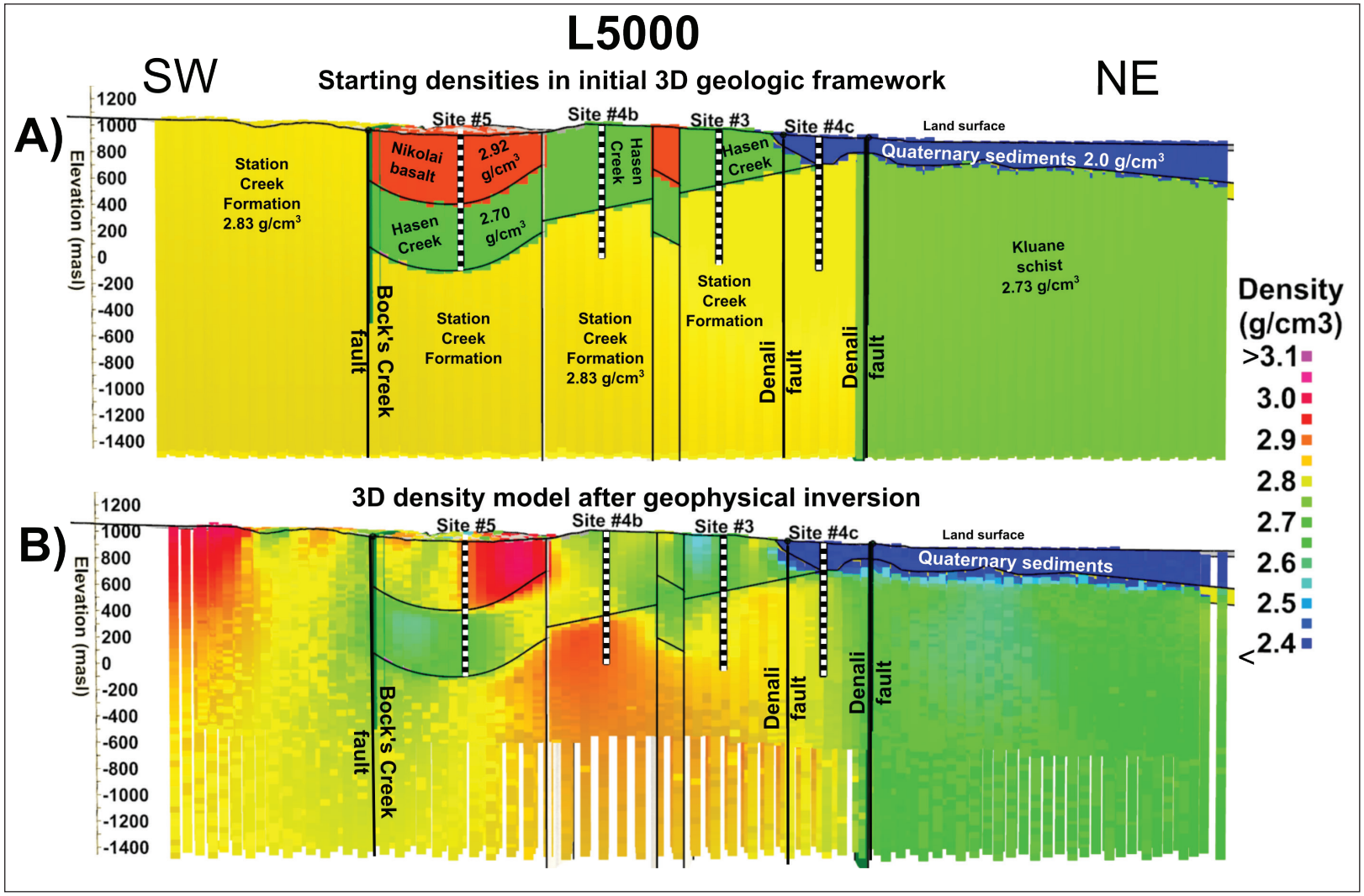

Figure 35. *Density models along profile L5000 showing:* **(A)** *starting density values in the initial 3D geologic model and* **(B)** *model densities generated by the geophysical inversion that are in agreement with the measured gravity survey data. One kilometre deep proposed boreholes are shown as black/white dashed lines and are labeled. The boreholes have been projected onto the cross-section from their original locations by <200 m. Horizontal and vertical scales are equal. Location of profile is shown in Figure 29.*

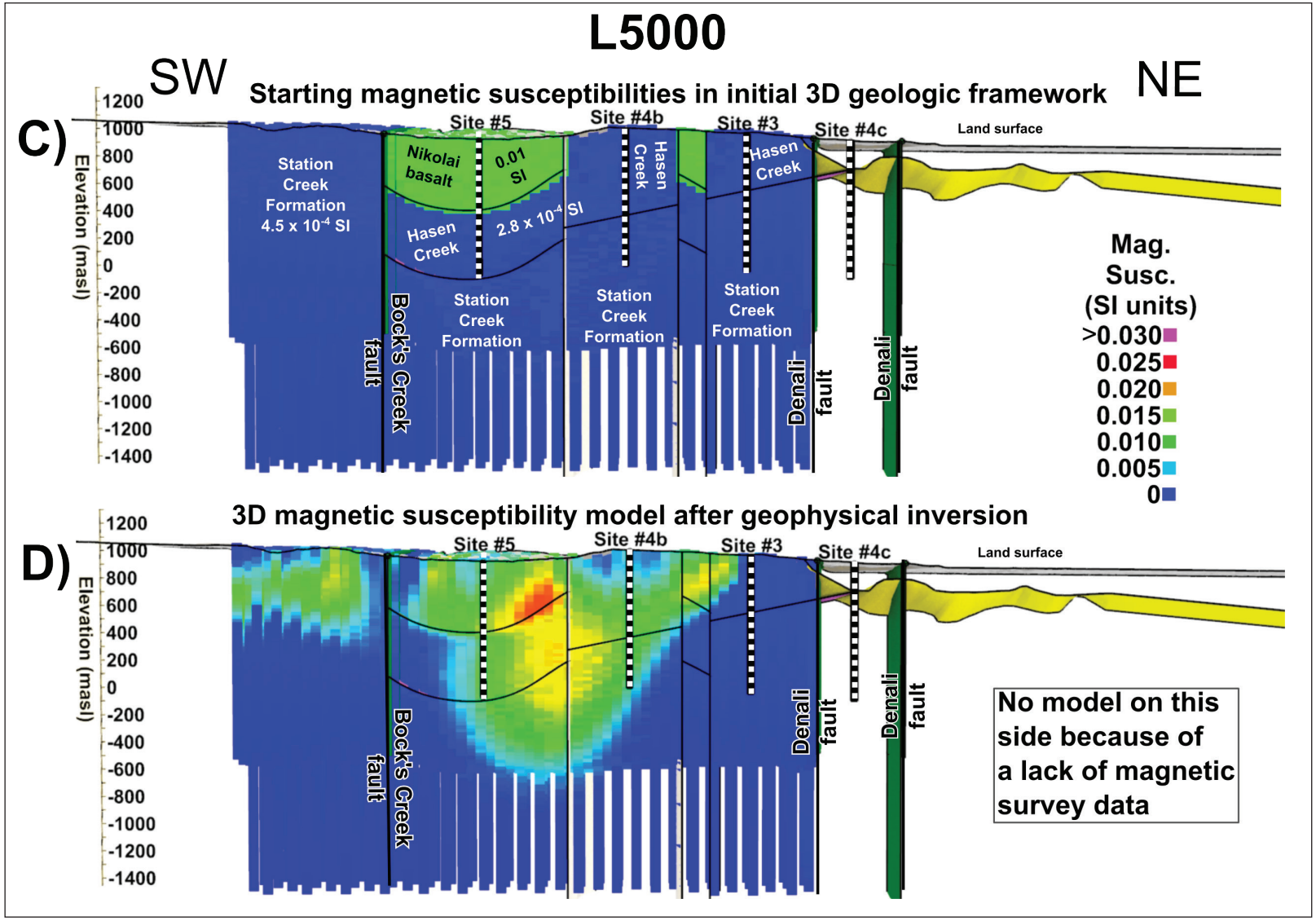

Figure 36. *Magnetic susceptibility models along profile L5000 showing:* ***(A)*** *starting magnetic susceptibility values in the initial 3D geologic model and* ***(B)*** *model magnetic susceptibility values generated by the geophysical inversion that are in agreement with the measured magnetic survey data. One kilometre deep proposed boreholes are shown as black/white dashed lines and are labeled. Horizontal and vertical scales are equal.*

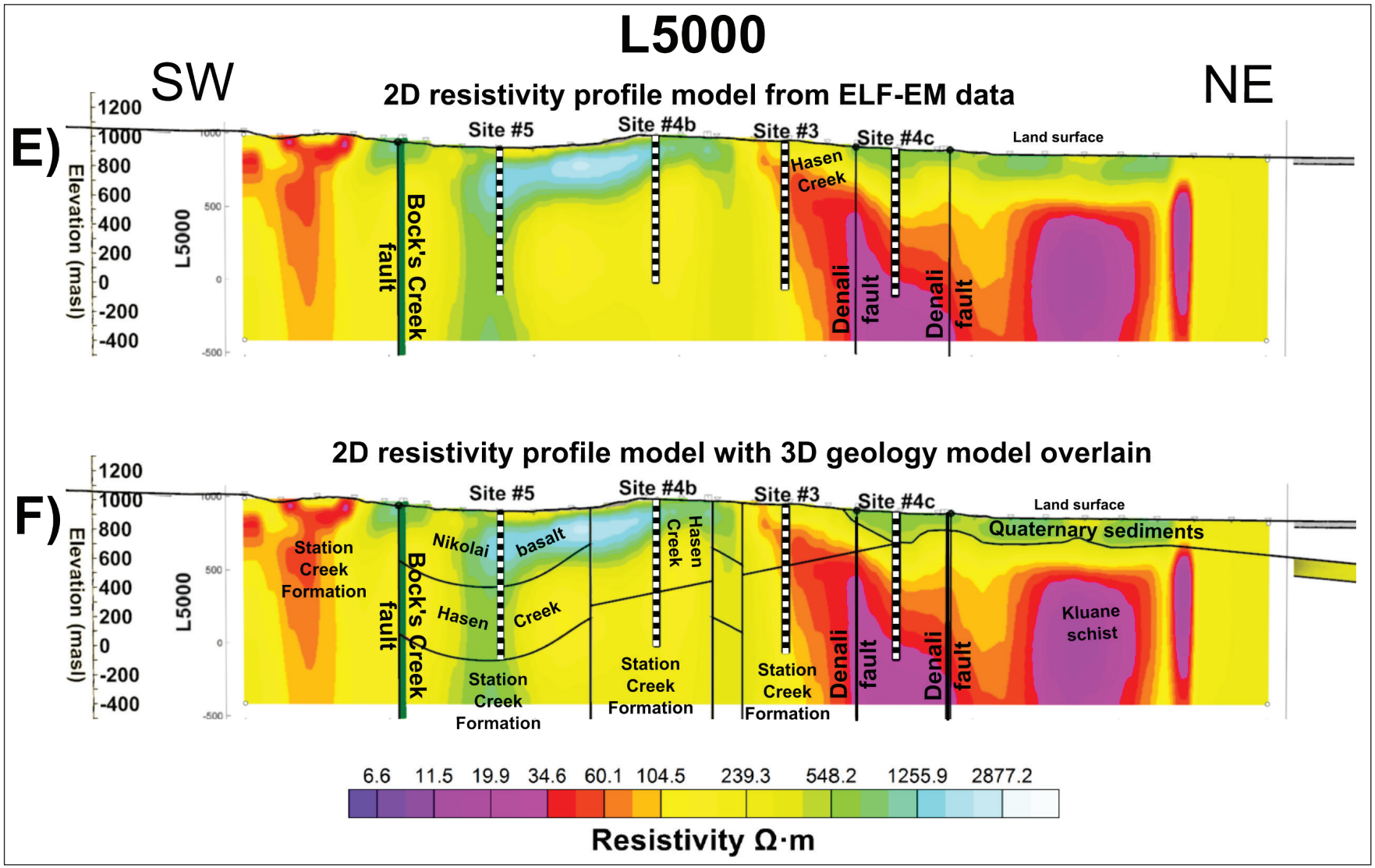

Figure 37. *ELF-EM resistivity model along profile L5000 showing:* ***(A)*** *the original model and* ***(B)*** *the resistivity profile with the 3D geologic model overlain. One kilometre deep proposed boreholes are shown as black/white dashed lines and are labeled. Horizontal and vertical scales are equal.*

Table 2. *Proposed exploratory drill sites ranked from most to least-favourable with descriptions of relevant geological and site access information.*

Drill site#	Access?	Site preparation needed?	Bedrock Geology?	Faults?	Near Right Step?
1	No apparent road access in GeoYukon satellite images. Flat area with few trees. Site is located 350 m SW from the end of a gravel spur road (*i.e.*, Site#2) which connects to the Alaska Highway	Likely need to build 350 m long access road (or may be accessible in winter when frozen?). Also may need to clear vegetation for a drill pad	Quaternary sediments underlain by Hasen Creek formation (Israel et al., 2005)	Located between the two strands of the eastern Denali fault	Yes, on the edge of the right-bend in the gravity map
2	Most easily accessible of all proposed sites. Located at end of a mapped spur road off of the Alaska Hwy.	May need to clear some trees on side of gravel road to make room for drill pad	Quaternary sediments underlain by Kluane schist or Hasen Creek formation?	On top of the main strand of the eastern Denali fault. Site is located between the USGS Denali fault trench and the Denali fault flower structure exposed in the bluff at Duke River	Yes, on the edge of the right-bend in the gravity map
3	Along a snowmobile trail (seen in GeoYukon satellite images)	Yes, need to build ~1.5 km long access road and clear the drill pad	Quaternary sediments underlain by Hasen Creek formation	Site located about 400 m SW of the southern strand of the eastern Denali fault and ~500 m NE of and ~650 m along strike from an antithetic (*i.e.*, NE-dipping) fault observed in the southern wall of the Duke River valley. This site would be in the hanging wall of this fault. Site located on margin of minor, inferred normal faults in the Duke River valley	Located halfway between the Denali fault "right-bend" and the "right-step" ELF-EM anomaly
4a	Accessible via gravel road that runs along N side of Duke River. Site is flat, but in area of dense trees on the bluff above the river.	Need to clear an area in the forest for the drill pad	Thin cover of surficial sediments underlain by Nikolai basalt (which outcrops in bluff only 100m to SE)	Site located ~1.1 km SW of the southern strand of the eastern Denali fault and ~100 m NE of and ~500 m along strike from an antithetic (*i.e.*, NE dipping) fault observed in the southern wall of the Duke River valley. This site would be in the hanging wall	Yes, located at the northern end of the "right-step" ELF-EM anomaly
4b	None. Would need to build an access road ~1 km from Site#4b (or ~2.5 km from Alaska Hwy)	Yes, need to build access road and clear the drill pad	Thin cover of surficial sediments underlain by Hasen Creek formation	Site located ~1.3 km SW of the southern strand of the eastern Denali fault and ~350 m SW of and ~450 m along strike from an antithetic (*i.e.*, NE dipping) fault observed in the southern wall of the Duke River valley. This site would be in the footwall of this fault	Yes, located in the middle of the "right-step" ELF-EM anomaly
4c	Along a snowmobile trail? (seen in GeoYukon satellite images)	Yes, need to build ~1 km long access road and clear a drill pad	Quaternary sediments underlain by Hasen Creek formation	Located between the two strands of the eastern Denali fault	Yes, located in the middle of the Denali fault "right-bend" anomaly
5	Accessible via gravel road that runs along N side of Duke River. Site is a flat, open area next to river near some miner's cabins	Probably not much	Thin cover of fluvial sediments underlain by Nikolai basalt	600 m NE of Bock's Creek Fault. Within the area of of minor, inferred normal faults in the Duke River valley	No

Table 3. *Proposed exploratory drill sites ranked from most to least-favourable with descriptions of relevant geophysical information.*

				Subsurface Information from geological & geophysical models			
Drill site#	**Information from Magnetic Map?**	**Information from Gravity Map?**	**Information from ELF-EM Map?**	**ELF-EM resistivity model?**	**3D geology model?**	**3D magnetic susceptibility model?**	**3D density model?**
1	No magnetic survey data	Located in the middle of the Horizontal Gradient high on one end of the right-bend in the gravity map	Located in the middle of the Denali fault ELF-EM anomaly	Strongly resistive in uppermost 300m and progressively more conductive in lower 700m	Quat. Seds. in upper 300m then 700m of Station Creek and faulted rocks?	No magnetic survey data	Upper 300 m is low density sediments underlain by 700 m of anomalously high density rock (basalt?)
2	No magnetic survey data	Located on margin of the Horizontal Gravity Gradient high situated at one end of the right-bend in the gravity map	Located on the margin of the Denali fault ELF-EM anomaly	Near-surface conductor underlain by moderately conductive rocks and then highly conductive rocks deeper	Quat. Seds. in upper 300m then 700m of Kluane schist and faulted rocks(?)	No magnetic survey data	Upper 300 m is low density sediments underlain by boundary between lower density rocks on the NE and higher density rocks on the SW
3	Not interesting. Located north of NW-trending mag high far from right-step in mag map.	Located just outside of the Horizontal Gradient high on one end of the right-bend in the gravity map	Located halfway between the Denali fault ELF-EM anomaly and the "right-step" ELF-EM anomaly	Goes right through resistivity boundary between conductive rocks on the NE and moderately resistive rocks on the SW	Hasen Creek in upper 400m; Station Creek in lower 600m	Low mag susc for entire length of hole	Upper 500 m moderate density; lower 500 m higher density
4a	Not interesting. Located south of NW-trending magnetic high far from right-step in magnetic map.	Located well outside of the Horizontal Gradient high on one end of the right-bend in the gravity map	Located at the northern end of the "right-step" ELF-EM anomaly.	Strongly resistive rocks for 1000m	Upper 400m Nikolai basalt; middle 400m Hasen Creek; lower 200m Station Creek	Upper 400m moderate mag susc then low magnetic susceptibility for rest of hole	upper 300 m in higher density rocks; middle 500m in moderate density rocks; lower 200 m in anomalously higher density rocks
4b	Interesting. Located on magnetic high on the north edge of the right-step in the magnetic map.	Located well outside of the Horizontal Gradient high on one end of the right-bend in the gravity map	Located in the middle of the "right-step" ELF-EM anomaly	Uppermost 200m strongly resistive but lower 800m has moderate resistivity	Hasen Creek in upper 700m; Station Creek in lower 300m	Moderate-high magnetic susceptibility for most of the length of hole	Moderate density in upper 700 m; Anomalously high density in lower 300 m
4c	No magnetic survey data	Located in the middle of the Horizontal Gradient high and in the middle of the right-bend in the gravity map	Located in the middle of the Denali fault ELF-EM anomaly	Moderately resistive Quat. Seds in upper few 100m underlain by moderate-to-strongly conductive rocks	Quat. Seds. In upper 200m then 800m of Station Creek formation	No magnetic survey data	Upper 200 m very low density underlain by gradational boundary between dense rocks on SW and lower density rocks on NE
5	Not interesting. Located south of NW-trending mag high and across the Duke River from the right-step in magnetic map.	on edge of minor gravity low that may be associated with extension in the Duke River valley	Far outside of right step shown on the ELF-EM map. This site is on the margin of the Bock's Creek fault ELF-EM anomaly.	Strongly resistive in upper 500m but only moderately resistive in lower 500m	Nikolai basalt in upper 600m; Hasen Creek in lower 400m	Moderate-high magnetic susceptibility for entire length of hole	On margin of high density body for upper 600 m; moderate density for lower 400 m

Table 4. *Locations of the seven proposed drill sites in WGS84 geographic coordinate system.*

Drill site#	Latitude	Longitude	Elevation (masl)
1	61.367905	-139.147378	877
2	61.370497	-139.143062	873
3	61.356423	-139.143592	952
4a	61.359827	-139.164972	978
4b	61.351632	-139.157042	995
4c	61.363220	-139.138441	904
5	61.344788	-139.170933	919

Conclusions and Recommendations

This study analyzed and interpreted an array of geological and geophysical data along the eastern Denali fault near the town of Burwash Landing in southwestern Yukon in an attempt to identify favourable locations for exploratory drilling for geothermal energy resources. This part of Yukon is considered to have high potential for geothermal resources because of relatively shallow Curie point depths derived for this area (which suggest elevated temperature) as well as the presence of the crustal-scale Denali fault zone (which suggests fractured rock and permeability in the subsurface). Data sets included in this study are: bedrock geological maps, surficial geological maps, fault maps, rock properties, gravity data, magnetic survey data, ELF-EM data, high resolution topographic data, and InSAR data.

A map-based investigation of these data revealed a right-step in the vicinity of the Denali fault (near Duke River) which has an orientation consistent with localized crustal extension. Such an extensional environment could potentially pull-apart the Earth's crust in a restricted area which could lead to fracturing of rocks in the subsurface and the formation of permeability. If such an environment has indeed been created, then the fractured, permeable subsurface could allow for the ascent of warm geothermal fluids to near surface, drillable depths. Drilling targets were chosen in the area of this observed right-step.

As an aid to selecting specific subsurface drill targets, a 3D geological model was constructed for the project area and it was tested using 3D geophysical modelling of gravity and magnetic data. The aim of this effort was to better understand the distribution of subsurface lithologic domains and structures prior to drilling.

Seven exploratory drill targets have been selected and ranked qualitatively from most to least-favourable. It is recommended that at least two out of the seven proposed holes are drilled in order to test the thermal and geologic variability across the geothermally prospective area. The recommended drilling depth of the exploratory boreholes is 500 m to 1 km. The key data sets extracted from the exploratory boreholes should be: downhole geology, water samples, and an equilibrated static temperature profile.

This geothermal study is the first of its kind in southwestern Yukon and, fortunately, we have been able to leverage large amounts of pre-existing, high quality geoscientific data for this project thanks to years of effort by the Yukon Geological Survey. That being said, additional data collection and analysis are needed to better understand the subsurface and the potential for geothermal resources in this area. The drilling of two or more exploratory drillholes, as proposed here, will only be the first step in a longer program to discover, define, and demarcate the potential size and temperature of geothermal resources in the region. There are specific geoscientific studies which would be helpful:

1. An airborne LIDAR survey over the project area to help define subtle topographic features that mark the surface traces of faults. Small patches of LIDAR data available near the Alaska Highway show that the Denali fault, for example, is clearly visible in LIDAR-derived DEMs. LIDAR coverage in other parts of the project area would, thus, be useful for identifying other faults, particularly those with Quaternary offset.
2. Higher resolution geological mapping of both bedrock distribution and geological structures would improve our understanding of the subsurface in the project area. The most recent bedrock mapping in the area is of high quality; however, it was done at a scale of 1:50 000. More detailed mapping at 1:24 000 scale or better is recommended. During the geologic mapping effort, additional rock samples should be collected for the measurement of rock properties (*i.e.*, density and magnetic susceptibility).
3. A magnetotelluric (MT) survey that covers about a 5 by 5 km area centered on the right-step is recommended. A 3D resistivity model should be generated using the new MT survey data as well as the existing ELF-EM data in a cooperative or joint 3D geophysical inversion. The existing ELF-EM resistivity models are 2D profiles and extend to only 1.5 km deep. An MT survey with a 3D inversion of the MT + ELF-EM data would result in a higher quality 3D resistivity model which would extend to a depth of several kilometres.
4. After new LIDAR, geologic mapping, rock property and MT data are collected and interpreted, and after the exploratory boreholes have been drilled and the downhole data analysed, the initial 3D geologic model created in this study should be updated and the 3D geophysical inversion modelling of the gravity and magnetic data should also be re-run as a means of testing the new, updated version of the 3D geologic model.

References

Bender, A.M. and Haeussler, P.J., 2017. Eastern Denali Fault Surface Trace Map, Eastern Alaska and Yukon, Canada. U.S. Geological Survey, Open-File Report 2017-1049, 10 p.

Blais-Stevens, A., Clague, J.J., Brahney, J., Lipovsky, P., Haeussler, P.J. and Menounos, B., 2020. Evidence for Large Holocene Earthquakes along the Denali Fault in Southwest Yukon, Canada. Environmental and Engineering Geoscience, vol. 26, no. 1, p. 1–18.

Brueseke, M.E., Benowitz, J.A., Trop, J.M., Davis, K.N., Berkelhammer, S.E., Layer, P.W. and Morter, B.K., 2019. The Alaska Wrangell Arc: ~30 Ma of subduction-related magmatism along a still active arc-transform junction. Terra Nova, vol. 31, p. 59–66.

Cockett, R., Kang, S., Heagy, L.J., Pidlisecky, A. and Oldenburg, D.W., 2015. SimPEG: An open source framework for simulation and gradient based parameter estimation in geophysical applications. Computers and Geosciences, vol. 85, p. 142–154.

Colpron, M. and Nelson, J.L., 2011. A Digital Atlas of Terranes for the Northern Cordillera. Yukon Geological Survey, www.geology.gov.yk.ca, accessed December 1, 2016.

Coyle, M. and Oneschuk, D., 2015. Residual Total Magnetic Field, Kluane Lake West Aeromagnetic Survey, Yukon, NTS 115-G/6 and parts of 115-G/5 and 7. Yukon Geological Survey, Open File 2015-17; *also Geological Survey of Canada, Open File 7913*, 1:50 000 scale.

Faulds, J.F. and Hinz, N.H., 2015. Favorable Tectonic and Structural Settings of Geothermal Systems in the Great Basin Region, Western USA: Proxies for Discovering Blind Geothermal Systems. Proceedings World Geothermal Congress, Melbourne, Australia, 19–25 April 2015, 6 p.

Feng, W., Samsonov, S., Liang, C., Li, J., Charbonneau, F., Yu, C. and Li, Z., 2019. Source parameters of the 2017 Mw 6.2 Yukon earthquake doublet inferred from co-seismic GPS and ALOS-2 deformation measurements. Geophysical Journal International, vol. 216, no. 3, p. 1517–1528.

Fournier, D. and Oldenburg, D., 2019. Inversion using spatially variable mixed Lp norms. Geophysical Journal International, vol. 218, p. 268–282.

Fraser, T.A., Grasby, S.E., Witter, J.B., Colpron, M. and Relf, C., 2018. Geothermal Studies in Yukon – Collaborative Efforts to Understand Ground Temperature in the Canadian North. Transactions Geothermal Resources Council, vol. 42, 20 p.

Fullagar, P.K. and Pears, G.A., 2007. Towards geologically realistic inversion. Proceedings of Exploration 07: Fifth Decennial International Conference on Mineral Exploration, Toronto. p. 444–460.

Fullagar, P.K., Pears, G.A. and McMonnies, B., 2008. Constrained inversion of geologic surfaces—Pushing the boundaries. The Leading Edge, vol. 27, p. 98–105.

GeoYukon, 2018. Geomatics Yukon website. Government of Yukon, http://mapservices.gov.yk.ca/GeoYukon/, accessed May 2018.

Global Volcanism Program, 2013. Volcanoes of the World, v. 4.8.4. Venzke, E (ed.). Smithsonian Institution. http://volcano.si.edu/, accessed December 6, 2019.

Hoffmann-Rothe, A., Ritter, O. and Janssen, C., 2004. Correlation of electrical conductivity and structural damage at a major strike-slip fault in northern Chile. Journal of Geophysical Research, vol. 109, B10101, doi:10.1029/2004JB003030.

Ingham, M. and Brown, C., 1998. A magnetotelluric study of the Alpine Fault, New Zealand. Geophysical Journal International, vol. 135, p. 542–552.

Israel, S., Tizzard, A. and Major, J., 2005. Bedrock geology of the Duke River area, parts of NTS 115G/2, 3, 4, 6 and 7, southwestern Yukon. *In*: Yukon Exploration and Geology 2005, D.S. Emond, G.D. Bradshaw, L.L. Lewis and L.H. Weston (eds.), Yukon Geological Survey, p. 139–154.

Kennedy, K.E. 2013. Surficial Geology of Burwash Landing and Destruction Bay (parts of NTS 115G/2, 6 and 7) Yukon. Yukon Geological Survey, Open File 2013-14.

Leonard, L.J., Mazzotti, S. and Hyndman, R.D., 2008. Deformation rates estimated from earthquakes in the northern Cordillera of Canada and eastern Alaska. Journal of Geophysical Research, vol. 113, B08406, doi:10.1029/2007JB005456.

Li, C.-F., Lu, Y. and Wang, J. 2017. A global reference model of Curie-point depths based on EMAG2. Nature, Scientific Reports, vol. 7, 9 p.

Marechal, A., Ritz, J.-F., Ferry, M., Mazzotti, S., Blard, P.-H., Braucher, R. and Saint-Carlier, D. 2018. Active tectonics around the Yakutat indentor: New geomorphological constraints on the eastern Denali, Totschunda and Duke River Faults. Earth and Planetary Science Letters, vol. 482, p. 71–80.

McDermott, R.G., Ault, A.K., Caine, J.S. and Thomson, S.N. 2019. Thermotectonic History of the Kluane Ranges and Evolution of the Eastern Denali Fault Zone in Southwestern Yukon, Canada. Tectonics, vol. 38, p. 2983–3010.

Nelson, J.L., Colpron, M. and Israel, S., 2013. The Cordillera of British Columbia, Yukon, and Alaska: Tectonics and Metallogeny. *In*: Tectonics, Metallogeny, and Discovery: The North American Cordillera and Similar Accretionary Settings, M. Colpron, T. Bissig, B.G. Rusk and J.F.H. Thompson (eds.), Society of Economic Geologists, Special Publication 17, p. 53–109.

Porter, C., Morin, P., Howat, I., Noh, M.-J., Bates, B., Peterman, K., Keesey, S., Schlenk, M., Gardiner, J., Tomko, K., Willis, M., Kelleher, C., Cloutier, M., Husby, E., Foga, S., Nakamura, H., Platson, M., Wethington, M., Williamson, C., Bauer, G., Enos, J., Arnold, G., Kramer, W., Becker, P., Doshi, A., D'Souza, C., Cummens, P., Laurier, F. and Bojesen, M., 2018. ArcticDEM, https://www.pgc.umn.edu/data/arcticdem/, accessed May 15, 2019.

Siripunvaraporn, W. and Egbert, G., 2000. An efficient data-subspace inversion method for 2-D magnetotelluric data. Geophysics, vol. 65, no. 3, p. 791–803.

Skulski, T., 1988. The origin and setting of anomalous arc magmatism in the Wrangell volcanic belt, southwest Yukon. *In*: Yukon Geology, vol. 2, Exploration and Geological Sciences Division, Yukon Region, Indian and Northern Affairs Canada, p. 88–98.

Skulski, T., Francis, D. and Ludden, J., 1992. Volcanism in an arc-transform transition zone: the stratigraphy of the St. Clare Creek volcanic field, Wrangell volcanic belt, Yukon, Canada. Canadian Journal of Earth Sciences, vol. 29, no. 3, p. 446–461.

Stanley, B., 2012. Structural geology and geochronology of the Kluane schist, southwestern Yukon Territory. Unpublished MSc thesis, University of Waterloo, Ontario, Canada, 113 p.

Townend, J., Sutherland, R., Toy, V.G., Doan, M.-L., Celerier, B., Massiot, C., et *al.*, 2017. Petrophysical, geochemical, and hydrological evidence for extensive fracture mediated fluid and heat transport in the Alpine Fault's hanging-wall damage zone. Geochemistry, Geophysics, Geosystems, vol. 18, p. 4709–4732.

Trop, J.M., Hart, W.K., Snyder, D. and Idleman, B. 2012. Miocene basin development and volcanism along a strike-slip to flat-slab subduction transition: Stratigraphy, geochemistry, and geochronology of the central Wrangell volcanic belt, Yakutat–North America collision zone. Geosphere vol. 8, no. 4, p. 805–834.

Unsworth, M. and Bedrosian, P.A., 2004a. Electrical resistivity structure at the SAFOD site from magnetotelluric exploration. Geophysical Research Letters, vol. 31, 4 p.

Unsworth, M., and Bedrosian, P.A., 2004b. On the geoelectric structure of major strike-slip faults and shear zones. Earth Planets Space, vol. 56, p. 1177–1184.

Witter, J.B., Miller, C.A., Friend, M. and Colpron, M., 2018. Curie Point Depths and Heat Production in Yukon, Canada. Proceedings 43rd Workshop on Geothermal Reservoir Engineering, Stanford University, Stanford, California, 11 p.

Younker, L.W., Kasameyer, P.W. and Tewhey, J.D., 1982. Geological, geophysical, and thermal characteristics of the Salton Sea Geothermal Field, California. Journal of Volcanology and Geothermal Research, vol. 12, no. 3-4, p. 221–258.

Yukon Geological Survey, 2018. Yukon Digital Bedrock Geology. http://data.geology.gov.yk.ca/Compilation/3, accessed May 2018.

Appendix 1. Statement of Qualifications

This report has been prepared by Jeffrey B. Witter, Principal Geoscientist at Innovate Geothermal Ltd. Dr. Witter holds an undergraduate degree in geophysics as well as Master's and Ph.D. degrees in geology. He has fifteen years of experience as an exploration geologist/geophysicist in the natural resource industry with over half of that time committed specifically to geothermal exploration and resource evaluation. He is a registered professional geoscientist in the province of British Columbia (Canada) and is a member of Engineers and Geoscientists of British Columbia (EGBC). EGBC has a defined and enforceable Code of Ethics which Dr. Witter agrees to abide by. Dr. Witter has been engaged as a Consultant by the Yukon Geological Survey but holds no financial interest in any geothermal energy project in Yukon.

Dated in Vancouver, British Columbia, Canada this 31st day of March 2020

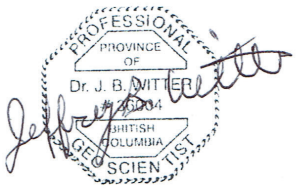

Jeffrey B. Witter Ph.D., PGeo (Province of British Columbia, No. 36004)

The following appendices are available as digital files only:

Appendix 2. Rock Property data

Appendix 3. Gravity data

Appendix 4. ELF-EM data

Appendix 5. InSar Report

Appendix 6. GIS files

Appendix 7. 3D animation